UNIVERSIDADE FEDERAL DE UBERLÂNDIA

INSTITUTO DE CIÊNCIAS BIOMÉDICAS

PROGRAMA DE PÓS-GRADUAÇÃO EM IMUNOLOGIA E PARASITOLOGIA APLICADAS

URIEL ENRIQUE AQUINO RUIZ

EFEITOS DA IMIDAZONAFTIRIDINA NA INFECÇÃO PELO VÍRUS CHIKUNGUNYA: ATIVIDADE ANTIVIRAL POR UMA VIA INDEPENDENTE DO INTERFERON TIPO 1?

UBERLÂNDIA-MG, BRASIL

2022

EFEITOS DA IMIDAZONAFTIRIDINA NA INFECÇÃO PELO VÍRUS CHIKUNGUNYA: ATIVIDADE ANTIVIRAL POR UMA VIA INDEPENDENTE DO INTERFERON TIPO 1?

Dissertação apresentada ao colegiado do Programa de Pós-Graduação em Imunologia e Parasitologia Aplicadas como parte de obtenção do título de Mestre.

Orientadora: Profa. Dra. Ana Carolina Gomes Jardim

Uriel Enrique Aquino Ruiz

Profa. Dra. Ana Carolina Gomes Jardim

Dados Internacionais de Catalogação na Publicação (CIP)
Sistema de Bibliotecas da UFU, MG, Brasil.

R934e 2022

Ruiz, Uriel Enrique Aquino, 1996-
Efeitos da Imidazonaftiridina na infecção pelo vírus Chikungunya [recurso eletrônico] : atividade antiviral por uma via independente do Interferon tipo 1? / Uriel Enrique Aquino Ruiz. - 2022.

Orientadora: Ana Carolina Gomes Jardim.
Dissertação (mestrado) - Universidade Federal de Uberlândia. Programa de Pós-Graduação em Imunologia e Parasitologia Aplicadas.
Modo de acesso: Internet.
Disponível em: http://doi.org/10.14393/ufu.di.2022.5348
Inclui bibliografia.
Inclui ilustrações.

1. Imunologia. I. Jardim, Ana Carolina Gomes, 1981-, (Orient.). II. Universidade Federal de Uberlândia. Programa de Pós-Graduação em Imunologia e Parasitologia Aplicadas. III. Título.

CDU: 612.017

Glória Aparecida
Bibliotecária - CRB-6/2047

UNIVERSIDADE FEDERAL DE UBERLÂNDIA
Coordenação do Programa de Pós-Graduação em Imunologia e Parasitologia Aplicada
Av. Amazonas, s/n, Bloco 4C, Sala 4C218 - Bairro Umuarama, Uberlândia-MG, CEP 38400-902
Telefone: (34) 3225-8672 - www.imunoparasito.ufu.br - coipa@ufu.br

ATA DE DEFESA - PÓS-GRADUAÇÃO

Programa de Pós-Graduação em:	Imunologia e Parasitologia Aplicadas				
Defesa de:	Dissertação de Mestrado Acadêmico nº 281 do PPGIPA				
Data:	Vinte e quatro de agosto de dois mil e vinte e dois	Hora de início:	13 h	Hora de encerramento:	16h e 35min
Matrícula do Discente:	12012IPA006				
Nome do Discente:	Uriel Enrique Aquino Ruiz				
Título do Trabalho:	Efeitos da Imidazonaftiridina na infecção pelo vírus chikungunya: atividade antiviral por uma via independente do interferon tipo 1?				
Área de concentração:	Imunologia e Parasitologia Aplicadas				
Linha de pesquisa:	Biologia das Interações entre Patógenos e seus Hospedeiros				
Projeto de Pesquisa de vinculação:	Terapia Antiviral: A Solução Está na Natureza?				

Reuniu-se no dia 24 de agosto, às 13 horas, por vídeo conferência, a Banca Examinadora designada pelo Colegiado do Programa de Pós-graduação em Imunologia e Parasitologia Aplicadas, assim composta pelos titulares: Fernando Moreira Simabuco - Unicamp; Samuel Cota Teixeira - ICBIM/UFU; Ana Carolina Gomes Jardim - PPGIPA/ICBIM/UFU (Presidente) orientadora do candidato.

Iniciando os trabalhos a presidente da mesa, Profa. Ana Carolina Gomes Jardim, apresentou a Comissão Examinadora e o candidato(a). Agradeceu a presença do público e concedeu ao discente a palavra para exposição do seu trabalho. A duração da apresentação do discente e o tempo de arguição e resposta foram conforme as normas do Programa.

A seguir o(a) senhor presidente concedeu a palavra, pela ordem sucessivamente, aos (às) examinadores(as) que passaram a arguir o(a) candidato(a). Ultimada a arguição, que se desenvolveu dentro dos termos regimentais, a Banca, em sessão secreta, atribuiu o resultado final, considerando o candidato(a):

APROVADO.

Esta defesa faz parte dos requisitos necessários à obtenção do título de Mestre.

O competente diploma será expedido após cumprimento dos demais requisitos, conforme as normas do Programa, a legislação pertinente e a regulamentação interna da UFU.

Nada mais havendo a tratar foram encerrados os trabalhos. Foi lavrada a presente ata que após lida e achada conforme foi assinada pela Banca Examinadora.

Documento assinado eletronicamente por **Ana Carolina Gomes Jardim**, **Professor(a) do Magistério Superior**, em 24/08/2022, às 16:37, conforme horário oficial de Brasília, com fundamento no art. 6º, § 1º, do Decreto nº 8.539, de 8 de outubro de 2015.

Documento assinado eletronicamente por **Samuel Cota Teixeira**, **Usuário Externo**, em 24/08/2022, às 16:37, conforme horário oficial de Brasília, com fundamento no art. 6º, § 1º, do Decreto nº 8.539, de 8 de outubro de 2015.

Documento assinado eletronicamente por **Fernando Moreira Simabuco**, **Usuário Externo**, em 24/08/2022, às 16:37, conforme horário oficial de Brasília, com fundamento no art. 6º, § 1º, do Decreto nº 8.539, de 8 de outubro de 2015.

A autenticidade deste documento pode ser conferida no site https://www.sei.ufu.br/sei/controlador_externo.php?acao=documento_conferir&id_orgao_acesso_externo=0, informando o código verificador **3834191** e o código CRC **FF06A7B3**.

LISTA DE ABREVIATURAS E SIGLAS

ANVISA Agência Nacional de Vigilância Sanitária

AUD Domínio único de alphavirus (tradução direta de *alphavirus unique domain*)

BHK-21 Fibroblastos de rim de Hamster bebê

C Proteína do capsídeo

CC_{50} Concentração citotóxica de 50%

CHIKV Vírus da Chikungunya

DENV Vírus da Dengue

DMEM Meio básico modificado por Dulbecco (tradução direta de *Dulbecco's Modified Eagle Medium*)

DMSO Dimetilsulfóxido

E Proteína do envelope

EC_{50} Concentração efetiva de 50%

ECSA Leste/Centro/Sul da África (tradução direta de *East/Central/South Africa*)

FDA Administração de Comidas e Remédios (tradução direta de F*ood and Drug Administration*)

HBV Hepacivírus B

HCV Hepacivírus C

IFN Interferon

IFNAR Receptor do Interferon de tipo 1

JAK Quinase Janus

MOI Multiplicidade de infecção (tradução direta de *Multiplicity of infection*)

MTT brometo de 3-4,5-dimetil-tiazol-2-il-2,5-difeniltetrazólio (tradução direta de *3-(4,5-dimethylthiazol-2-yl)-2,5-diphenyltetrazolium-bromide*)

mL Mililitros

nsP Proteínas não estruturais (tradução direta de *nonstructural proteins*)

OMS Organização Mundial da Saúde

ORFs Regiões de leitura aberta (tradução direta de *open reading frame*)

PAHO Organizacao Pan-America de Saúde (tradução direta de *The Pan American Health Organization*)

RdRp RNA-Polimerase dependente de RNA (tradução direta de *RNA dependent RNA polymerase*)

RE Retículo endoplasmático

RNA Ácido ribonucleico (tradução direta de *ribonucleic acid*)

RO8191 RO4948191 (8-(1, 3, 4-oxadiazol-2-yl)-2, 4-bis (trifluorometil) imidazo [1, 2-a] [1, 8] naftiridina)

SI Índice de Selectividade (tradução direta de *selective index*)

STAT Transdutor de sinal e Ativador de Transcrição (tradução direta de *Signal Transducer and Activator of Transcription*)

Tyk Tirosina quinase (tradução direta de *tyrosine kinases*)

VERO-E6 Células de rim de macaco verde africano, clone E6

ZIKV Vírus Zika

µL Microlitro

µg Microgramas

LISTA DE FIGURAS

SUMÁRIO

RESUMO

O vírus Chikungunya (CHIKV), agente causador da febre Chikungunya, é transmitido principalmente pela picada de mosquitos hematófagos do gênero *Aedes*. A doença é caracterizada por sintomas como artralgias e poliartralgias debilitantes, as quais podem permanecer por meses ou anos. Até o momento, não existem medicamentos antivirais disponíveis para tratar as manifestações do CHIKV. Neste contexto, a Imidazolnaftiridina (RO8191) é um composto sintético com atividade antiviral previamente documentada contra o Hepacivirus C (HCV) e o Zika vírus (ZIKV), porém, a atividade anti-CHIKV do RO8191 ainda não foi elucidada. Portanto, este trabalho teve como objetivo avaliar os efeitos do RO8191 na infecção por CHIKV *in vitro*, utilizando o CHIKV-*nanoluc*, uma construção viral inserida de um gene r*eporter* (-*nanoluc*), para infectar células de rim de hamster bebê (BHK-21). A análise de viabilidade celular foi avaliada por meio de ensaios de MTT e a taxa de infectividade pela quantificação de luminescência. Ensaios de adição do composto em diferentes estágios do ciclo replicativo do CHIKV foram realizados, bem como células BHK-CHIKV-NCT, que expressam proteínas não estruturais do CHIKV e os genes *Renilla* luciferase e EGFP, também foram utilizadas para avaliar o efeito do RO8191 na replicação viral. O RO8191 inibiu fortemente a replicação do CHIKV com um índice de seletividade (SI) de 12,3 e 18,7 em células BHK-21 e BHK-CHIKV-NCT, respetivamente. Além disso, o composto inibiu todos os estágios virais avaliados, com maiores taxas de inibição nas etapas viricida (75,4%) e pós-tratamento (87%). RO8191 é um agonista do IFN-α, e para avaliar o efeito independente dessa via, os ensaios também foram realizados em células VERO-E6, que não expressam os genes que codificam interferons tipo I (IFN-$I^{-/-}$). Como resultado, RO8191 demonstrou um SI de 37,3 apresentando efeito em todas as etapas, principalmente na virucida (70,5%) e pós-tratamento (91,6%). Ensaios de espectroscopia de infravermelho (ATR-FTIR) e experimentos de ancoragem molecular foram realizados e demonstraram interações de RO8191 principalmente com as glicoproteínas do CHIKV. Os resultados aqui apresentados enfatizam o potencial anti-CHIKV do RO8191, o qual pode ser futuramente capitalizado como uma alternativa terapêutica para o tratamento da febre Chikungunya.

Palavras-chave: Imidazolnaftiridina; Atividade antiviral; Vírus da Chikungunya; Febre Chikungunya; Doenças negligenciadas; Atividade independente de IFN-I

ABSTRACT

The Chikungunya virus (CHIKV), the causative agent of Chikungunya fever, is transmitted mainly by the bite of hematophagous mosquitoes of the *Aedes* genus. The disease is characterized by symptoms such as disabling arthralgias and polyarthralgia, which can persistent for months or years. Up to date, there are no antiviral drugs available to treat CHIKV manifestations. In this context, Imidazolnaphtyridine (RO8191) is a compound with antiviral activity previously reported against the Hepacivirus C (HCV) and Zika virus (ZIKV), however, the anti-CHIKV activity of RO8191 has not yet been elucidated. Therefore, this work aimed to evaluate the effects of RO8191 on CHIKV infection *in vitro*, employing CHIKV-*nanoluc*, a viral construct inserted of a reporter gene (-*nanoluc*), to infect baby hamster kidney cells (BHK-21). Cell viability analysis was evaluated through MTT assays and infectivity rates through luminescence assays. We developed time of drug-addition assays in different stages of the CHIKV replicative cycle, as well as BHK-CHIKV-NCT cells, that express CHIKV non-structural proteins and *Renilla* luciferase and EGFP reporters, were also used to analyze the effects of RO8191 on viral replication. RO8191 strongly inhibits the CHIKV replication with a selectivity index (SI) of 12.3 and 18.7 in BHK-21 and BHK-CHIKV-NCT cells, respectively. Additionally, the compound inhibited all viral stages evaluated, with higher rates of inhibition in viricidal (75.4%) and post-treatment (87%). Due to the IFN-α agonism by RO8191, and to analyze an independent of this pathway effect, assays were also developed all employing VERO-E6 cells, which do not encode type I interferons (IFN-$I^{-/-}$). As a result, RO8191 presented SI of 37.3 and had effects in all viral replication steps, but mainly in viricidal (70.5%) and post-treatment (91.6%) assays. Infrared spectroscopy assays (ATR-FTIR) and molecular docking experiments were carried out and demonstrated interactions mainly between RO8191 and CHIKV glycoproteins. Our data highlights the anti-CHIKV potential exerted by RO8191, that could be future capitalized as an alternative treatment against Chikungunya fever.

Keywords: Imidazonaphthyridine; Antiviral activity; Chikungunya virus; Chikungunya Fever; Neglected tropical diseases; IFN-I independent activity

CAPÍTULO I

FUNDAMENTAÇÃO TEÓRICA

1. INTRODUÇÃO

1.1. Febre Chikungunya: Epidemiologia e Transmissão

A Febre Chikungunya é uma doença causada pelo vírus da Chikungunya (CHIKV), identificada pela primeira vez na Tanzânia, África Oriental, em 1952 (ACOSTA-REYES; NAVARRO-LECHUGA; MARTÍNEZ-GARCÉS, 2015). No 2004, se reportaram surtos de Febre Chikungunya na África, nas ilhas do Oceano Índico, na Austrália, e no sudeste da Ásia (Índia, Indonésia, Mianmar, Maldivas, Sri Lanka e Tailândia) (STAIKOWSKY et al., 2009). Em 2007, a PAHO e a Organização Mundial da Saúde (OMS) notificaram o primeiro caso de transmissão local na Europa, em um surto localizado na região Nordeste da Itália, no qual foram registrados 197 casos, sendo posteriormente disseminado para o sudeste Asiático, ilhas do Oceano Índico, regiões da Europa, Estados Unidos e Taiwan (BETTIS et al., 2022). Em 2013, os primeiros casos nativos na ilha de Saint Martin, no Caribe, foram reportados, confirmando o primeiro caso de febre Chikungunya com transmissão autóctone nas Américas (WEAVER; FORRESTER, 2015) (Figura 1).

Figura 1. Panorâmica mundial da Febre Chikungunya. Países no mundo que registraram pelo menos um caso de Febre Chikungunya não importado até junho 2022

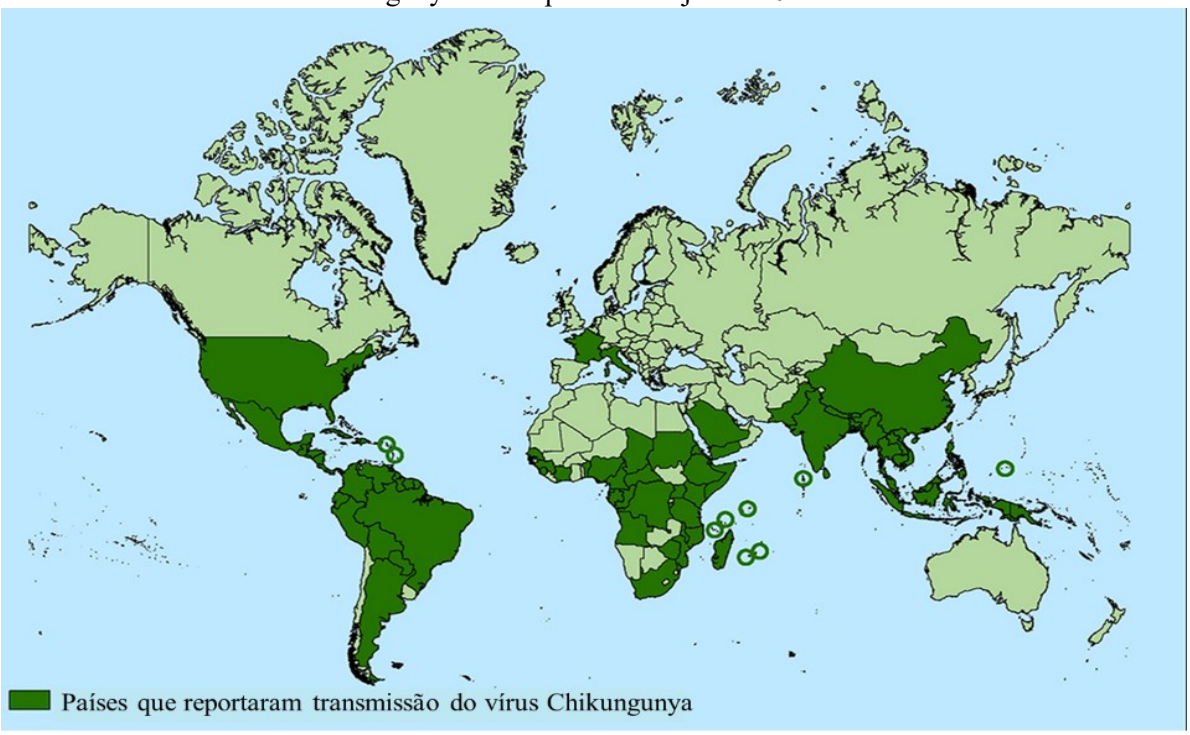

Disponível em https://www.cdc.gov/chikungunya/geo/index.html. (Consultado em 30 de julho, 2022)

No Brasil, o Ministério da Saúde confirmou em setembro de 2014 os primeiros casos autóctones, ou seja, nativos no país (SILVA et al., 2018). Em março de 2015, mais de 1.200.000 casos suspeitos foram notificados no continente americano (MORENS; FAUCI, 2014). Até junho de 2022 foram reportados 122.075 casos prováveis de infecções por CHIKV no Brasil, afetando principalmente a região Nordeste do país, com uma média de 175,7 casos por cada 100 mil habitantes. Adicionalmente, em junho de 2022, 23 óbitos por Febre Chikungunya foram confirmados e mais 50 estão em investigação (MINISTÉRIO DE SAÚDE, 2022) (**Figura 2**).

Figura 2. Taxa de incidência da Febre da Chikungunya no Brasil em 2022. Mapa com dados de casos confirmados para infecção por CHIKV no Brasil até junho de 2022

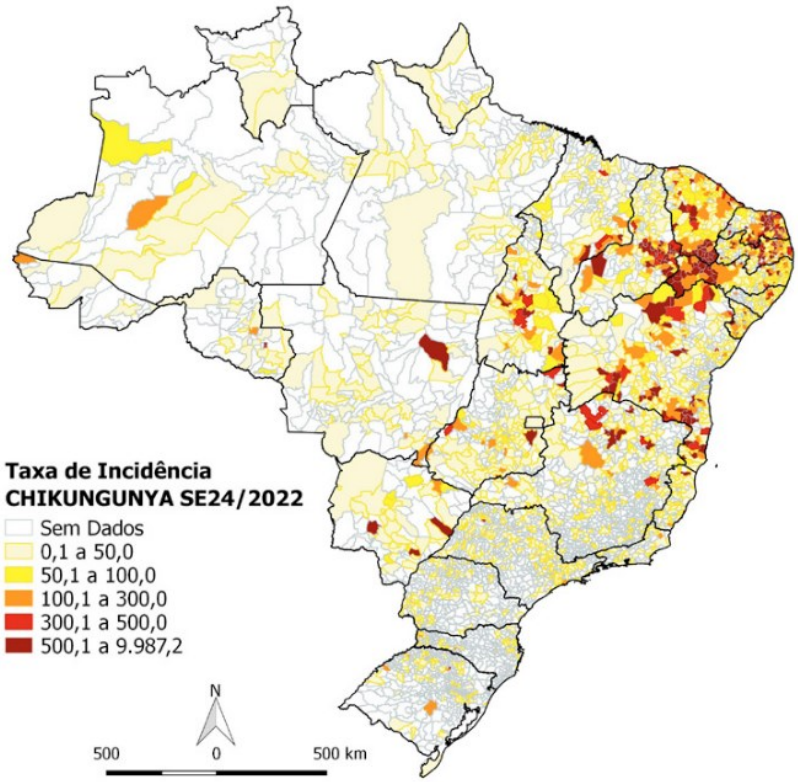

Disponível em https://www.gov.br/saude/pt-br/centrais-de-conteudo/publicacoes/boletins/boletins-epidemiologicos/edicoes/2022/boletim-epidemiologico-vol-53-no24/view. (Consultado em 30 de julho, 2022)

A transmissão do CHIKV se dá principalmente por meio da picada de mosquitos *Aedes aegypti* e *Aedes albopictus* (MAVALANKAR; SHASTRI; RAMAN, 2007).

Entretanto, outros vetores foram identificados como potenciais transmissores do vírus, como os mosquitos *Haemagogus sp.* pertencentes à família Culicidae (SCHWARTZ; ALBERT, 2010). Após a inoculação do vírus pela picada do mosquito, inicia-se o período de incubação, que dura em média entre 3 e 4 dias, seguido do início da fase aguda, com sintomas como febre alta (39 a 40 °C), inchaço nas articulações, dores intensas e manchas vermelhas com coceira (SILVA et al., 2018; THIBERVILLE et al., 2013). A fase subaguda ou convalescente inicia-se na segunda semana (aproximadamente 10 dias após os primeiros sintomas) e pode durar até 12 semanas. Neste período não há mais febre ou viremia, porém alguns sintomas como dores nas articulações podem reaparecer (BARR; VAIDHYANATHAN, 2019). A permanência de dor constante, principalmente nas articulações, marca o início da fase crônica, caracterizada por inflamações recorrentes nas articulações, e com maior intensidade, afetando a qualidade de vida dos indivíduos infectados (MICHLMAYR et al., 2018; SCHILTE et al., 2013).

1.2 Vírus da Chikungunya

O CHIKV pertence ao gênero *Alphavirus* e família *Togaviridae* (BURT et al., 2017), sendo subdivido em 3 principais genótipos: asiático, oeste da África e centro-leste da África do Sul (ECSA, *East/Central/South African*) (GANESAN; DUAN; REID, 2017).

A partícula viral possui um genoma de RNA de fita simples e polaridade positiva (RNAss+) de aproximadamente 12 kb, e um capsídeo proteico, envolto por um envelope lipídico inserido de glicoproteínas virais (CAGLIOTI et al., 2013) (Figura 3). O genoma do CHIKV possui duas regiões de leitura aberta (ORFs, *open reading frame*), sendo a primeira localizada na região 5', a qual promove a tradução de proteínas não estruturais (nsP) designadas como nsP1, nsP2, nsP3 e nsP4, e a segunda ORF, localizada após a sequência da proteína nsP4, é responsável pela expressão das proteínas estruturais C, E3, E2, 6k e E1 (CARISSIMO; NG, 2019) (**Figura 3**).

Figura 3. Partícula viral e genoma do vírus Chikungunya. Constituintes do vírion do CHIKV e regiões genômicas referentes às proteínas estruturais e não estruturais que conformam o genoma do CHIKV.

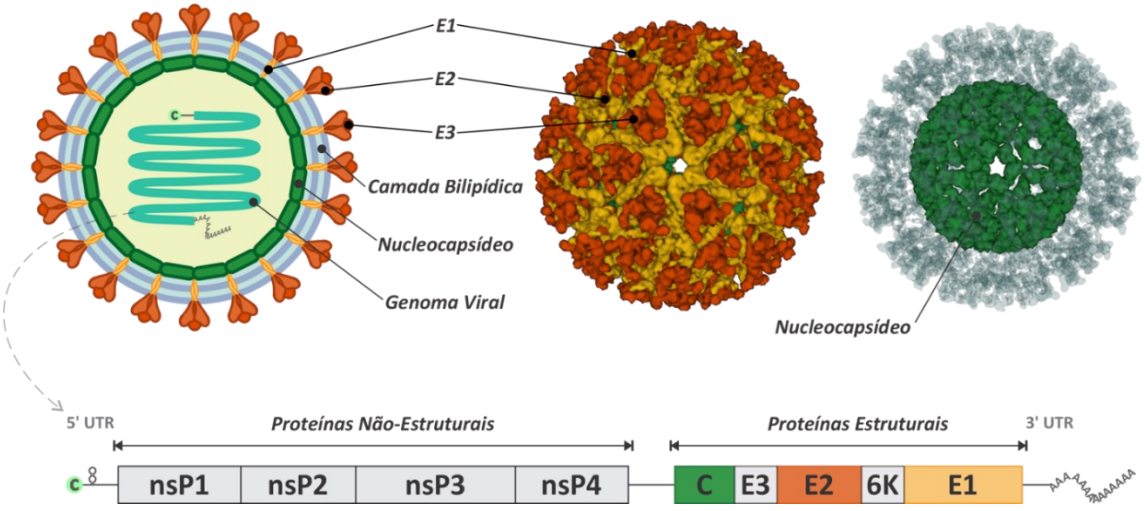

As nsP1-4 são essenciais para a replicação (GHILDIYAL; GABRANI, 2020), sendo responsáveis pela proteção do RNA, clivagem da poliproteína e funções necessárias para a replicação viral (HOORNWEG et al., 2016; MOIZÉIS et al., 2018). A proteína nsP1 possui 535 aminoácidos e está envolvida no encapsulamento do RNA, além de atuar na replicação com atividades de metiltransferase e guaniltransferase (SREEJITH et al., 2012). Diferentemente, a nsP2 possui 798 aminoácidos e atua como trifosfatase de nucleosídeo e trifosfatase de RNA (GHILDIYAL; GABRANI, 2020; RUPP et al., 2015). A nsP3 é essencial para a síntese de RNA devido à sua atividade replicase, e é dividida em três domínios: o macro-domínio na região N-terminal que se liga a polímeros carregados negativamente; o domínio único de alfavírus (AUD); e o domínio hiper variável na região C-terminal (HVR), o qual é responsável pela ligação às proteínas do hospedeiro (GAO et al., 2019; RATHORE et al., 2014; SREEJITH et al., 2012). Por fim, a nsP4 do CHIKV atua como RNA polimerase dependente de RNA (RdRp) (RATHORE et al., 2014) (Figura 3).

Considerando as proteínas codificadas a partir da ORF 3', a proteína viral E1 é encarregada de promover a fusão do envelope viral com a membrana do endossomo, e a E2 estabelece uma ligação entre a partícula viral e os receptores da célula hospedeira (processo de adsorção) (SOLIGNAT et al., 2009; WONG; CHU, 2018). Entretanto, não há atividade descrita para a proteína E3. A proteína 6k é uma proteína formadora de canais iônicos e

possui a função de viroporina (HOLMES et al., 2020), e a proteína C constitui o capsídeo viral, que envolve o RNA sintetizado (LEUNG; NG; CHU, 2011).

1.3 Ciclo replicativo do CHIKV

O ciclo replicativo do CHIKV tem início após a ligação da proteína E2 com os receptores das células hospedeiras, como as proteínas de ligação fosfatidilserina da família TIM (TIM-1 e 4) (JEMIELITY et al., 2013; KIRUI et al., 2021; MOLLER-TANK et al., 2013), glicosaminoglicanos (SOLIGNAT et al., 2009), Mxra8 e limitrina (ZHANG et al., 2018), desencadeando a endocitose dependente e independente de clatrina. Dentro do endossomo ocorre um processo de acidificação, que desencadeia o rearranjo conformacional das glicoproteínas e exposição da proteína E1, induzindo a fusão entre o envelope viral e a membrana endossômica, o que resulta na liberação do nucleocapsídeo e, consequentemente, do RNA no citosol (LEUNG; NG; CHU, 2011; SOLIGNAT et al., 2009). A ORF 5' do RNAss+ é traduzida nas poliproteínas P123 e P1234, as quais formam a nsP1, nsP2, nsP3 e nsP4 por processos de clivagem, e se associam para formar o complexo replicativo (CUNHA et al., 2020; RUPP et al., 2015). Posteriormente, a ORF 3' é transcrita em um RNA subgenômico (26S) de polaridade negativa, que serve como molde para produção de fitas de RNA 26S positivas complementares. O RNA 26S é traduzido em uma poliproteína precursora que dará origem às proteínas estruturais E1, E2, E3, 6K e C (JONSSON; GOODMAN; RASMUSSEN, 2019). O processo de tradução e clivagem da poliproteína acontece principalmente no retículo endoplasmático (ER), e as proteínas são empacotadas e enviadas ao Complexo de Golgi para o processamento pós-traducional (maturação e glicosilação), e sua posterior inserção na membrana da célula hospedeira (FIELDS; KNIPE; HOWLEY, 2007). Simultaneamente, as proteínas C se associam no citoplasma e interagem com o RNA genômico, formando novos nucleocapsídeos, os quais são liberados das células infectadas por brotamento (SOLIGNAT et al., 2009) (Figura 4).

Figura 4. Ciclo replicativo do CHIKV. Processos celulares e extracelulares envolvidos no ciclo de replicação do vírus CHIKV

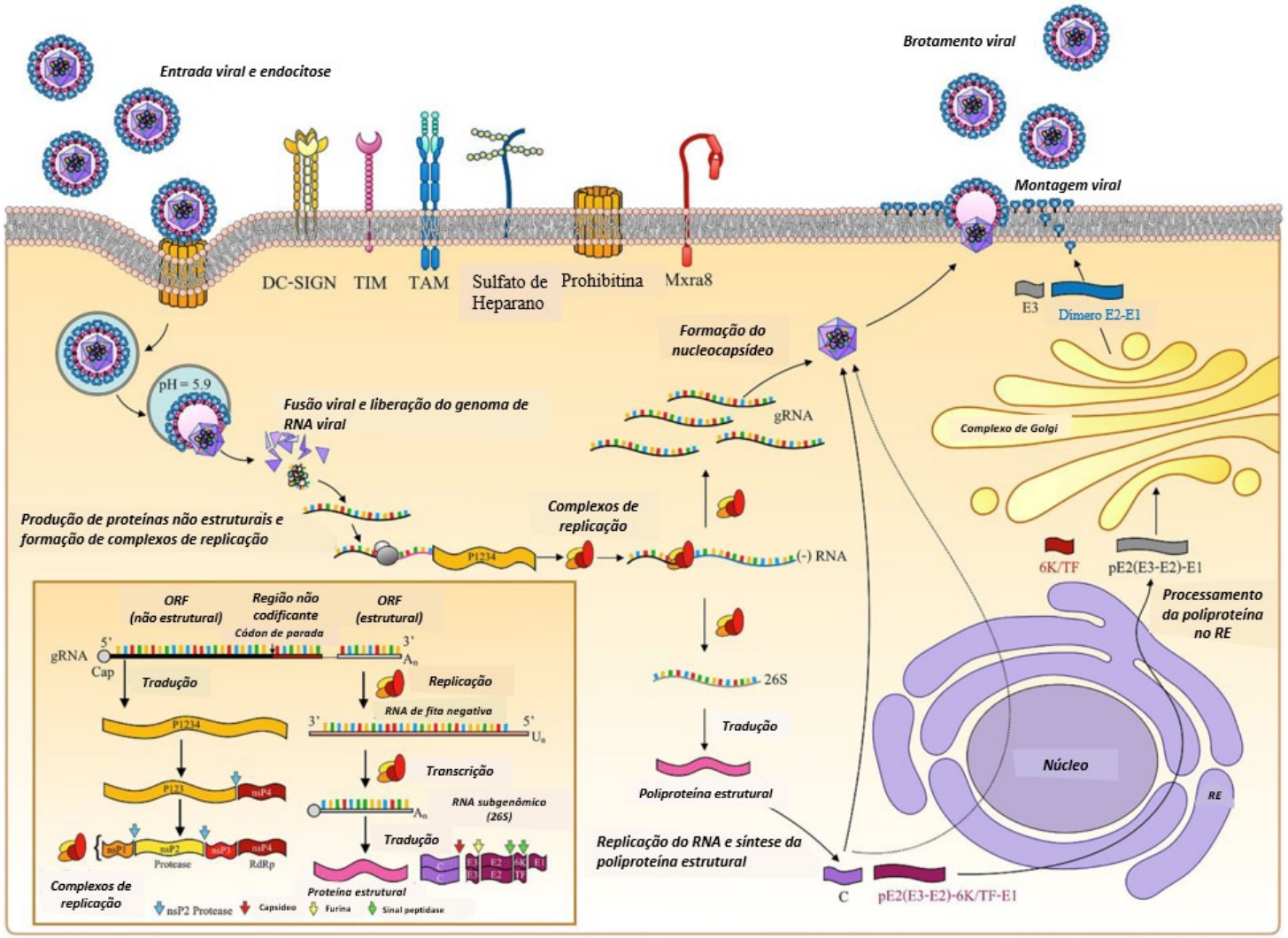

Adaptado de (WICHIT et al., 2021)

1.4 Tratamento da Febre Chikungunya e Compostos sintéticos contra o CHIKV

Atualmente, o tratamento de indivíduos infectados com o CHIKV é baseado no uso de anti-inflamatórios não-esteroides e analgésicos sistêmicos a fim de aliviar os sintomas da infecção (THARMARAJAH; MAHALINGAM; ZAID, 2017). Não existem vacinas e/ou medicamentos antivirais aprovados pelas agências reguladoras, como a Agência Nacional de Vigilância Sanitária (ANVISA) e a Administração de Alimentos e Medicamentos dos Estados Unidos da América (FDA, *Food and Drug Administration*) (SUBUDHI et al., 2018), o que dificulta o manejo dos pacientes infectados, impacta diretamente a qualidade de vida da população e acarreta problemas econômicos para países em desenvolvimento.

Neste contexto, os avanços nas pesquisas de antivirais contra o CHIKV sugerem potenciais alvos que reduzem a infecção viral, como as proteínas virais estruturais ou não-estruturais, bloqueadores da entrada e fusão do vírus com a célula, e alvos da célula hospedeira (BATTISTI; URBAN; LANGER, 2021). Estudos com fármacos como a suramina, aprovada para tratar a tripanossomíase, demonstraram que essa molécula é capaz de inibir os estágios iniciais da infecção pelo CHIKV (ALBULESCU et al., 2015), principalmente pela interação com os vírions, inibindo a ligação a receptores da célula hospedeira (ALBULESCU et al., 2020; HENSS et al., 2016). Estudos *in vivo* corroboraram o potencial da suramina como um potencial candidato para tratar a Febre Chinkunguya, reduzindo consideravelmente o inchaço e a inflamação nos camundongos testados (KUO et al., 2016). Além disso, um tratamento combinado com o composto natural galato de epigalocatequina demostrou um efeito sinérgico contra a infecção viral (LU et al., 2017).

A amantadina é um medicamento antiviral aprovado pela FDA para o tratamento de infecções pelo vírus da influenza, que demonstrou atividade na proteína estrutural 6K (viroporina) do CHIKV, alterando assim a formação de novos vírions (DEY et al., 2019). O cloridrato de rimantadina, fármaco também utilizado no tratamento da influenza A, demonstrou inibir efetivamente os estágios iniciais da infecção por CHIKV, interagindo com os vírions, e interrompendo assim a replicação viral (SANTOS et al., 2022).

Dentre os alvos virais mais promissores para o desenvolvimento de fármacos antivirais, a nsP4 do CHIKV é um alvo conservado entre os *alphavirus*, por possuir atividade de RNA polimerase dependente de RNA (RdRp) (PICARAZZI et al., 2020; RUPP et al.,

2015). O flavipiravir é uma molécula análoga de nucleosídeo que tem como alvo principal a nsP4 do CHIKV (ABDELNABI et al., 2017). Estudos *in vivo* avaliaram o potencial desse composto para tratar infecção aguda por CHIKV, diminuindo doenças neurológicas graves e a replicação nas articulações, e aumentando a taxa de sobrevida dos indivíduos infectados (JULANDER et al., 2020). Análogos do Sofosbuvir, outro análogo de nucleosídeo aprovado pelo FDA para tratar a infecção por HCV, apresentou atividade *in vitro* e *in vivo* contra a infecção por CHIKV, tendo como alvo a nsP4 (FERREIRA et al., 2019). Finalmente, Freire e colaboradores caracterizaram a estrutura da CHIKV-nsP4 e identificaram o LabMol-309 como um potente ligante da nsP4 do CHIKV, inibindo significativamente a replicação viral *in vitro* (FREIRE et al., 2022).

Adicionalmente, moléculas que potencializam ou estimulam mecanismos do hospedeiro também têm se mostrado eficazes na redução da infecção viral por CHIKV, como inibidores da sintase de ácidos graxos (HITAKARUN et al., 2020; WICHIT et al., 2017), inibidores de purinas e pirimidinas (MISHRA et al., 2016; RASHAD et al., 2018), inibidores de proteínas e receptores celulares (ABDELNABI et al., 2017; ASHBROOK et al., 2016; CRUZ et al., 2013; VARGHESE et al., 2016), e agentes imunorreguladores (ASHBROOK et al., 2016; CARISSIMO et al., 2019; LI et al., 2012).

1.5 Imidazonaftiridina como um potencial inibidor das infecções virais

As imidazonaftiridinas são moléculas com grande potencial para tratar infecções produzidas por vírus, como as infecções pelos vírus da família *Flaviviridae* (FERNANDES et al., 2021; KONISHI et al., 2012; WANG et al., 2015). Como exemplo, o RO8191 é uma imidazonaftiridina descrita previamente como um candidato promissor para o tratamento da infecção pelo HCV (EC_{50}=0.20μM) (KONISHI et al., 2012). O principal mecanismo de ação do RO8191 foi descrito como um agonista do interferon alfa (IFN-α), que se liga à subunidade 2 do receptor de interferon tipo 1 (IFNAR2), ativando a via JAK/STAT e desencadeando uma resposta imune intracelular para combater a infecção viral (KONISHI et al., 2012) (**Figura 5**). RO8191 é responsável por desencadear a fosforilação e ativação da proteína STAT, principalmente STAT1 e STAT2, e por consequência, a ativação da quinase JAK1, relacionada a subunidade IFNAR2. Como resultado, há a alteração da expressão

gênica para induzir a transcrição e tradução de genes ISG similares ao IFN-α que resultam na atividade antiviral intracelular (KONISHI et al., 2012).

Figura 5. Mecanismo de ação do RO8191. Comparação entre as vias de sinalização ativadas por RO8191 e IFN-α

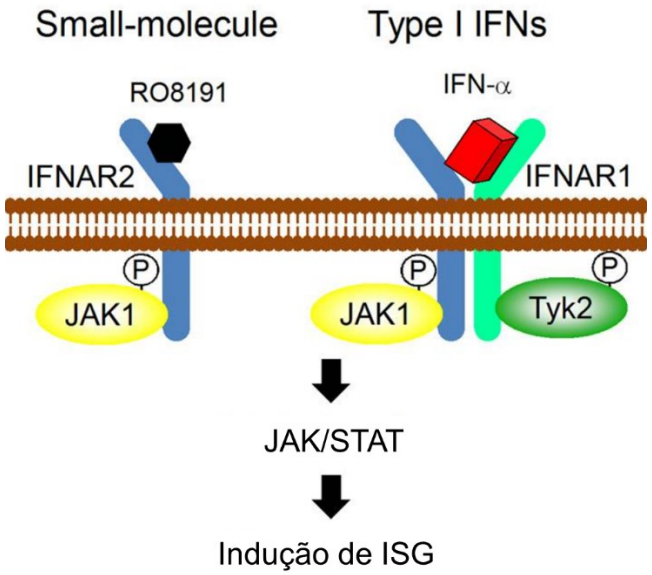

Adaptado de (KONISHI et al., 2012)

A atividade de agonista de IFN-α foi observada como mecanismo de ação antiviral das imidazonaftiridinas, e em alguns casos resultou na potencialização da atividade de compostos análogos sintetizados a partir do RO8191. O CDM-3008, um análogo de RO8191, demonstrou atividade contra o vírus da Hepatite B (HBV) mediante a ativação de ISGs, bem como a dependência ao receptor IFNAR2 em hepatócitos humanos (TAKAHASHI et al., 2019). Adicionalmente, o potencial desta molécula foi ainda mais evidenciado em estudos em que os análogos do RO8191 inibiram a infecção do HCV em concentrações dez vezes menores (EC_{50}=0.017μM), e mediante um mecanismo distinto do previamente descrito, interferindo com a entrada do vírus na célula (WANG et al., 2015).

O efeito antiviral do RO8191 também foi avaliado em células expressando o *replicon* subgenômico do ZIKV, e resultou em um EC_{50} de 0.042 μM (FERNANDES et al., 2021), além de mostrar permeabilidade hematoencefálica e proteger camundongos infectados com príones, propondo este composto como um potencial inibidor da replicação de um dos arbovírus com maior interesse clínico na última década (ISHIBASHI et al., 2019).

De forma mais interessante, o RO8191 é uma molécula pequena (**Figura 6**), que demostra potencial para ser administrada oralmente e oferece vantagens como tratamento eficaz, barato e com efeitos secundários aparentemente reduzidos para o tratamento de distintas infecções virais (KONISHI et al., 2012; TAKAHASHI et al., 2019). Nesse contexto, se torna um composto candidato a ser avaliado contra o CHIKV.

Figura 6. Estrutura do RO8191. Estrutura química da Imidazonaftiridina RO8191

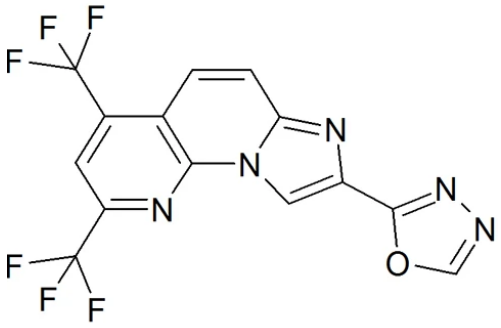

Adaptado de (KONISHI et al., 2012)

2. OBJETIVOS

2.1 Objetivo geral

Avaliar a atividade antiviral da Imidazonaftiridina RO8191 no ciclo replicativo do CHIKV *in vitro*.

2.2 Objetivos específicos

- Avaliar o efeito antiviral da Imidazonaftiridina RO8191 nas células infectadas com o CHIKV;
- Determinar a concentração efetiva de 50% (EC_{50}), concentração citotóxica em 50% (CC_{50}) e índice de seletividade ($IS=CC_{50}/EC_{50}$) em células infectadas por CHIKV e tratadas com RO8191;
- Avaliar a associação de interferon I (IFN-I) na atividade antiviral de RO8191;
- Avaliar a atividade do composto em diferentes etapas do ciclo replicativo do CHIKV, utilizando diferentes tempos de adição do composto;
- Investigar o modo de ação do RO8191 no ciclo do CHIKV, por meio de técnicas de ancoragem molecular (*docking* molecular), espectrofotometria no infravermelha (ATR-FTIR), interação biofísica com a proteína nsP4, e pelo uso de células com *replicon* subgenômico do CHIKV.

3 REFERÊNCIAS

ABDELNABI, R. et al. Protein kinases C as potential host targets for the inhibition of chikungunya virus replication. **Antiviral Research**, v. 139, p. 79–87, 1 mar. 2017. https://doi.org/10.1016/j.antiviral.2016.12.020

ABDELNABI, R. et al. Understanding the Mechanism of the Broad-Spectrum Antiviral Activity of Favipiravir (T-705): Key Role of the F1 Motif of the Viral Polymerase. **Journal of Virology**, v. 91, n. 12, 15 jun. 2017. https://doi.org/10.1128/JVI.00487-17

ACOSTA-REYES, J.; NAVARRO-LECHUGA, E.; MARTÍNEZ-GARCÉS, J. C. Chikungunya fever: history and epidemiology. **Salud Uninorte**, v. 31, n. 3, p. 621–630, 1 jun. 2015. https://doi.org/10.14482/sun.31.3.7486

ALBULESCU, I. C. et al. Suramin inhibits chikungunya virus replication through multiple mechanisms. **Antiviral Research**, v. 121, p. 39–46, 1 set. 2015. https://doi.org/10.1016/j.antiviral.2015.06.013

ALBULESCU, I. C. et al. Suramin Inhibits Chikungunya Virus Replication by Interacting with Virions and Blocking the Early Steps of Infection. **Viruses**, v. 12, n. 3, p. 314, 17 mar. 2020. https://doi.org/10.3390/v12030314

ASHBROOK, A. W. et al. Antagonism of the Sodium-Potassium ATPase Impairs Chikungunya Virus Infection. **mBio**, v. 7, n. 3, 6 jul. 2016. https://doi.org/10.1128/mBio.00693-16

BARR, K.; VAIDHYANATHAN, V. Chikungunya in Infants and Children: Is Pathogenesis Increasing? **Viruses**, v. 11, n. 3, p. 294, 23 mar. 2019. https://doi.org/10.3390/v11030294

BATTISTI, V.; URBAN, E.; LANGER, T. Antivirals against the Chikungunya Virus. **Viruses**, v. 13, n. 7, p. 1307, 5 jul. 2021. https://doi.org/10.3390/v13071307

BETTIS, A. A. et al. The global epidemiology of chikungunya from 1999 to 2020: A systematic literature review to inform the development and introduction of vaccines. **PLOS Neglected Tropical Diseases**, v. 16, n. 1, p. e0010069, 12 jan. 2022. https://doi.org/10.1371/journal.pntd.0010069

BURT, F. J. et al. Chikungunya virus: an update on the biology and pathogenesis of this emerging pathogen. **The Lancet Infectious Diseases**, v. 17, n. 4, p. e107–e117, 1 abr. 2017. https://doi.org/10.1016/S1473-3099(16)30385-1

CAGLIOTI, C. et al. Chikungunya virus infection: an overview. **NEW MICROBIOLOGICA**, v. 36, p. 211–227, 2013. https://pubmed.ncbi.nlm.nih.gov/23912863/

CARISSIMO, G. et al. *Viperin* controls chikungunya virus–specific pathogenic T cell IFNγ Th1 stimulation in mice. **Life Science Alliance**, v. 2, n. 1, p. e201900298, 21 fev. 2019. https://doi.org/10.26508/lsa.201900298

CARISSIMO, G.; NG, L. F. P. Understanding Molecular Pathogenesis with Chikungunya Virus Research Tools. In: **Current Topics in Microbiology and Immunology**. [s.l: s.n.]. https://doi.org/10.1007/82_2019_158

CRUZ, D. J. M. et al. Identification of Novel Compounds Inhibiting Chikungunya Virus-Induced Cell Death by High Throughput Screening of a Kinase Inhibitor Library. **PLoS Neglected Tropical Diseases**, v. 7, n. 10, p. e2471, 31 out. 2013. https://doi.org/10.1371/journal.pntd.0002471

CUNHA, M. S. et al. Chikungunya Virus: An Emergent Arbovirus to the South American Continent and a Continuous Threat to the World. **Frontiers in Microbiology**, v. 11, 26 jun. 2020. https://doi.org/10.1371/journal.pntd.0002471

DEY, D. et al. The effect of amantadine on an ion channel protein from Chikungunya virus. **PLOS Neglected Tropical Diseases**, v. 13, n. 7, p. e0007548, 24 jul. 2019. https://doi.org/10.1371/journal.pntd.0007548

FERNANDES, R. S. et al. Discovery of an imidazonaphthyridine and a riminophenazine as potent anti-Zika virus agents through a replicon-based high-throughput screening. **Virus Research**, v. 299, p. 198388, 2 jul. 2021. https://doi.org/10.1016/j.virusres.2021.198388

FERREIRA, A. C. et al. Beyond Members of the Flaviviridae Family, Sofosbuvir Also Inhibits Chikungunya Virus Replication. **Antimicrobial Agents and Chemotherapy**, v. 63, n. 2, fev. 2019. https://doi.org/10.1128/AAC.01389-18

FIELDS, B. N.; KNIPE, D. M. (DAVID M.; HOWLEY, P. M. **Fields virology**. 5th ed. ed. Philadelphia: Wolters Kluwer Health/Lippincott Williams & Wilkins, 2007. pp. 1023. https://www.worldcat.org/title/fields-virology/oclc/71812790#.YtSPxOn0z9E.mendeley

FREIRE, M. C. L. C. et al. Characterization of the RNA-dependent RNA polymerase from Chikungunya virus and discovery of a novel ligand as a potential drug candidate. **Scientific Reports**, v. 12, n. 1, p. 10601, 22 dez. 2022. https://doi.org/10.21203/rs.3.rs-1280888/v1

GANESAN, V.; DUAN, B.; REID, S. Chikungunya Virus: Pathophysiology, Mechanism, and Modeling. **Viruses**, v. 9, n. 12, p. 368, 1 dez. 2017. https://doi.org/10.3390/v9120368

GAO, Y. et al. Multiple roles of the non-structural protein 3 (nsP3) alphavirus unique domain (AUD) during Chikungunya virus genome replication and transcription. **PLOS Pathogens**, v. 15, n. 1, p. e1007239, 22 jan. 2019. https://doi.org/10.1371/journal.ppat.1007239

GHILDIYAL, R.; GABRANI, R. Antiviral therapeutics for chikungunya virus. **Expert Opinion on Therapeutic Patents**, v. 30, n. 6, p. 467–480, 2 jun. 2020. https://doi.org/10.1080/13543776.2020.1751817

HENSS, L. et al. Suramin is a potent inhibitor of Chikungunya and Ebola virus cell entry. **Virology Journal**, v. 13, n. 1, p. 149, 31 dez. 2016. https://doi.org/10.1186/s12985-016-0607-2

HITAKARUN, A. et al. Evaluation of the antiviral activity of orlistat (tetrahydrolipstatin) against dengue virus, Japanese encephalitis virus, Zika virus and chikungunya virus. **Scientific Reports**, v. 10, n. 1, p. 1499, 30 dez. 2020. https://doi.org/10.1038/s41598-020-58468-8

HOLMES, A. C. et al. A molecular understanding of alphavirus entry. **PLOS Pathogens**, v. 16, n. 10, p. e1008876, 22 out. 2020. https://doi.org/10.1371/journal.ppat.1008876

HOORNWEG, T. E. et al. Dynamics of Chikungunya Virus Cell Entry Unraveled by Single-Virus Tracking in Living Cells. **Journal of Virology**, v. 90, n. 9, p. 4745–4756, maio 2016. https://doi.org/10.1128/JVI.03184-15

ISHIBASHI, D. et al. Type I interferon protects neurons from prions in in vivo models. **Brain**, v. 142, n. 4, p. 1035–1050, 1 abr. 2019. https://doi.org/10.1093/brain/awz016

JEMIELITY, S. et al. TIM-family Proteins Promote Infection of Multiple Enveloped Viruses through Virion-associated Phosphatidylserine. **PLoS Pathogens**, v. 9, n. 3, p. e1003232, 28 mar. 2013. https://doi.org/10.1371/journal.ppat.1003232

JONSSON, C. B.; GOODMAN, A. G.; RASMUSSEN, A. L. Editorial: Host-Pathogen Interactions During Arboviral Infections. **Frontiers in Cellular and Infection Microbiology | www.frontiersin.org**, v. 1, p. 77, 2019. https://doi.org/10.3389/fcimb.2019.00077

JULANDER, J. G. et al. Strain-dependent disease and response to favipiravir treatment in mice infected with Chikungunya virus. **Antiviral Research**, v. 182, p. 104904, 1 out. 2020. https://doi.org/10.1016/j.antiviral.2020.104904

KIRUI, J. et al. The Phosphatidylserine Receptor TIM-1 Enhances Authentic Chikungunya Virus Cell Entry. **Cells**, v. 10, n. 7, p. 1828, 20 jul. 2021. https://doi.org/10.3390/cells10071828

KONISHI, H. et al. An orally available, small-molecule interferon inhibits viral replication. **Scientific Reports**, v. 2, n. 1, p. 259, 10 dez. 2012. https://doi.org/10.1038/srep00259

KUO, S. C. et al. Suramin treatment reduces chikungunya pathogenesis in mice. **Antiviral Research**, v. 134, p. 89–96, 1 out. 2016. https://doi.org/10.1016/j.antiviral.2016.07.025

LEUNG, J. Y.-S.; NG, M. M.-L.; CHU, J. J. H. Replication of Alphaviruses: A Review on the Entry Process of Alphaviruses into Cells. **Advances in Virology**, v. 2011, p. 1–9, 2011. https://doi.org/10.1155/2011/249640

LI, Y.-G. et al. Poly (I:C), an agonist of toll-like receptor-3, inhibits replication of the Chikungunya virus in BEAS-2B cells. **Virology Journal**, v. 9, n. 1, p. 114, 14 dez. 2012. https://doi.org/10.1186/1743-422X-9-114

LU, J. W. et al. Synergistic effects of combination treatment using EGCG and suramin against the chikungunya virus. **Biochemical and Biophysical Research Communications**, v. 491, n. 3, p. 595–602, 23 set. 2017. https://doi.org/10.1016/j.bbrc.2017.07.157

MAVALANKAR, D.; SHASTRI, P.; RAMAN, P. Chikungunya epidemic in India: a major public-health disaster. **The Lancet Infectious Diseases**, v. 7, n. 5, p. 306–307, maio 2007. https://doi.org/10.1016/S1473-3099(07)70091-9

MICHLMAYR, D. et al. Comprehensive innate immune profiling of chikungunya virus infection in pediatric cases. **Molecular Systems Biology**, v. 14, n. 8, p. 7862, 27 ago. 2018. https://doi.org/10.15252/msb.20177862

MISHRA, P. et al. Inhibition of Chikungunya Virus Replication by 1-[(2-Methylbenzimidazol-1-yl) Methyl]-2-Oxo-Indolin-3-ylidene] Amino] Thiourea(MBZM-N-IBT). **Scientific Reports**, v. 6, n. 1, p. 20122, 4 abr. 2016. https://doi.org/10.1038/srep20122

MOIZÉIS, R. N. C. et al. Chikungunya fever: a threat to global public health. **Pathogens and Global Health**, v. 112, n. 4, p. 182–194, 19 maio 2018. https://doi.org/10.1080/20477724.2018.1478777

MOLLER-TANK, S. et al. Role of the Phosphatidylserine Receptor TIM-1 in Enveloped-Virus Entry. **Journal of Virology**, v. 87, n. 15, p. 8327–8341, ago. 2013. https://doi.org/10.1128/JVI.01025-13

MORENS, D. M.; FAUCI, A. S. Chikungunya at the Door — Déjà Vu All Over Again? **New England Journal of Medicine**, v. 371, n. 10, p. 885–887, 4 set. 2014. https://doi.org/10.1056/NEJMp1408509

PICARAZZI, F. et al. Targeting the RdRp of Emerging RNA Viruses: The Structure-Based Drug Design Challenge. **Molecules**, v. 25, n. 23, p. 5695, 3 dez. 2020. https://doi.org/10.3390/molecules25235695

RASHAD, A. A. et al. A reassessment of mycophenolic acid as a lead compound for the development of inhibitors of chikungunya virus replication. **Tetrahedron**, v. 74, n. 12, p. 1294–1306, 22 mar. 2018. https://doi.org/10.1016/j.tet.2017.12.053

RATHORE, A. P. S. et al. Chikungunya virus nsP3 & nsP4 interacts with HSP-90 to promote virus replication: HSP-90 inhibitors reduce CHIKV infection and inflammation in vivo. **Antiviral Research**, v. 103, n. 1, p. 7–16, 1 mar. 2014. https://doi.org/10.1016/j.antiviral.2013.12.010

RUPP, J. C. et al. Alphavirus RNA synthesis and non-structural protein functions. **Journal of General Virology**, v. 96, n. 9, p. 2483–2500, 1 set. 2015. https://doi.org/10.1099/jgv.0.000249

SANTOS, I. A. et al. Repurposing potential of rimantadine hydrochloride and development of a promising platinum(II)-rimantadine metallodrug for the treatment of Chikungunya virus infection. **Acta Tropica**, v. 227, p. 106300, 1 mar. 2022. https://doi.org/10.1016/j.actatropica.2021.106300

SCHILTE, C. et al. Correction: Chikungunya Virus-associated Long-term Arthralgia: A 36-month Prospective Longitudinal Study. **PLoS Neglected Tropical Diseases**, v. 7, n. 3, p. null, 22 mar. 2013. https://doi.org/10.1371/annotation/850ee20f-2641-46ac-b0c6-ef4ae79b6de6

SCHWARTZ, O.; ALBERT, M. L. Biology and pathogenesis of chikungunya virus. **Nature Reviews Microbiology**, v. 8, n. 7, p. 491–500, jul. 2010. https://doi.org/10.1038/nrmicro2368

SILVA, N. M. DA et al. Chikungunya surveillance in Brazil: challenges in the context of Public Health. **Epidemiology and health services: Journal of the Sistema Unico de Saude do Brasil**, v. 27, n. 3, p. e2017127, 3 set. 2018. https://doi.org/10.5123/s1679-49742018000300003

SOLIGNAT, M. et al. Replication cycle of chikungunya: A re-emerging arbovirus. **Virology**, v. 393, n. 2, p. 183–197, 25 out. 2009. https://doi.org/10.1016/j.virol.2009.07.024

SREEJITH, R. et al. Mapping interactions of Chikungunya virus nonstructural proteins. **Virus Research**, v. 169, n. 1, p. 231–236, 1 out. 2012. https://doi.org/10.1016/j.virusres.2012.08.006

STAIKOWSKY, F. et al. Prospective Study of Chikungunya Virus Acute Infection in the Island of La Réunion during the 2005–2006 Outbreak. **PLoS ONE**, v. 4, n. 10, p. e7603, 28 out. 2009. https://doi.org/10.1371/journal.pone.0007603

SUBUDHI, B. et al. Current Strategies for Inhibition of Chikungunya Infection. **Viruses**, v. 10, n. 5, p. 235, 3 maio 2018. https://doi.org/10.3390/v10050235

TAKAHASHI, N. et al. Development of an anti-hepatitis B virus (HBV) agent through the structure-activity relationship of the interferon-like small compound CDM-3008. **Bioorganic & Medicinal Chemistry**, v. 27, n. 3, p. 470–478, 1 fev. 2019. https://doi.org/10.1016/j.bmc.2018.11.039

THARMARAJAH, K.; MAHALINGAM, S.; ZAID, A. Chikungunya: vaccines and therapeutics. **F1000Research**, v. 6, p. 2114, 8 dez. 2017. https://doi.org/10.12688/f1000research.12461.1

THIBERVILLE, S. D. et al. Chikungunya fever: Epidemiology, clinical syndrome, pathogenesis and therapy. **Antiviral Research**, v. 99, n. 3, p. 345–370, 1 set. 2013. https://doi.org/10.1016/j.antiviral.2013.06.009

VARGHESE, F. S. et al. The Antiviral Alkaloid Berberine Reduces Chikungunya Virus-Induced Mitogen-Activated Protein Kinase Signaling. **Journal of Virology**, v. 90, n. 21, p. 9743–9757, nov. 2016. https://doi.org/10.1128/JVI.01382-16

WANG, H. et al. Discovery of Imidazo[1,2-α][1,8]naphthyridine Derivatives as Potential HCV Entry Inhibitor. **ACS Medicinal Chemistry Letters**, v. 6, n. 9, p. 977–981, 10 set. 2015. https://doi.org/10.1021/acsmedchemlett.5b00159

WEAVER, S. C.; FORRESTER, N. L. Chikungunya: Evolutionary history and recent epidemic spread. **Antiviral Research**, v. 120, p. 32–39, 1 ago. 2015. https://doi.org/10.1016/j.antiviral.2015.04.016

WICHIT, S. et al. Imipramine Inhibits Chikungunya Virus Replication in Human Skin Fibroblasts through Interference with Intracellular Cholesterol Trafficking. **Scientific Reports**, v. 7, n. 1, p. 3145, 9 dez. 2017. https://doi.org/10.1038/s41598-017-03316-5

WICHIT, S. et al. Chikungunya and Zika Viruses: Co-Circulation and the Interplay between Viral Proteins and Host Factors. **Pathogens**, v. 10, n. 4, p. 448, 9 abr. 2021. https://doi.org/10.3390/pathogens10040448

WONG, K. Z.; CHU, J. J. H. The Interplay of Viral and Host Factors in Chikungunya Virus Infection: Targets for Antiviral Strategies. **Viruses**, v. 10, n. 6, p. 294, 30 maio 2018. https://doi.org/10.3390/v10060294

ZHANG, R. et al. Mxra8 is a receptor for multiple arthritogenic alphaviruses. **Nature**, v. 557, n. 7706, p. 570–574, 16 maio 2018. https://doi.org/10.1038/s41586-018-0121-3

CAPÍTULO II

ARTIGO CIENTÍFICO:

IMIDAZONAPHTHYRIDINE EFFECTS ON CHIKUNGUNYA VIRUS INFECTION: ANTIVIRAL ACTIVITY BY INDEPENDENT OF INTERFERON TYPE 1 PATHWAYS

*****Este capítulo está em formato de manuscrito com algumas alterações estruturais para melhor se adequar ao formato da dissertação. O artigo em questão foi submetido à revista ***Antiviral Research.***

IMIDAZONAPHTHYRIDINE EFFECTS ON CHIKUNGUNYA VIRUS INFECTION: ANTIVIRAL ACTIVITY BY INDEPENDENT OF INTERFERON TYPE 1 PATHWAY

Uriel Enrique Aquino Ruiz[1], Igor Andrade Santos[1], Victória Riquena Grosche[1,4], Rafaela Sachetto Fernandes[2], Andre Schutzer de Godoy[2], Marjorie Caroline Liberato Cavalcanti Freire[2], Nathalya Cristina de Moraes Roso Mesquita[2], Marco Guevara-Vega[1], Nilson Nicolau-Junior[3], Robinson Sabino-Silva[1], Glaucius Oliva[2], Ana Carolina Gomes Jardim[1,4]

[1]Institute of Biomedical Science, Federal University of Uberlândia (UFU), Uberlândia, MG, Brazil.

[2]Sao Carlos Institute of Physics, University of Sao Paulo (USP), São Carlos, SP, Brazil

[3]Institute of Biotechnology, Federal University of Uberlândia (UFU), Uberlândia, MG, Brazil.

[4]Institute of Biosciences, Humanities and Exact Sciences, São Paulo State University (UNESP), Campus São José do Rio Preto, SP, Brazil.

ABSTRACT

The Chikungunya virus (CHIKV) causes Chikungunya fever, a disease characterized by symptoms such as arthralgia/polyarthralgia. Currently, there are no antiviral approved against CHIKV, emphasizing the need to develop novel therapies. The imidazonaphthyridine compound (RO8191), an interferon-α (IFN-α) agonist, was reported as a potent inhibitor of HCV. Here RO8191 was investigated for its potential to inhibit CHIKV replication *in vitro*. RO8191 inhibited CHIKV infection in BHK-21 and Vero-E6 cells with a selectivity index (SI) of 12.3 and 35.2, respectively. Additionally, RO8191 was capable to protect cells against CHIKV infection, inhibiting entry by virucidal activity, and strongly impairing post-entry steps of viral replication. An effect of RO8191 on CHIKV replication was demonstrated in Vero-E6 IFN-I knockout cells, suggesting an IFN-I independent mode of action. Molecular docking calculations demonstrated interactions of RO8191 with the CHIKV E proteins, corroborated by the ATR-FTIR assay, and with non-structural proteins, supported by the CHIKV-subgenomic replicon cells assay.

Keywords: Imidazonaphthyridine; Antiviral activity; Chikungunya virus; Chikungunya Fever; Neglected tropical diseases; IFN-I independent activity

1. INTRODUCTION

Chikungunya fever is a viral disease with an acute phase characterized by *dengue-like* symptoms, such as high fever, nausea, severe arthralgia and polyarthralgia, and rashes, which can appear up to 12 weeks after the onset of viral infection (Kril et al., 2021; Silva et al., 2018; Thiberville et al., 2013). Aggravatingly, most CHIKV-infected patients develop chronic conditions of arthralgia and polyarthralgia, which persist for months to years, affecting the quality of life of infected people (Bedoui et al., 2021; Hibl et al., 2021; Kril et al., 2021; Schilte et al., 2013).

The Chikungunya virus (CHIKV) is the causative agent of Chikungunya fever, belonging to the *Alphavirus* genus within the *Togaviridae* family (Burt et al., 2017; Silva and Dermody, 2017). The viral particle consists of a positive single-stranded RNA genome (ssRNA+) of approximately 12 kb, protected by a protein capsid shell and a lipid envelope inserted with glycoproteins (Caglioti et al., 2013). The transmission of CHIKV occurs mainly through the bite of *Aedes spp.* Mosquitoes (Burt et al., 2017; Coffey et al., 2014), and since its first identification in Tanzania, East Africa, in 1952 (Schwartz and Albert, 2010), it has spread throughout the world, mainly affecting tropical and subtropical regions, such as the Americas (Pan American Health Organization, 2013).

Until December 2021, 131,630 cases of CHIKV fever were reported only in the Americas, of which about 127,487 cases and 11 deaths were confirmed in Brazil (Pan American Health Organization, 2021). Despite that, there are no approved vaccines or antiviral drugs by the Brazilian National Health Surveillance Agency (ANVISA) or the Food and Drug Administration of the United States of America (FDA) to manage Chikungunya fever (Subudhi et al., 2018). Therefore, the treatment of CHIKV infection is palliative, relying on non-steroidal anti-inflammatory and analgesics drugs, emphasizing the demand for antiviral development to treat this infection (Battisti et al., 2021; Tharmarajah et al., 2017).

The Pandemic Response Box (PRB), proposed by the Medicines for Malaria Venture (MMV) and the Drugs for Neglected Diseases initiative (DNDi), was designed with compounds that are highly active against malaria disease, and possess the potential to present biologic activities against other pathogens, being potentially applied in future outbreaks (Medicines for Malaria Venture and Drugs for Neglected Diseases initiative, n.d.; van Voorhis et al.,

2016). Within the PRB, the imidazonaphthyridine (RO4948191 or RO8191) is a potent orally active interferon (IFN) agonist, binding directly to the IFNα/β receptor 2 (IFNAR2), triggering the JAK/STAT pathway, and consequently resulting in the activation and expression of IFN genes (Hwang et al., 2019; Konishi et al., 2012; Kota et al., 2018; Ying et al., 2021; Zeng et al., 2020). RO8191 was previously described as an inhibitor of Hepacivirus C (HCV) (Huang et al., 2014; Konishi et al., 2012; Wang et al., 2015), Hepatitis B virus (HBV) (Furutani et al., 2019; Takahashi et al., 2019), and Zika virus (ZIKV) (Fernandes et al., 2021) infections, and recently, as an enhancer compound in antiviral treatments against CHIKV (Hwang et al., 2019). However, to the best of our knowledge, there is no description of RO8191 as an anti-CHIKV-specific inhibitor, as well as insights into its mechanism of action. Therefore, herein, RO8191 was evaluated as a potential inhibitor of CHIKV replication *in vitro* by the evaluation of its activity on several steps of the CHIKV replicative cycle in wild-type (BHK-21) and knockout for type 1 interferon gene locus (Vero-E6) (Emeny and Morgan, 1979; Prescott et al., 2010) cells, associated to bioinformatics and infrared spectroscopy analyzes that revealed the possible interactions between the RO8191 and CHIKV proteins.

2. METHODS

2.1 Cells, Virus and compound

Vero-E6 (isolated from the kidney of an African green monkey; ATCC CRL-1587) and BHK-21 cells (fibroblasts derived from Syrian golden hamster kidney; ATCC CCL-10) were maintained as previously described (Santos et al., 2021). Briefly, cells were maintained in Dulbecco's modified Eagle's medium (DMEM, SIGMA-ALDRICH), supplemented with 100U/mL of penicillin (HYCLONE LABORATORIES), 100 mg/mL of streptomycin (HYCLONE LABORATORIES), 1% dilution of stock of non-essential amino acids (Hyclone Laboratories) and 1% of fetal bovine serum (FBS, HYCLONEN LABORATOIRES) in a humidified 5% CO_2 incubator at 37 °C. Subgenomic replicon (SGR) harboring cells (BHK-CHIKV-NCT) (Pohjala et al., 2011) were maintained under the same conditions of BHK-21 cells (ATCC CCL-10), except for the addition of G418 (SIGMA-ALDRICH) at 5 mg/mL.

The CHIKV expressing *nanoluciferase* reporter (CHIKV-*nanoluc*) **(Fig. 1A)** used for the antiviral assays is based on the CHIKV isolate LR2006OPY1 (East/Central/South African genotype) and was produced, rescued, and titrated as previous described (Oliveira et al., 2020; Santos et al., 2021).

The imidazonaphthyridine compound (RO4948191 or RO8191) **(Fig. 1B)** was selected from PRB compounds (purity of > 90%) and was dissolved in 100% DMSO (v/v) to the concentration of 5 mM. The compound was diluted in the medium immediately before the assays (Fernandes et al., 2021).

2.2 Cell viability assay

Cell viability assays were performed as previously described (Oliveira et al., 2020; Santos et al., 2021), employing MTT [3-(4,5-dimethylthiazol-2-yl)-2,5-diphenyl tetrazolium bromide] (Sigma-Aldrich®) method. Briefly, BHK-21 and Vero-E6 cells were plated into 48-well plates at a density of 5 x 10^4 cells per well and incubated overnight at 37 °C and 5% CO_2. Medium containing serial dilutions of RO8191 ranging from 60 µM to 0.46 µM was added to cells and incubated for 16 h. After this, the medium was replaced by MTT solution at 1 mg/ml, and cells were incubated for 30 minutes, after which the MTT solution was removed and replaced by 300 µL of DMSO (dimethyl sulfoxide) to solubilize the formazan crystals. The absorbance was measured at 490 nm on the Glomax microplate reader (Promega®). Cell viability was calculated according to the equation (T/C) × 100%, where T and C represent the mean optical density of the treated and untreated control groups, respectively. The cytotoxic concentration of 50% (CC_{50}) was calculated using GraphPad Prism 8.

2.3 Antiviral assays

To assess the antiviral activity of RO8191, BHK-21 and Vero-E6 cells were seeded at a density of 5 x 10^4 cells per well into 48-well plates 24 h prior the assays. Cells were infected with CHIKV-*nanoluc* at a multiplicity of infection (MOI) of 0.1 in the presence of the compound in two-fold serial dilutions ranging from 60 µM to 0.46 µM for BHK-21 cells and three-fold serial dilutions from 60 µM to 0.02 µM for Vero-E6 cells (Oliveira et al., 2020; Santos et al., 2021). Samples were harvested using *Renilla* luciferase lysis buffer (Promega®) at 16 h post-infection (h.p.i.), and virus replication levels were quantified by measuring

nanoluciferase activity using the *Renilla* luciferase Assay System (Promega®). The effective concentration of 50% inhibition (EC_{50}) was calculated using GraphPad Prism 8 software. The values of CC_{50} and EC_{50} were used to calculate the selectivity index ($SI = CC_{50}/ EC_{50}$) (Oliveira et al., 2020; Santos et al., 2021).

2.4 Time of drug-addition assay

For the time-of-drug addition assays, BHK-21 and Vero-E6 cells were seeded at a density of 5×10^4 cells per well into 48 well plates overnight, and infected with CHIKV-*nanonluc* at a MOI of 0.1. The samples were harvested using *Renilla* luciferase lysis buffer (Promega®) 16 h after infection, and virus replication levels were quantified by measuring *nanoluciferase* activity using the *Renilla* luciferase Assay System (Promega®).

In the pre-treatment assay, cells were treated for 1 h at 37 °C with RO8191, washed with PBS for compound removal, and then infected with the virus for 1 h at 37 °C. Then, cells were washed again to remove the unbound virus and replaced with fresh medium for 16 h. For virus entry assays, cells were infected using medium containing RO8191 and virus for 1 h at 37 °C, extensively washed with PBS, and incubated with a fresh medium for 16 h. The virucidal activity was performed using the same protocol of virus entry assay, with exception that the inoculum containing compound and virus at MOI of 5 was incubated for an extra hour before being added to the cells. In the post-entry assay, cells were infected with CHIKV-*nanoluc* for 1 h, washed with PBS to remove unbound virus, and incubated with medium containing compound for 16 h at 37 °C.

2.5 Replication assay using BHK-CHIKV-NCT cells

BHK-CHIKV-NCT cells harboring CHIKV replicon that expresses the non-structural proteins of the virus, a selection marker (puromycin acetyltransferase, Pac), and reporter genes of *Renilla* luciferase and EGFP (Pohjala et al., 2011), at a density of 1×10^4 cells per well in a 96-well plate and incubated overnight at 37 °C. Medium containing serial dilutions of RO8191 at concentrations ranging from 60 µM to 0.46µM was added to cells and incubated for 72 h. Samples were harvested using *Renilla* luciferase lysis buffer (Promega®), and the luminescence levels were quantified with the *Renilla* luciferase Assay System (Promega®). In parallel, cell viability values were analyzed by performing MTT assay. The

effective concentration of 50% inhibition (EC_{50}) was calculated using GraphPad Prism 8 software. The values of CC_{50} and EC_{50} were used to calculate the selectivity index (SI = CC_{50}/ EC_{50}).

2.6 Molecular Docking assays

The compound RO8191 (PDB: 3R0L) and the CHIKV proteins were docked employing the GOLD program(Jones et al., 1997). GOLD performs a search for the best pose of the chosen molecule in the receptor-binding site using a genetic algorithm (GA) and the score ChemPL. The docking focused on the envelope glycoprotein complex (PDBid: 3N42), nsP1 (PDBid: 7DOP), nsP2 (PDBid:4ZTB), nsP3 (PDBid:6W8Z), and nsP4 were performed. For the nsP4, a database representative sequence of the nsP4 extracted from the virus polyprotein (uniport-id: Q8JUX6) was modeled using the RoseTTAFold (Minkyung et al., 2021) in Robetta online server (https://robetta.bakerlab.org/). The nsP4 tridimensional model was assessed using ERRAT (Colovos, 1993) Ramachandran Plot (Laskowski et al., 1993), and Verify 3D (Eisenberg et al., 1997) tools in SAVES v6.0 (https://saves.mbi.ucla.edu/). The nsP4 binding site was predicted using COACH (Yang et al., 2013) based on the RoseTTAFold structure prediction. COACH is a meta-server approach that combines multiple function annotation results to generate ligand binding site predictions. COACH results indicate a binding site similar to the site where the Uridine 5'-Triphosphate (UTP) interacts with the crystal structure of HCV ns5B polymerase (PDBid: 4RY5). The binding site was defined by the UTP position based on the 4RY5 structure and extrapolated to the modeled nsP4. The GA run parameters were maintained at default. The poses generated were then ranked and the solution with the best score was chosen. For the proteins nsP1-3 the interaction was analyzed using blind docking, while the envelop glycoprotein complex was directed to the seven probable ligand sites that were defined whit the support of Rashad and Keller (2013). The interaction on the best solution were analyzed using the program DS Visualizer (BIOVIA, Dassault Systèmes, Discovery Studio Visualizer, v 20.1, San Diego: Dassault Systèmes, 2020).

2.7 Infrared spectroscopy spectral assay through ATR-FTIR

Samples were recorded in a Fourier transform infrared connected to a micro-attenuated total reflectance spectrophotometer (ATR-FTIR Agilent Cary 630 FTIR, Agilent Technologies,

Santa Clara, CA, USA), as previously described (Oliveira et al., 2020; Santos et al., 2021). The diamond unit in the ATR system performs an internal-reflection element to record the fingerprint infrared signature in 1800 cm^{-1} to 800 cm^{-1} regions. The samples were prepared as previously described (Oliveira et al., 2020; Santos et al., 2021), where RO8191 (50 µM) was mixed with CHIKV-*nanoluc* virions (1 x 10^6 PFU/mL). A volume of 1.5 µL of each sample was inserted into the diamond unit and dehydrated for 6 min using airflow, forming a thin layer on the surface of the ATR crystal. The spectra were then recorded in triplicate (24 cm^{-1} resolution, 32 scans). All spectra were normalized by the vector method and corrected using the rubber-band baseline correction (Caixeta et al., 2020). Subsequently, the second derivative spectra were created based on raw data plotted in the Origin Pro 9.0 (OriginLab, Northampton, MA, USA) software, and corrected using the Savitzky-Golay algorithm with polynomial order 5 and 20 points of the window. To further elucidate the expression of the functional group evaluated we used the value of the valley heights (Oliveira et al., 2020; Santos et al., 2022, 2021).

2.8 dsRNA intercalation assay

A migration retardation assay was performed based on the previously described protocol (Campos et al., 2017; Krawczyk et al., 2009; Silva et al., 2019). The HCV JFH-1 3' untranslated region (UTR) known for forming a dsRNA was amplified through PCR. The reaction product of 273 bp was purified by ReliaPrep™ DNA Clean-Up and Concentration System (Promega®) and used for *in vitro* transcription by the HiScribe™ T7 High Yield RNA Synthesis Kit (New England BioLabs®). The dsRNA molecule was obtained by complementary annealing, later incubated at 30 nM with compound at 5 µM for 45 min and analyzed in 1% agarose TAE 1x gel stained with ethidium bromide. The lack of band in the gel confirms the compound intercalation activity since it competes with ethidium bromide. Doxorubicin (100 µM) was used as a positive control of intercalation. The band quantification was performed using ImageJ.JS version 1.53j.

2.9 CHIKV nsP4 cloning, overexpression, and purification

The coding region of nsP4 was cloned into a pET-SUMO expression vector, generating the nsP4_pET-SUMO/LIC expression vector, as previously described (Freire et al., 2022). Rosetta (DE3) *E. coli* (Novagen) cells were transformed with nsP4_pET-SUMO/LIC and

grown in TB medium, supplemented with 50 μM kanamycin and 34 μM chloramphenicol at 37 °C, until the OD_{600} reached 1.0. The protein expression was induced by adding 1 mM of Isopropyl β-D-1-thiogalactopyranoside (IPTG), at 18 °C for 16 h. Cells were harvested by centrifugation and cell pellets were resuspended in 50 mM Tris pH 8.0, 500 mM NaCl and 10% glycerol. Cells were lysed by sonication and cell debris was separated by centrifugation. The nsP4 was purified using an AKTA Purifier System (GE Healthcare). The first purification step was an affinity chromatography using a HisTrap HP 5.0 mL column (GE Healthcare). Concomitantly, the buffer was exchanged through dialysis and the His-tag-SUMO was cleavage by TEV protease during overnight at 4 °C. Another affinity chromatography was performed using the same system to collect the protein after cleavage. The protein was concentrated, and a final purification step was done through size-exclusion chromatography on a XK 26/1000 Superdex 75 column (GE Healthcare) pre-equilibrated in buffer 50 mM Tris pH 8.0, 200 mM NaCl and 10% glycerol. The final protein sample was analyzed in SDS-PAGE 12.5% to confirm its purity. Concentration was determined in a Nanodrop 1000 spectrophotometer.

2.10 MicroScale Thermophoresis (MST)

Experiments were performed on a Monolith® NT.115 (Nanotemper technol-ogies), as previously descrived (Freire et al., 2022). The nsP4 was labelled on cysteine residues with NT-647-Maleimide dye (Nanotemper Technologies) as per manufacturer's instructions. The concentration of protein indicated for MicroScale Thermophoresis experiments was 25 nM and a serial dilution of the compound from 250 μM to 0.0076 μM (7.6 nM). The dissociation constant K_d was obtained by fitting the binding curve with the Hill function.

2.11 Statistical analysis

All experiments were performed in triplicates and all tests were performed a minimum of three times (events) to confirm the reproducibility of the results. GraphPad Prism 8 software was used to evaluate the statistical differences in the means of the readings using the student t-test for paired data or the Mann-Whitney for unpaired data. Values of $p<0.01$ were considered statistically significant.

3. RESULTS

3.1 RO8191 is a potent inhibitor of CHIKV replication in BHK-21 cells

To assess the antiviral activity of RO8191 (**Fig. 1B**), a dose-response assay was carried out to determine the 50% effective concentration (EC_{50}) and 50% cytotoxicity concentration (CC_{50}) of this compound using previously described protocols (Oliveira et al., 2020; Santos et al., 2021). BHK-21 cells were treated with a two-fold serial dilution of RO8191 at concentrations ranging from 0.46 μM to 60 μM in the presence or absence of CHIKV-*nanoluc* (**Fig. 1A**) for 16 h (**Fig. 1C**). As a result, RO8191 demonstrated to possess CC_{50} of 10.9 μM and EC_{50} of 0.88 μM, with a selectivity index (SI) of 12.3 (**Fig. 1D**), emphasizing that this compound is a strong inhibitor of CHIKV replication *in vitro*. For further analysis, cells were treated with RO8191 at 5 μM, which significantly inhibited 95.7% of the CHIKV infection (cell viability > 100%).

3.2 RO8191 mainly inhibits post-entry stages of CHIKV replication

Since RO8191 compound exhibited a potent antiviral action against CHIKV, time of drug-addition assay was carried out to investigate the effects of this molecule on different stages of viral replication (Santos et al., 2022, 2021). A protective assay was performed by pre-treating cells with RO8191 for 1 h at 37 °C, extensively washing cells with PBS, and infecting them with CHIKV-*nanoluc* for 1 h. Then, the virus-containing medium was removed, and a fresh medium was added (**Fig. 2A**). As a result, 16 h.p.i. RO8191 inhibited 52.9% of CHIKV infection (p=0.04) (**Fig. 2A**), suggesting an effect of RO8191 as a protective molecule against CHIKV infection, providing an antiviral effect in host cells that blocked virus infection.

To further elucidate the activity of RO8191 in the early stages of CHIKV infection, virus and compound were simultaneously added to the cells for 1 h at 37°C. Later, cells were washed with PBS and a fresh medium was added until 16 h.p.i. (**Fig. 2B**). As an outcome, the compound significantly inhibited 62.4% of CHIKV replication (p=0.002), demonstrating the effect of RO8191 on viral entry into the cells (**Fig. 2B**). Additionally, we performed a virucidal assay by incubating the CHIKV particles with the compound for 1 h at 37 °C, and subsequently adding this inoculum to BHK-21 cells for an additional hour. Finally, the supernatant was removed, the cells were washed, and fresh medium was added (**Fig. 2C**). The results demonstrated that RO8191 possesses a virucidal activity inhibiting 75.4% of the

CHIKV replication (p=0.0024) (**Fig. 2C**), potentially by interacting with viral particles and blocking virus entry to the host cells.

To elucidate the post-entry effect of RO8191, the cells were infected with CHIKV-*nanoluc* for 1 h at 37 °C, then, the supernatant was removed, cells were washed with PBS, and medium with RO8191 was added (**Fig. 2D**). The results showed that the compound strongly inhibited CHIKV-*nanoluc* replication by 87% (p=0.0004) (**Fig. 2D**).

Altogether, data obtained from the time of drug-addition assay demonstrated that the main effect of RO8191 is on post-entry stages of virus replication (**Fig. 2**). Therefore, to further assess the RO8191 potential as a post-entry inhibitor, the effects of the compound on the replication stage of CHIKV replicative cycle, with no viral particles production and virion spread, were assessed through the employment of BHK-CHIKV-NCT cells, a subgenomic replicon system which expresses CHIKV non-structural proteins and the reporter genes of *Renilla* luciferase and EGFP (Pohjala et al., 2011). As previously described, the measurement of the activity of these reporters allows the evaluation of the effect of compounds on replication complexes formed during the replication stage, as well as on the transcription and translation of subgenomic RNAs (Pohjala et al., 2011; Santos et al., 2021). Thus, BHK-CHIKV-NCT cells were treated with two-fold serial dilution of the RO8191, at concentrations ranging from 0.46 to 60 µM for 16 h, and the expression of *Renilla* was subsequently measured (**Fig. 2E**). The results demonstrate that the compound strongly impaired viral replication, with an EC_{50} and CC_{50} of 1.4 µM and 26.2 µM, respectively, and SI of 18.7 (**Fig. 2E**), indicating a decrease in subgenomic RNA synthesis and/or translation, suggesting possible interactions of RO8191 with the virus nonstructural proteins or with the dsRNA intermediate of CHIKV replication.

3.3 RO8191 impairs CHIKV replication independently of the IFN-I pathway

RO8191 was described as an agonist of IFN-I (Konishi et al., 2012), and BHK-21 cells possess the IFN-I pathway (MacDonald et al., 2007), which might suggest that the effect observed here is dependent on the intrinsic cellular immune response, and not only by the effects of the compound on CHIKV machinery. To further evaluate the RO8191 activity on CHIKV infection, Vero-E6 cells, which do not express type 1 interferon genes (Emeny and Morgan, 1979; Prescott et al., 2010), were employed to perform the dose-response (**Fig. 3A**)

and time of drug-addition assay (**Fig. 3B-E**) assays on the same conditions used for BHK-21. The results demonstrated that RO8191 possesses CC_{50} and EC_{50} of 11.2 and 0.3 μM, respectively, with an SI of 37.3 (**Fig. 3A**). The time of drug-addition assay demonstrated that RO8191 protected the cells from infection in 72% (p=0.0005) (**Fig. 3B**), inhibited viral entry in 70.5% (p=0.0008) (**Fig. 3C**), and presented virucidal activity in 51.8% (p=0.0336) (**Fig. 3D**). The strongest effect observed using Vero-E6 cells was also in the post-entry stages, with inhibition of 91.6% of CHIKV replication (p<0.0001) (**Fig. 3E**). Altogether, the data suggest a direct effect of RO8191 on the CHIKV replicative machinery, mainly on post-entry steps, however, in an independent of interferon genes expression manner. It is important to emphasize that, since RO8191 protects cells against CHIKV infection and also interferes with the entry and post-entry stages, the antiviral effects of this compound might also be due to an additional interference with host factors, other than IFN-I-related ones.

3.4 Molecular docking suggests the interaction of RO8191 with CHIKV glycoproteins and nonstructural proteins

Considering the effects of RO8191 on CHIKV replication stages, molecular docking data were generated by GOLD and suggested interesting interactions between the compound and CHIKV proteins. Based on the observed *in vitro* virucidal effect, interactions between CHIKV glycoproteins and the compounds were observed mainly in the domain II of viral protein E1, with docking ChemPLP scores ranging between 47.37 and 57.12, and in the domain A-B of the viral protein E2 and domain B of viral protein E3, with score 45.26 (**Table 1, Fig. 4A**). Alkyl and Pi-Alkyl interactions were identified between the compound and the residues VAL F:54, ARG B:36, ILE F:55, and PRO B:240 on the domain II; a Halogen interaction with residue GLU B:35; two conventional hydrogen bonds, one at residue LYS F:52 and other with Pi-Pi Stacked at TYR B:237 residues. The carbon-hydrogen bonds with the residue ASN B:238 and TYR F:233; and Van der Waals interaction at GLU B:168, PRO F:56, LEU B:241, THR F:53, and ILE B:37, were seen between RO8191 and CHIKV glycoproteins (**Fig. 4A**).

The molecular docking performed with CHIKV nonstructural proteins (**Fig. 4B-E**) demonstrated the ChemPLP scores of 50.11, 35.26, 65.04, and 65.17 for nsP1, nsP2, nsP3, and nsP4, respectively (**Table 1**). The higher scores were observed for nsP3 and nsP4 (**Table**

1), in which at the nsP3 ADP-Ribose site the residues VAL A:33 and VAL A:113 interacted by alkyl and pi-alky bonds; the residues ALA A:23 and ALA A:22 by alkyl, amide-pi stacked, and halogen interactions; LEU A:109 by alkyl carbon-hydrogen bonds interaction; SER A:110 and GLY A:70 by halogen bond, TYR A:114 alkyl bond, and THR A:111 by amide-pi stacked and conventional hydrogen bonds, whereas the residue GLY A:112 interacted by van der Walls bond (**Table 1, Fig. 4D**). Additionally, nsP4 interacted with RO8191 through a pi-anion bond at ASP A:466, two halogen bonds at LYS A:429 and MET A:428; carbon-hydrogen bonds at THR A:435 and SER A:430; three conventional hydrogen bonds at GLN A:310, SER A:374, and ASP A:376 (with Pi-Anion ligands) (**Table 1**, **Fig. 4E**). Altogether, these data corroborate the *in vitro* effects shown by the compound.

3.5 RO8191 induces molecular changes into CHIKV glycoproteins

A scheme of the ATR-FTIR technology based on infrared analysis to evaluate sample of CHIKV virions, RO8191, and CHIKV virions plus RO8191 is represented in **Fig. 5A.** We found a minimum of five molecular changes in CHIKV virions after incubation with RO8191 using ATR-FTIR analyses. The samples RO8191 at 50 μM, CHIKV-*nanoluc* virions (1 x 10^6 PFU/mL), and the mixture RO8191 (50 μM) and CHIKV-*nanoluc* virions were recorded in ATR-FTIR and the representative infrared spectra are shown in **Fig. 5B**. The biofingerprint in the range of 1800–800 cm^{-1} are capable to indicates absorption bands of glycoproteins, proteins, lipids, and RNA of CHIKV, and it may be exploited to suggest the interaction between the virus and RO8191. The second derivative spectrum is capable to identify the accurate spatial distribution of each wavenumber referring to each biochemical component (Kohler et al., 2007; Rieppo et al., 2012). In this context, infrared spectra can also detect binding among different functional groups of materials and biological samples (Haris, 2013). The second derivative function spectrum is capable to isolate and determine the suitable spatial distribution of each wavenumber related to the unique molecular component in each sample (Kohler et al., 2007; Rieppo et al., 2012). In this context, infrared spectra can also indicate molecular interactions between different functional groups of substances with biological samples (Haris, 2013). We highlighted the functional groups when a vibrational mode was present in the second derivative spectrum of CHIKV and it was totally absent (above zero) after incubation of CHIKV with RO8191 (**Fig. 5C–G**). As an outcome, the

binding interactions between CHIKV and RO8191 were suggested in five vibrational modes at 1496 cm^{-1}, 1465 cm^{-1}, 1448 cm^{-1}, 1333 cm^{-1}, and 1078 cm^{-1}. The vibrational modes at 1496 cm^{-1} correspond to the in plane CH bending vibrations (**Fig. 5C)**. The vibrational mode at 1465 cm^{-1} represents CH_2 scissoring mode of the acyl chain in lipids (**Fig. 5D)**. The vibrational modes at 1448 cm^{-1} can be assigned to the asymmetric CH3 bending in methyl groups of proteins (**Fig. 5E)**. The vibrational mode at 1333 cm^{-1} represents CH vibrations in polysaccharides (**Fig. 5F)**, and 1078 cm^{-1} can be assigned to symmetric vibrations of PO_2^- in RNA (**Fig. 5G)**. Altogether, these interactions displayed in infrared spectroscopy analyses are in accordance with the molecular docking analysis described above.

3.6 Effects of RO8191 on virus dsRNA and CHIKV nsP4

The replication of ssRNA+ viruses is dependent on the dsRNA, a viral replicating intermediator (Rampersad and Tennant, 2018), and the viral RNA-dependent RNA polymerase (Rupp et al., 2015). Since RO8191 displayed activity in post-entry stages of infection and on subgenomic RNA synthesis and/or translation, and molecular docking calculations suggested interactions between RO8191 and CHIKV, interaction assays employing synthetic dsRNA and the CHIKV nsP4 were performed.

Employing the 3' UTR region of JFH-1 HCV as a template, an amplicon flanked by a T7 promoter was produced and used for *in vitro* transcription, synthesizing a dsRNA molecule of 273 bp (Campos et al., 2017; Krawczyk et al., 2009; Silva et al., 2019). Then, RO8191 at 5 µM was incubated with 30 nM of dsRNA and loaded in an agarose gel for electrophoresis. The results showed that RO8191 did not intercalate with the dsRNA (90.6% of band density) compared with the band of the sample treated with doxorubicin, the positive control of dsRNA interaction (1.3% of band density), that does not appear in the gel (**Supplementary Fig. 1**).

The purified CHIKV nsP4 was obtained by cloning the nsP4 genomic region into pET-SUMO (nsP4_pET-SUMO/LIC) expression vector and transforming Rosetta (DE3) *E. coli* (Novagen) cells, as previously described (Freire et al., 2022). The nsP4 was purified using an AKTA Purifier System (GE Healthcare) and concentration was determinated using spectrophotometry. The CHIKV nsP4 size is 54 kDa, and its presence has been verified and confirmed in all purification steps, as shown in SDS-PAGE gels (**Supplementary Fig. 2A**).

The assessment of nsP4 binding affinity was performed by MicroScale Thermophoresis (MST) on a Monolith® NT.115 (Nanotemper technol-ogies). The CHIKV nsP4 was labeled on cysteine residues with NT-647-Maleimide dye (Nanotemper Technologies) and the protein concentration was 25 nM. In addition, to estimate the interaction between RO8191 and CHIKV nsP4, we used a dissociation constant K_d, obtained by fitting the binding curve with the Hill function, and serial dilutions of the compound from 250 μM to 0.0076 μM. The results obtained for RO8191 are shown in **Supplementary Fig. 3**, where it is possible to observe the presence of the unbound states well defined, but not a bound state, suggesting that the occurrence of interaction between the protein and the compound is on a major scale concentration, approximated $k_d \pm \Delta k_d = >207 \pm 10$ μM. With these results is possible to conclude that CHIKV nsP4 presented a low interaction with RO8191.

4. DISCUSSION

CHIKV has shown an evident evasion of the first immune responses during infection (Tanabe et al., 2018), and also a high percentage of the infected people develop a chronic condition (Amaral et al., 2020; McCarthy et al., 2018). It highlights the clinical importance of chikungunya fever and the urgency to develop effective treatments. The data presented here suggest that RO8191 has strong anti-CHIKV activity *in vitro*, potentially through several antiviral mechanisms, making it an interesting promising treatment. Additionally, *in vivo* studies have shown the pharmacological potential of RO8191 as a small molecule that can be administered orally in a more controlled, simple, rapid, and economical way (Ishibashi et al., 2019; Konishi et al., 2012). RO8191 was described as a possible enhancer drug to be employed in combined therapy against CHIKV (Hwang et al., 2019), however, to the best of our knowledge, there is no description of the effect of the monotherapy with this compound on the CHIKV replicative cycle, as well as data on its mode of action. Data obtained here emphasized and supported the anti-CHIKV activity of RO8191 *in vitro* and provided insights into the mechanisms of action of this drug. Therefore, our results present RO8191 as a promising drug for the treatment of chikungunya fever.

RO8191 was previously described with antiviral activity by activating the interferon type-I pathway by specifically binding the IFNAR receptor (IFNAR2) subunit 2, resulting in a similar response to the interferon-alpha (IFN-α) and JAK/STAT signaling pathway (Furutani

et al., 2019; Konishi et al., 2012; Takahashi et al., 2019). Herein, our data demonstrate that RO8191 has anti-CHIKV activity in cells with or without the expression of type 1 interferon (α/β) *in vitro*, an interesting, novel, and unreported activity for RO8191, likely suggesting multiple mechanisms of action for this compound. RO8191 exerts strong activity toward CHIKV infection in BHK-21 and Vero-E6 cells, emphasized by the SI of 12.3 and 37.3, respectively. Also, RO8191 previously showed anti-ZIKV activity in infected Vero-E6 cells, with a strong antiviral effect (SI of 121.4) (Fernandes et al., 2021). Other authors described the effect of RO8191 impairing Hepatitis C and B virus infection (Furutani et al., 2019; Huang et al., 2014; Konishi et al., 2012; Takahashi et al., 2019; Wang et al., 2015), among them, Konishi and coworkers demonstrated RO8191 activity against HCV with an EC_{50} of 0.2 μM (Konishi et al., 2012), as well as its synthetic analogs with an improved anti-HCV entry action (Wang et al., 2015). Additionally, Takahashi and collaborators described that a RO8191 analog (CDM-3008), with strong activity against HCV and HBV, impaired 92.1% and 90.1% of infection, respectively (Takahashi et al., 2019). These works corroborate our data, and altogether demonstrate a strong antiviral activity against important clinical viruses, suggesting a broad-spectrum activity for RO8191. Moreover, RO8191 exerts a potential antiviral effect mediated by distinct mechanisms of action.

Another point observed here is the potent effect of RO8191 in different cell lineages, inhibiting over 50% of viral replication at all stages, with the strongest effect observed in post-entry stages of the CHIKV replicative cycle. Even though RO8191 was previously described as an effective agonist of interferon signaling (Furutani et al., 2021; Ishibashi et al., 2019; Kitamura et al., 2022; Zeng et al., 2020), when the antiviral assays were performed in Vero-E6 cells, which do not naturally express IFN-I genes (Emeny and Morgan, 1979; Prescott et al., 2010), the compound still triggered a strong anti-CHIKV activity, probably through an independent of IFN-α production mechanism of action. The effect observed here is in agreement with Konishi and collaborators who demonstrated that RO8191 inhibited HCV virus through a similar mechanism to IFN-α (Konishi et al., 2012). Interestingly, Wang and coworkers demonstrated the activity of RO8191 analogs impairing HCV entry by interacting with the virions (Wang et al., 2015), which agrees with our results, and with the antiviral data in IFN-I knockout cells (Furutani et al., 2019; Konishi et al., 2012). It might explain and emphasizes the potential of this molecule as antiviral through a different

mechanism of action, being supported by the bioinformatics data that demonstrated strong interactions with the subunit E1, also corroborated by the ATR-IFTR results, which indicated interactions between RO8191 and viral glycoproteins and lipids from CHIKV virions.

The RO8191 post-entry activity was demonstrated to be the strongest effect in the time-of-drug-addition assays, supported by the potent effect on the CHIKV subgenomic expressing cells. Additionally, the *in-silico* data showed the highest docking values for nsP3 and nsP4, suggesting that RO8191 might be also interacting and interfering with the nsP4 polymerase activity and/or with the ADP-ribose site of nsP3, both representing interesting antiviral targets for antiviral discovery against CHIKV (Chaudhary and Sehgal, 2021; Shimizu et al., 2020). Also, to the best of our knowledge, the inhibition of the nsP3 and/or nsP4 activities has not been described for RO8191 yet. It is important to highlight that our data did show an interaction between RO8191 and CHIKV nsP4, suggesting a low interference with nsP4. However, further analyses are needed to investigate the interference of RO8191 with the ADP-ribose site of nsP3 or with other viral and cellular proteins, which may potentially disrupt the CHIKV replication.

5. CONCLUSION

Altogether, the data presented here support RO8191 as a potent CHIKV inhibitor, mainly by affecting post-entry stages of viral replication, but also through an IFN-I independent pathway of intrinsic cellular response. The combined mechanisms of action exhibited by RO8191 highlight its potential to be further studied for its effects against CHIKV replication *in vivo* and present this compound as an interesting alternative for antiviral development against arboviruses. Therefore, this data might be useful for further approaches against CHIKV and provide a potential treatment for Chikungunya fever.

Acknowledgments

We thank Andres Merits (Institute of Technology, University of Tartu, Tartu, Estonia) for the provision of the CHIKV expressing-*nanoluciferase*. IAS thanks Conselho Nacional de Desenvolvimento Científico e Tecnológico (CNPq), scholarship #142495/2020–4. ACGJ and RSS are grateful to Coordenação de Aperfeiçoamento de Pessoal de Nível Superior (CAPES)-Brasil-Prevention and Combat of Outbreaks, Endemics, Epidemics and Pandemics-Finance Code #88881.506794/2020–01. ACGJ is also grateful to FAPEMIG

(Minas Gerais Research Foundation APQ-03385–18) and CAPES-Finance Code 001. This work was also supported by Fundação de Amparo à Pesquisa do Estado de São Paulo (FAPESP), CEPID grant 2013/07600-3 to GO, grant 2018/05130-3 to RSF, and 2016/19712-9 to ASG, and Coordenaçao de Aperfeiçoamento de Pessoal de Nível Superior (grant 88887.516153/2020-00) to ASG. We are grateful to the Medicine for Malaria Ventures (MMV, www.mmv.org) and the Drugs for Neglected Diseases initiative (DNDi, www.dndi.org) for their support, for the design of the Pandemic Response Box and for supplying the compounds. MarvinSketch was used to draw the chemicals, MarvinSketch version 20.17.0, ChemAxon (https://www.chemaxon.com).

REFERENCES

Amaral, J.K., Bilsborrow, J.B., Schoen, R.T., 2020. Chronic Chikungunya Arthritis and Rheumatoid Arthritis: What They Have in Common. Am J Med 133, e91–e97. https://doi.org/10.1016/J.AMJMED.2019.10.005

Basore, K., Kim, A.S., Nelson, C.A., Zhang, R., Smith, B.K., Uranga, C., Vang, L., Cheng, M., Gross, M.L., Smith, J., Diamond, M.S., Fremont, D.H., 2019. Cryo-EM Structure of Chikungunya Virus in Complex with the Mxra8 Receptor. Cell 177, 1725-1737.e16. https://doi.org/10.1016/J.CELL.2019.04.006

Battisti, V., Urban, E., Langer, T., 2021. Antivirals against the Chikungunya Virus. Viruses 13, 1307. https://doi.org/10.3390/v13071307

Bedoui, Y., Septembre-Malaterre, A., Giry, C., Jaffar-Bandjee, M.C., Selambarom, J., Guiraud, P., Gasque, P., 2021. Robust cox-2-mediated prostaglandin response may drive arthralgia and bone destruction in patients with chronic inflammation post-Chikungunya. PLoS Negl Trop Dis 15. https://doi.org/10.1371/journal.pntd.0009115

Burt, F.J., Chen, W., Miner, J.J., Lenschow, D.J., Merits, A., Schnettler, E., Kohl, A., Rudd, P.A., Taylor, A., Herrero, L.J., Zaid, A., Ng, L.F.P., Mahalingam, S., 2017. Chikungunya virus: an update on the biology and pathogenesis of this emerging pathogen. Lancet Infect Dis 17, e107–e117. https://doi.org/10.1016/S1473-3099(16)30385-1

Caglioti, C., Lalle, E., Castilletti, C., Carletti, F., Capobianchi, M.R., Bordi, L., 2013. Chikungunya virus infection: an overview. NEW MICROBIOLOGICA 36, 211–227.

Caixeta, D.C., Aguiar, E.M.G., Cardoso-Sousa, L., Coelho, L.M.D., Oliveira, S.W., Espindola, F.S., Raniero, L., Crosara, K.T.B., Baker, M.J., Siqueira, W.L., Sabino-Silva, R., 2020. Salivary molecular spectroscopy: A sustainable, rapid and non-invasive monitoring tool for diabetes mellitus during insulin treatment. PLoS One 15, e0223461. https://doi.org/10.1371/journal.pone.0223461

Campos, G.R.F., Bittar, C., Jardim, A.C.G., Shimizu, J.F., Batista, M.N., Paganini, E.R., Assis, L.R. de, Bartlett, C., Harris, M., Bolzani, V. da S., Regasini, L.O., Rahal, P., 2017. Hepatitis C virus in vitro

replication is efficiently inhibited by acridone Fac4. Journal of General Virology 98, 1693–1701. https://doi.org/10.1099/jgv.0.000808

Chaudhary, M., Sehgal, D., 2021. In silico identification of natural antiviral compounds as a potential inhibitor of chikungunya virus non-structural protein 3 macrodomain. J Biomol Struct Dyn 1–11. https://doi.org/10.1080/07391102.2021.1960195

Coffey, L.L., Failloux, A.-B., Weaver, S.C., 2014. Chikungunya Virus–Vector Interactions. Viruses 6, 4628–4663. https://doi.org/10.3390/v6114628

Colovos, C., 1993. Verification of protein structures: Patterns of nonbonded atomic interactions. Mol Biol 2, 1511–1519.

Eisenberg, D., Lüthy, R., Bowie, J.U., 1997. VERIFY3D: Assessment of protein models with three-dimensional profiles. Methods Enzymol 277, 396–404. https://doi.org/10.1016/S0076-6879(97)77022-8

Emeny, J.M., Morgan, M.J., 1979. Regulation of the Interferon System: Evidence that Vero Cells have a Genetic Defect in Interferon Production. Journal of General Virology 43, 247–252. https://doi.org/10.1099/0022-1317-43-1-247

Fernandes, R.S., de Godoy, A.S., Santos, I.A., Noske, G.D., de Oliveira, K.I.Z., Gawriljuk, V.O., Gomes Jardim, A.C., Oliva, G., 2021. Discovery of an imidazonaphthyridine and a riminophenazine as potent anti-Zika virus agents through a replicon-based high-throughput screening. Virus Res 299, 198388. https://doi.org/10.1016/J.VIRUSRES.2021.198388

Freire, M.C.L.C., Basso, L.G.M., Mendes, L.F.S., Mesquita, N.C.M.R., Mottin, M., Fernandes, R.S., Policastro, L.R., Godoy, A.S., Santos, I.A., Ruiz, U.E.A., Caruso, I.P., Sousa, B.K.P., Jardim, A.C.G., Almeida, F.C.L., Gil, L.H.V.G., Andrade, C.H., Oliva, G., 2022. Characterization of the RNA-dependent RNA polymerase from Chikungunya virus and discovery of a novel ligand as a potential drug candidate. Sci Rep 12, 10601. https://doi.org/10.1038/S41598-022-14790-X

Furutani, Y., Toguchi, M., Higuchi, S., Yanaka, K., Gailhouste, L., Qin, X.-Y., Masaki, T., Ochi, S., Matsuura, T., 2021. Establishment of a Rapid Detection System for ISG20-Dependent SARS-CoV-2 Subreplicon RNA Degradation Induced by Interferon-α. Int J Mol Sci 22, 11641. https://doi.org/10.3390/ijms222111641

Furutani, Y., Toguchi, M., Shiozaki-Sato, Y., Qin, X.-Y., Ebisui, E., Higuchi, S., Sudoh, M., Suzuki, H., Takahashi, N., Watashi, K., Wakita, T., Kakeya, H., Kojima, S., 2019. An interferon-like small chemical compound CDM-3008 suppresses hepatitis B virus through induction of interferon-stimulated genes. PLoS One 14, e0216139. https://doi.org/10.1371/journal.pone.0216139

Haris, P.I., 2013. Probing protein–protein interaction in biomembranes using Fourier transform infrared spectroscopy. Biochimica et Biophysica Acta (BBA) - Biomembranes 1828, 2265–2271. https://doi.org/10.1016/j.bbamem.2013.04.008

Hibl, B.M., Dailey Garnes, N.J.M., Kneubehl, A.R., Vogt, M.B., Spencer Clinton, J.L., Rico-Hesse, R.R., 2021. Mosquito-bite infection of humanized mice with chikungunya virus produces systemic

disease with long-term effects. PLoS Negl Trop Dis 15, e0009427. https://doi.org/10.1371/journal.pntd.0009427

Huang, S., Qing, J., Wang, S., Wang, H., Zhang, L., Tang, Y., 2014. Design and synthesis of imidazo[1,2-α][1,8]naphthyridine derivatives as anti-HCV agents via direct C–H arylation. Org. Biomol. Chem. 12, 2344–2348. https://doi.org/10.1039/C3OB42525H

Hwang, J., Wang, Y., Fikrig, E., 2019. Inhibition of Chikungunya Virus Replication in Primary Human Fibroblasts by Liver X Receptor Agonist. Antimicrob Agents Chemother. https://doi.org/10.1128/AAC

Ishibashi, D., Homma, T., Nakagaki, T., Fuse, T., Sano, K., Satoh, K., Mori, T., Atarashi, R., Nishida, N., 2019. Type I interferon protects neurons from prions in *in vivo* models. Brain 142, 1035–1050. https://doi.org/10.1093/brain/awz016

Jones, G., Willett, P., Glen, R.C., Leach, a R., Taylor, R., 1997. Development and validation of a genetic algorithm for flexible docking. J Mol Biol 267, 727–48. https://doi.org/10.1006/jmbi.1996.0897

Kitamura, H., Tanigawa, T., Kuzumoto, T., Nadatani, Y., Otani, K., Fukunaga, S., Hosomi, S., Tanaka, F., Kamata, N., Nagami, Y., Taira, K., Uematsu, S., Watanabe, T., Fujiwara, Y., 2022. Interferon-α exerts proinflammatory properties in experimental radiation-induced esophagitis: Possible involvement of plasmacytoid dendritic cells. Life Sci 289, 120215. https://doi.org/10.1016/J.LFS.2021.120215

Kohler, A., Bertrand, D., Martens, H., Hannesson, K., Kirschner, C., Ofstad, R., 2007. Multivariate image analysis of a set of FTIR microspectroscopy images of aged bovine muscle tissue combining image and design information. Anal Bioanal Chem 389, 1143–1153. https://doi.org/10.1007/s00216-007-1414-9

Konishi, H., Okamoto, K., Ohmori, Y., Yoshino, H., Ohmori, H., Ashihara, M., Hirata, Y., Ohta, A., Sakamoto, H., Hada, N., Katsume, A., Kohara, M., Morikawa, K., Tsukuda, T., Shimma, N., Foster, G.R., Alazawi, W., Aoki, Y., Arisawa, M., Sudoh, M., 2012. An orally available, small-molecule interferon inhibits viral replication. Sci Rep 2, 259. https://doi.org/10.1038/srep00259

Kota, S.K., Roening, C., Patel, N., Kota, S.B., Baron, R., 2018. PRMT5 inhibition promotes osteogenic differentiation of mesenchymal stromal cells and represses basal interferon stimulated gene expression. Bone 117, 37–46. https://doi.org/10.1016/J.BONE.2018.08.025

Krawczyk, M., Wasowska-Lukawska, M., Oszczapowicz, I., Boguszewska-Chachulska, A.M., 2009. Amidinoanthracyclines - A new group of potential anti-hepatitis C virus compounds. Biol Chem 390, 351–360. https://doi.org/10.1515/BC.2009.040

Kril, V., Aïqui-Reboul-Paviet, O., Briant, L., Amara, A., 2021. New Insights into Chikungunya Virus Infection and Pathogenesis. Annu Rev Virol. https://doi.org/10.1146/annurev-virology-091919

Laskowski, R.A., Macarthur, M.W., Moss, D.S., Thornton, J.M., 1993. PROCHECK: a program to check the stereochemical quality of protein structures. J. Appl. Cryst. 26, 283–291.

MacDonald, M.R., Machlin, E.S., Albin, O.R., Levy, D.E., 2007. The Zinc Finger Antiviral Protein Acts Synergistically with an Interferon-Induced Factor for Maximal Activity against Alphaviruses. J Virol 81, 13509–13518. https://doi.org/10.1128/jvi.00402-07

McCarthy, M.K., Davenport, B.J.J., Morrison, T.E., 2018. Chronic Chikungunya Virus Disease, in: Heise, M. (Ed.), Chikungunya Virus. Springer International Publishing, Cham, pp. 55–80. https://doi.org/10.1007/82_2018_147

Medicines for Malaria Venture, Drugs for Neglected Diseases initiative, n.d. Pandemic Response Box [WWW Document]. URL https://www.mmv.org/mmv-open/pandemic-response-box (accessed 3.27.22).

Metz, S.W., Pijlman, G.P., 2016. Function of Chikungunya Virus Structural Proteins, in: Okeoma, C.M. (Ed.), Chikungunya Virus. Springer International Publishing, Cham, pp. 63–74. https://doi.org/10.1007/978-3-319-42958-8_5

Minkyung, B., Frank, D., Ivan, A., Justas, D., Sergey, O., Rie, L.G., Jue, W., Qian, C., N., K.L., Dustin, S.R., Claudia, M., Hahnbeom, P., Carson, A., R., G.C., Andy, D., H., P.J., V., R.A., A., van D.A., C., E.A., J., O.D., Theo, S., Christoph, B., Tea, P.-K., K., R.M., Udit, D., K., Y.C., E., B.J., Christopher, G.K., V., G.N., D., A.P., J., R.R., David, B., 2021. Accurate prediction of protein structures and interactions using a three-track neural network. Science (1979) 373, 871–876. https://doi.org/10.1126/science.abj8754

Oliveira, D.M. de, Santos, I. de A., Martins, D.O.S., Gonçalves, Y.G., Cardoso-Sousa, L., Sabino-Silva, R., von Poelhsitz, G., Franca, E. de F., Nicolau-Junior, N., Pacca, C.C., Merits, A., Harris, M., Jardim, A.C.G., 2020. Organometallic Complex Strongly Impairs Chikungunya Virus Entry to the Host Cells. Front Microbiol 11. https://doi.org/10.3389/fmicb.2020.608924

Pan American Health Organization, 2021. Epidemiological Update Dengue, chikungunya and Zika in the context of COVID-19 [WWW Document]. URL https://iris.paho.org/handle/10665.2/55639 (accessed 3.27.22).

Pan American Health Organization, 2013. Epidemiological Alert, Chikungunya Fever [WWW Document]. URL https://iris.paho.org/handle/10665.2/50703 (accessed 3.27.22).

Pohjala, L., Utt, A., Varjak, M., Lulla, A., Merits, A., 2011. Inhibitors of Alphavirus Entry and Replication Identified with a Stable Chikungunya Replicon Cell Line and Virus-Based Assays. PLoS One 6, 28923. https://doi.org/10.1371/journal.pone.0028923

Prescott, J., Hall, P., Acuna-Retamar, M., Ye, C., Wathelet, M.G., Ebihara, H., Feldmann, H., Hjelle, B., 2010. New World Hantaviruses Activate IFNλ Production in Type I IFN-Deficient Vero E6 Cells. PLoS One 5, e11159. https://doi.org/10.1371/journal.pone.0011159

Rampersad, S., Tennant, P., 2018. Replication and Expression Strategies of Viruses, in: Viruses. Elsevier, pp. 55–82. https://doi.org/10.1016/B978-0-12-811257-1.00003-6

Rieppo, L., Saarakkala, S., Närhi, T., Helminen, H.J., Jurvelin, J.S., Rieppo, J., 2012. Application of second derivative spectroscopy for increasing molecular specificity of fourier transform infrared spectroscopic imaging of articular cartilage. Osteoarthritis Cartilage 20, 451–459. https://doi.org/10.1016/J.JOCA.2012.01.010

Rupp, J.C., Sokoloski, K.J., Gebhart, N.N., Hardy, R.W., 2015. Alphavirus RNA synthesis and non-structural protein functions. Journal of General Virology 96, 2483–2500. https://doi.org/10.1099/jgv.0.000249

Santos, I.A., Pereira, A.K. dos S., Guevara-Vega, M., de Paiva, R.E.F., Sabino-Silva, R., Bergamini, F.R.G., Corbi, P.P., Jardim, A.C.G., 2022. Repurposing potential of rimantadine hydrochloride and development of a promising platinum(II)-rimantadine metallodrug for the treatment of Chikungunya virus infection. Acta Trop 227, 106300. https://doi.org/10.1016/J.ACTATROPICA.2021.106300

Santos, I.A., Shimizu, J.F., de Oliveira, D.M., Martins, D.O.S., Cardoso-Sousa, L., Cintra, A.C.O., Aquino, V.H., Sampaio, S.V., Nicolau-Junior, N., Sabino-Silva, R., Merits, A., Harris, M., Jardim, A.C.G., 2021. Chikungunya virus entry is strongly inhibited by phospholipase A2 isolated from the venom of Crotalus durissus terrificus. Sci Rep 11, 8717. https://doi.org/10.1038/s41598-021-88039-4

Schilte, C., Staikovsky, F., Couderc, T., Madec, Y., Carpentier, F., Kassab, S., Albert, M.L., Lecuit, M., Michault, A., 2013. Correction: Chikungunya Virus-associated Long-term Arthralgia: A 36-month Prospective Longitudinal Study. PLoS Negl Trop Dis 7, null. https://doi.org/10.1371/annotation/850ee20f-2641-46ac-b0c6-ef4ae79b6de6

Schwartz, O., Albert, M.L., 2010. Biology and pathogenesis of chikungunya virus. Nat Rev Microbiol 8, 491–500. https://doi.org/10.1038/nrmicro2368

Shimizu, J.F., Martins, D.O.S., McPhillie, M.J., Roberts, G.C., Zothner, C., Merits, A., Harris, M., Jardim, A.C.G., 2020. Is the ADP ribose site of the Chikungunya virus NSP3 Macro domain a target for antiviral approaches? Acta Trop 207, 105490. https://doi.org/10.1016/J.ACTATROPICA.2020.105490

Silva, N.M. da, Teixeira, R.A.G., Cardoso, C.G., Siqueira Junior, J.B., Coelho, G.E., Oliveira, E.S.F. de, 2018. Chikungunya surveillance in Brazil: challenges in the context of Public Health. Epidemiology and health services: Journal of the Sistema Unico de Saude do Brasil 27, e2017127. https://doi.org/10.5123/S1679-49742018000300003

Silva, L.A., Dermody, T.S., 2017. Chikungunya virus: epidemiology, replication, disease mechanisms, and prospective intervention strategies. Journal of Clinical Investigation 127, 737–749. https://doi.org/10.1172/JCI84417

Silva, S., Shimizu, J.F., Oliveira, D.M. de, Assis, L.R. de, Bittar, C., Mottin, M., Sousa, B.K. de P., Mesquita, N.C. de M.R., Regasini, L.O., Rahal, P., Oliva, G., Perryman, A.L., Ekins, S., Andrade, C.H., Goulart, L.R., Sabino-Silva, R., Merits, A., Harris, M., Jardim, A.C.G., 2019. A diarylamine derived from anthranilic acid inhibits ZIKV replication. Sci Rep 9, 17703. https://doi.org/10.1038/s41598-019-54169-z

Subudhi, B., Chattopadhyay, S., Mishra, P., Kumar, A., 2018. Current Strategies for Inhibition of Chikungunya Infection. Viruses 10, 235. https://doi.org/10.3390/v10050235

Takahashi, N., Hayashi, K., Nakagawa, Y., Furutani, Y., Toguchi, M., Shiozaki-Sato, Y., Sudoh, M., Kojima, S., Kakeya, H., 2019. Development of an anti-hepatitis B virus (HBV) agent through the structure-

activity relationship of the interferon-like small compound CDM-3008. Bioorg Med Chem 27, 470–478. https://doi.org/10.1016/J.BMC.2018.11.039

Tanabe, I.S.B., Tanabe, E.L.L., Santos, E.C., Martins, W. v., Araújo, I.M.T.C., Cavalcante, M.C.A., Lima, A.R. v., Câmara, N.O.S., Anderson, L., Yunusov, D., Bassi, Ê.J., 2018. Cellular and Molecular Immune Response to Chikungunya Virus Infection. Front Cell Infect Microbiol 8, 345. https://doi.org/10.3389/fcimb.2018.00345

Tharmarajah, K., Mahalingam, S., Zaid, A., 2017. Chikungunya: vaccines and therapeutics. F1000Res 6, 2114. https://doi.org/10.12688/f1000research.12461.1

Thiberville, S.D., Moyen, N., Dupuis-Maguiraga, L., Nougairede, A., Gould, E.A., Roques, P., de Lamballerie, X., 2013. Chikungunya fever: Epidemiology, clinical syndrome, pathogenesis and therapy. Antiviral Res 99, 345–370. https://doi.org/10.1016/J.ANTIVIRAL.2013.06.009

van Voorhis, W.C., Adams, J.H., Adelfio, R., Ahyong, V., Akabas, M.H., Alano, P., Alday, A., Alemán Resto, Y., Alsibaee, A., Alzualde, A., Andrews, K.T., Avery, S. v., Avery, V.M., Ayong, L., Baker, M., Baker, S., ben Mamoun, C., Bhatia, S., Bickle, Q., Bounaadja, L., Bowling, T., Bosch, J., Boucher, L.E., Boyom, F.F., Brea, J., Brennan, M., Burton, A., Caffrey, C.R., Camarda, G., Carrasquilla, M., Carter, D., Belen Cassera, M., Chih-Chien Cheng, K., Chindaudomsate, W., Chubb, A., Colon, B.L., Colón-López, D.D., Corbett, Y., Crowther, G.J., Cowan, N., D'Alessandro, S., le Dang, N., Delves, M., DeRisi, J.L., Du, A.Y., Duffy, S., Abd El-Salam El-Sayed, S., Ferdig, M.T., Fernández Robledo, J.A., Fidock, D.A., Florent, I., Fokou, P.V.T., Galstian, A., Gamo, F.J., Gokool, S., Gold, B., Golub, T., Goldgof, G.M., Guha, R., Guiguemde, W.A., Gural, N., Guy, R.K., Hansen, M.A.E., Hanson, K.K., Hemphill, A., Hooft van Huijsduijnen, R., Horii, T., Horrocks, P., Hughes, T.B., Huston, C., Igarashi, I., Ingram-Sieber, K., Itoe, M.A., Jadhav, A., Naranuntarat Jensen, A., Jensen, L.T., Jiang, R.H.Y., Kaiser, A., Keiser, J., Ketas, T., Kicka, S., Kim, S., Kirk, K., Kumar, V.P., Kyle, D.E., Lafuente, M.J., Landfear, S., Lee, N., Lee, S., Lehane, A.M., Li, F., Little, D., Liu, L., Llinás, M., Loza, M.I., Lubar, A., Lucantoni, L., Lucet, I., Maes, L., Mancama, D., Mansour, N.R., March, S., McGowan, S., Medina Vera, I., Meister, S., Mercer, L., Mestres, J., Mfopa, A.N., Misra, R.N., Moon, S., Moore, J.P., Morais Rodrigues da Costa, F., Müller, J., Muriana, A., Nakazawa Hewitt, S., Nare, B., Nathan, C., Narraidoo, N., Nawaratna, S., Ojo, K.K., Ortiz, D., Panic, G., Papadatos, G., Parapini, S., Patra, K., Pham, N., Prats, S., Plouffe, D.M., Poulsen, S.A., Pradhan, A., Quevedo, C., Quinn, R.J., Rice, C.A., Abdo Rizk, M., Ruecker, A., st. Onge, R., Salgado Ferreira, R., Samra, J., Robinett, N.G., Schlecht, U., Schmitt, M., Silva Villela, F., Silvestrini, F., Sinden, R., Smith, D.A., Soldati, T., Spitzmüller, A., Stamm, S.M., Sullivan, D.J., Sullivan, W., Suresh, S., Suzuki, B.M., Suzuki, Y., Swamidass, S.J., Taramelli, D., Tchokouaha, L.R.Y., Theron, A., Thomas, D., Tonissen, K.F., Townson, S., Tripathi, A.K., Trofimov, V., Udenze, K.O., Ullah, I., Vallieres, C., Vigil, E., Vinetz, J.M., Voong Vinh, P., Vu, H., Watanabe, N.A., Weatherby, K., White, P.M., Wilks, A.F., Winzeler, E.A., Wojcik, E., Wree, M., Wu, W., Yokoyama, N., Zollo, P.H.A., Abla, N., Blasco, B., Burrows, J., Laleu, B., Leroy, D., Spangenberg, T., Wells, T., Willis, P.A., 2016. Open Source Drug Discovery with the Malaria Box Compound Collection for Neglected Diseases and Beyond. PLoS Pathog 12. https://doi.org/10.1371/journal.ppat.1005763

Wang, H., Wang, S., Cheng, L., Chen, L., Wang, Yongguang, Qing, J., Huang, S., Wang, Yuanhao, Lei, X., Wu, Y., Ma, Z., Zhang, L., Tang, Y., 2015. Discovery of Imidazo[1,2-α][1,8]naphthyridine Derivatives as Potential HCV Entry Inhibitor. ACS Med Chem Lett 6, 977–981. https://doi.org/10.1021/acsmedchemlett.5b00159

Yang, J., Roy, A., Zhang, Y., 2013. Protein-ligand binding site recognition using complementary binding-specific substructure comparison and sequence profile alignment. Bioinformatics 29, 2588–2595. https://doi.org/10.1093/bioinformatics/btt447

Ying, Z.H., Li, H.M., Yu, W.Y., Yu, C.H., 2021. Iridin prevented against lipopolysaccharide-induced inflammatory responses of macrophages via inactivation of pkm2-mediated glycolytic pathways. J Inflamm Res 14, 341–354. https://doi.org/10.2147/JIR.S292244

Zeng, J., Wu, D., Hu, H., Young, J.A.T., Yan, Z., Gao, L., 2020. Activation of the Liver X Receptor Pathway Inhibits HBV Replication in Primary Human Hepatocytes. Hepatology 72. https://doi.org/10.1002/hep.31217/suppinfo

TABLES

Table 1. Localization and ChemPLP values showed between RO8191 and CHIKV proteins by molecular docking calculations

		ChemPLP	Coordinates (x, y, z)	Volume ($Å^3$)	Localization
Glycoproteins	**Site 1**	50.41	−15.687, 2.019, −19.939	651.375	Between II domain of E1 and C of E2.
	Site 2	57.12	−33.937, −18.731, −31.939	357.375	Between II domain of E1 and beta-sheet of E2.
	Site 3	47.37	−33.437, −6.731, −33.189	156.125	Adjacent to site 2.
	Site 4	45.26	−42.937, −28.731, −22.939	183.875	Behind the fusion loop, between B domain of E3, and E2 domain B, and A domain of E2.
	Site 5	-34.73	−44.437, −14.731, −23.439	124	Between beta-sheet of E2 and of E3.
	Site 6	*	−16.187, −18.231, −36.439	20.5	Inside the E3 cavity.
	Site 7	10.30	−59.187, −15.731,−26.189	22.5	Replacing the furin loop.
nsP1		50.11			Catalytic amino acid H37
nsP2		35.26			Catalytic amino acid H548
nsP3		65.04			ADP-ribose
nsP4		65.17			Amino acid site ASP466

LEGENDS OF FIGURES

Figure 1. RO8191 activity on CHKV replication. A) Representative structure of CHIKV-*nanoluc* genome [PDB: 6NK5](Basore et al., 2019; Metz and Pijlman, 2016). **B)** Imidazonaphthyridine chemical structure (RO4948191 or RO8191) (CAS No.: 691868-88-9; https://www.medchemexpress.com/ro8191.html). **C)** Representative scheme of the infection assays. BHK-21 cells were treated with two-fold serial dilutions of RO8191 at concentrations ranging from 0.46 to 60 µM. CHIKV replication was quantified by measuring *nanoluciferase* activity (indicated by a black square) and cell viability using MTT assay (indicated by a gray circle). Mean ± SD values from a minimum of three independent experiments, each measured in triplicate, are represented. All images were generated using GraphPad Prism 8 and GIMP 2.1v.

Figure 2. RO8191 activity on different stages of CHIKV replicative cycle in BHK-21 cells. A) BHK-21 cells were treated with RO8191 for 1 h, cells were washed with PBS to remove the compound, and were infected with CHIKV-*nanoluc* at MOI 0.1 for 1 h. Then, the medium was removed, cells were washed to remove unbound virus, and fresh medium was added. **B)** BHK-21 cells were infected with CHIKV-*nanoluc* (MOI 0.1) and simultaneously treated with RO8191 for 1 h. Then, cells were washed to completely remove the inoculum, and a fresh medium was added. **C)** RO8191 and CHIKV-*nanoluc* at MOI 5 were incubated for 1 h (representative inoculum). Then, the inoculum was added to the cells for an additional hour. Cells were washed to remove the inoculum and fresh medium was added. **D)** BHK-21 cells were infected with CHIKV-*nanoluc* (MOI 0.1) for 1 h, cells were washed with PBS to remove unbound virus, and were treated with RO8191. All infection assays were quantified 16 h.p.i through the measurement of luminescence levels. Schematic representation of each time-based assay as indicated by BHK-21 cells (black bars), RO8191 (gray bars), CHIKV-*nanoluc* (orange bars), and CHIKV-RO8191 inoculum (blue tube). **E)** Schematic representation of the time-based BHK-CHIKV cell assay as indicated by the BHK-CHIKV-NCT cells (black bars) and RO8191 (gray bars). BHK-CHIKV-NCT cells were incubated for 72 h with the RO8191 compound at concentrations ranging from 60 to 0.46 µM. Then, cells were washed with PBS and lysed with Passive Lysis Buffer to measure the activity of *Renilla*. The reduction of *Renilla* activity in BHK-CHIKV-NCT cells is shown

by more than 50% from the lowest concentrations of RO8191. Mean ± SD values of a minimum of three independent experiments, each measured in triplicate (****) P <0.0001, (***) P<0.001, (**) P<0.01 and (*) P <0.05 are represented. Images were generated using GraphPad Prism 8 and GIMP 2.1v.

Figure 3. RO8191 activity against CHIKV infection in Vero-E6 cells. A) Representative scheme of the infection assays. Vero-E6 cells were treated with three-fold serial dilutions of RO8191 at concentrations ranging from 0.02 to 60 μM. CHIKV replication was quantified by measuring *nanoluciferase* activity (indicated by a black square) and cell viability using an MTT assay (indicated by a gray circle). Values of EC_{50}, $CC_{50,}$ and SI were obtained from the treatment of Vero-E6 cells treated with RO8191. **B)** Vero-E6 cells were treated with RO8191 for 1 h, then the cells were washed with PBS and infected with CHIKV-*nanoluc* virus at MOI 0.1 for 1 h. The medium was removed, cells were washed with PBS and fresh medium was added. **C)** Vero-E6 cells were infected with CHIKV-*nanoluc* (MOI 0.1) and simultaneously treated with RO8191 for 1h. Then, cells were washed, and fresh medium was added. **D)** RO891 and CHIKV-*nanoluc* at MOI 5 were incubated for 1 h, then the inoculum was added to cells for an extra 1 h, cells were washed, and fresh medium was added. **E)** Vero-E6 cells were infected with CHIKV-*nanoluc* (MOI 0.1) for 1h, cells were washed with PBS and treated with RO8191. Schematic representation of each time-based assay as indicated by Vero-E6 cells (blue bars), RO8191 (gray bars), CHIKV-*nanoluc* (orange bars), and CHIKV-RO8191 inoculum (blue tube). Mean ± SD values of a minimum of three independent experiments, each measured in triplicate, are represented. (****) P <0.0001, (***) P <0.001 and (*) P <0.05. Images were generated using GraphPad Prism 8 and GIMP 2.1v.

Figure 4. 2D and 3D interactions between RO8191 and CHIKV proteins showed by molecular docking analysis. A) RO8181 interacts with CHIKV glycoproteins mainly through Hydrogen Bond (green lines) and alkyl ligands (pink lines). **B)** RO8191 showed interactions with nsP1 protein mainly through Conventional Hydrogen Bonds (green circles) interactions. **C)** RO8191 interacts with nsP2 mainly through Alkyl (pink lines) and Hydrogen Bonds (green lines) interactions. **D)** RO8191 interacts with nsP3 mainly through Hydrogens Bonds ligands and interactions (green lines and circles). **E)** RO8191 interactions with nsP4 mainly through Conventional Hydrogens Bonds (green lines) and Halogen (blue lines)

ligands. RO8191 (PDB: 3R0L) and the CHIKV proteins (glycoprotein complex [PDBid: 3N42], nsP1 [PDBid: 7DOP], nsP2 [PDBid:4ZTB], nsP3 [PDBid:6W8Z], and database representative sequence of the nsP4 extracted from the virus polyprotein [uniport-id: Q8JUX6]) were docked employing the GOLD program site using a genetic algorithm (GA) and the score ChemPL. Images were generated using GraphPad Prism 8 and GIMP 2.1v.

Figure 5. Infrared spectroscopy indicates molecular interactions between CHIKV virions with RO8191. A) Representative scheme of the ATR-FTIR technology with CHIKV virions (black line), RO8191 (blue line), and CHIKV virion plus incubation with RO8191 (red line). **B)** The representative infrared average spectrum of normalized mean spectra of CHIKV virion (black line), RO8191 (blue line), and CHIKV virion plus RO8191 (red line) employing ATR-FTIR platform from 1800 to 800 cm^{-1}. **B-F)** The representative mean spectra of second derivative analysis to the vibrational modes at 1496 cm^{-1} (**B**), 1465 cm^{-1} (**C**), 1448 cm^{-1} (**D**), 1333 cm^{-1} (**E**), and 1078 cm^{-1} (**F**). Images were generated using GraphPad Prism 8 and GIMP 2.1v.

FIGURES

Figure 1

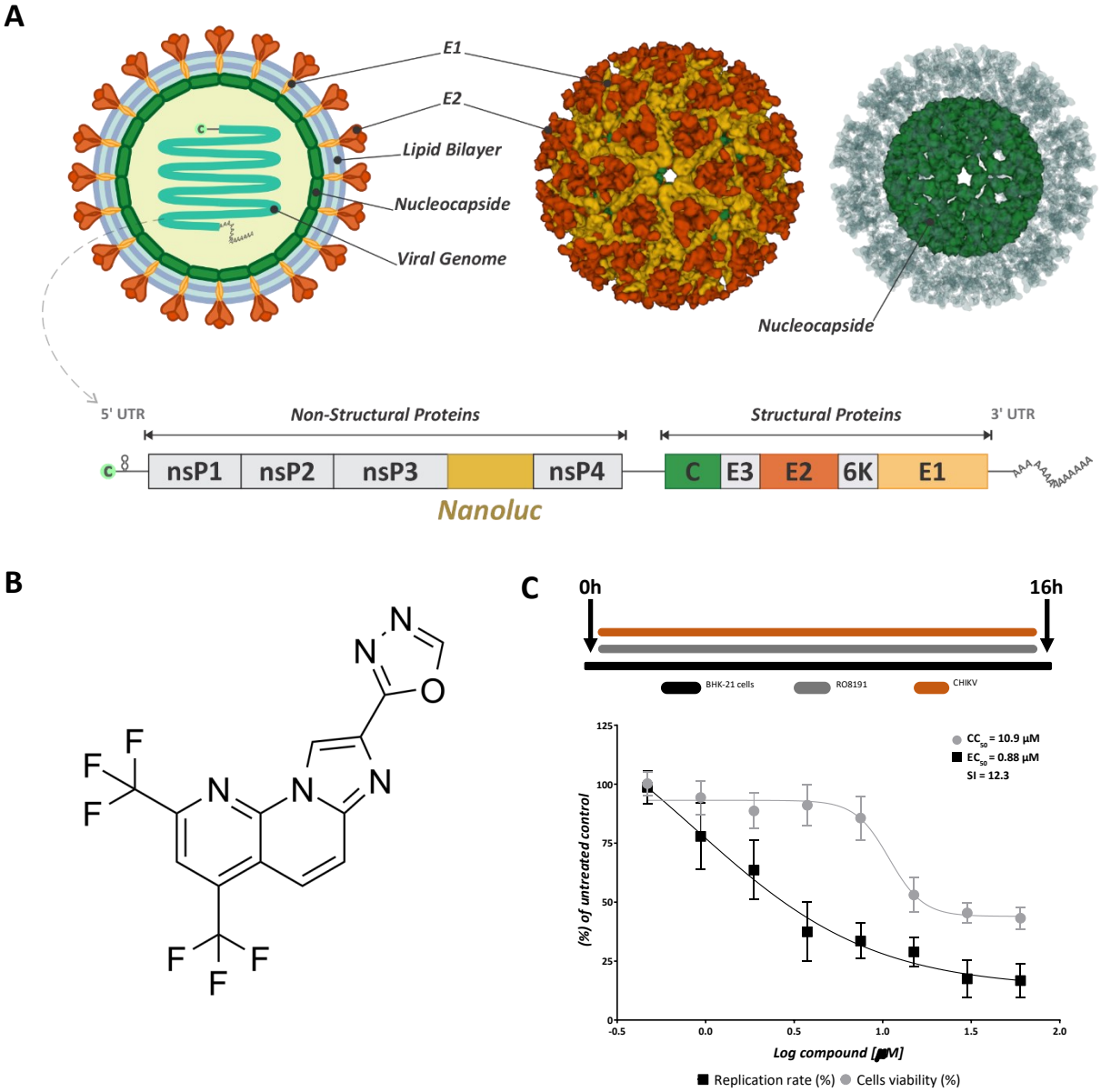

Figure 2

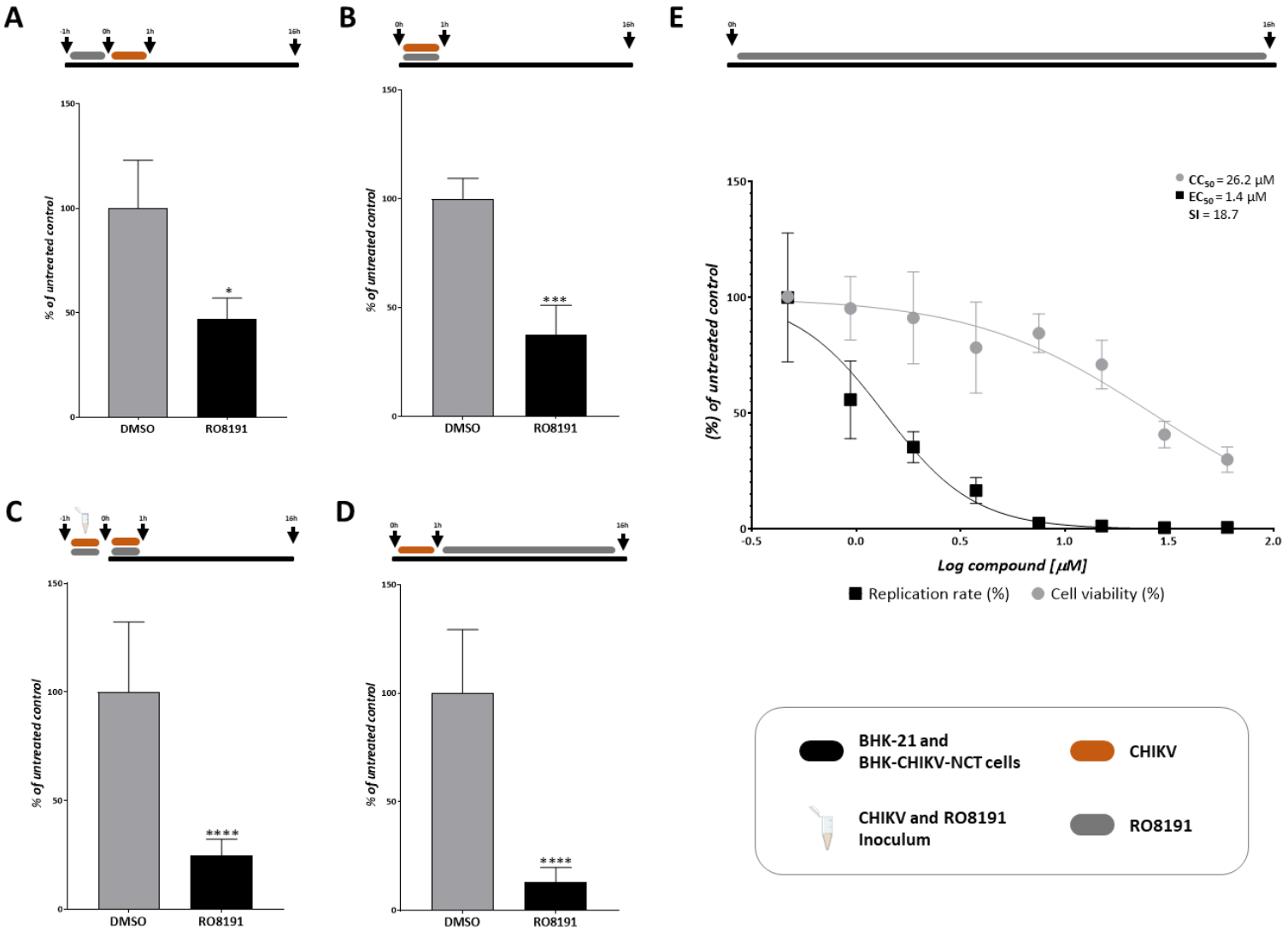
A
B
C
D
E
-1h
0h
1h
16h
% of untreated control
DMSO
RO8191
*
***
****
(%) of untreated control
Log compound [µM]
CC50 = 26.2 µM
EC50 = 1.4 µM
SI = 18.7
Replication rate (%)
Cell viability (%)
BHK-21 and BHK-CHIKV-NCT cells
CHIKV
CHIKV and RO8191 Inoculum
RO8191

Figure 3

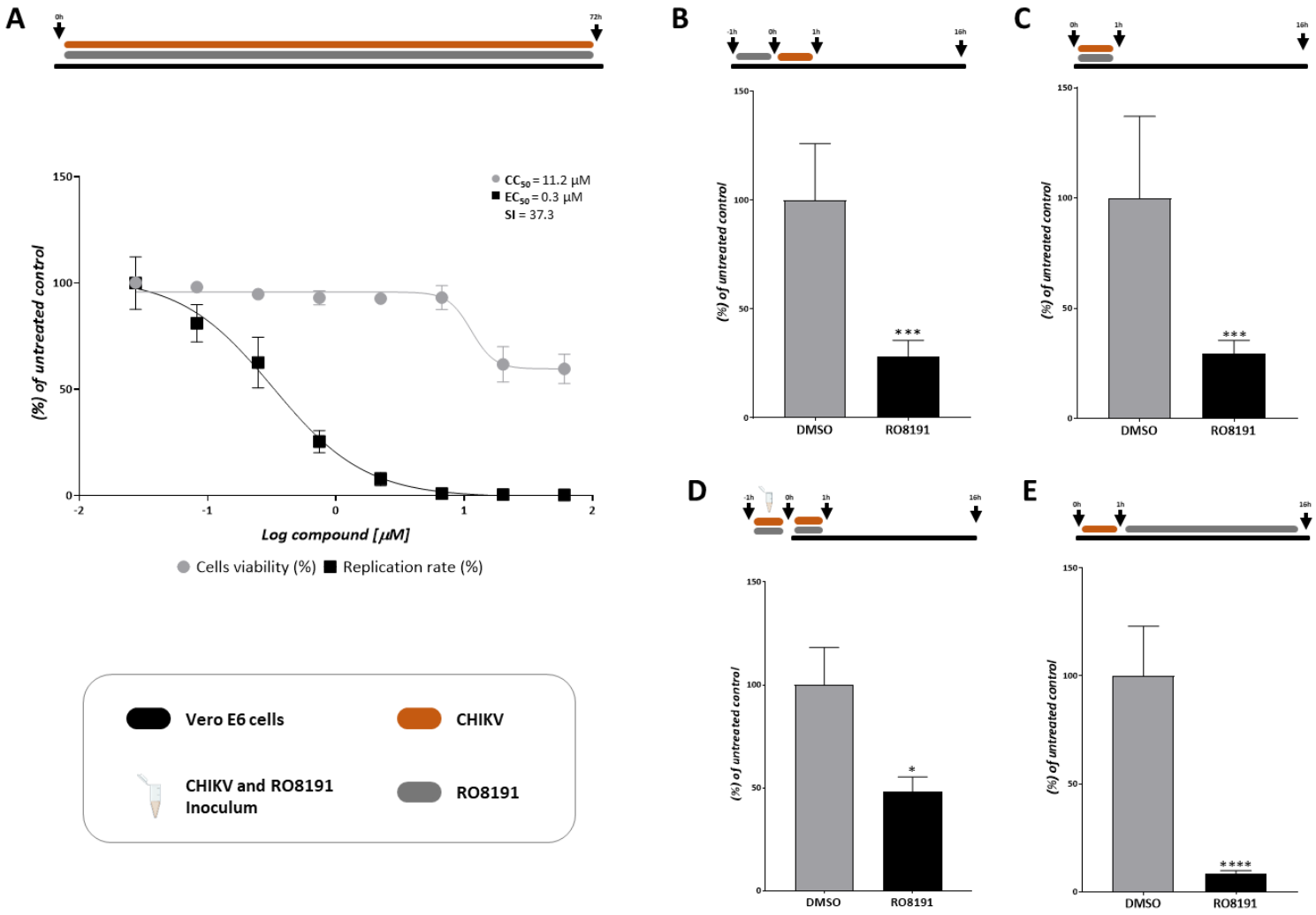
A
0h
72h
150
100
50
0
-2
-1
0
1
2
(%) of untreated control
Log compound [µM]
CC50 = 11.2 µM
EC50 = 0.3 µM
SI = 37.3
Cells viability (%)
Replication rate (%)
Vero E6 cells
CHIKV
CHIKV and RO8191 Inoculum
RO8191
B
-1h
0h
1h
16h
(%) of untreated control
***
DMSO
RO8191
C
0h
1h
16h
(%) of untreated control
***
DMSO
RO8191
D
-1h
0h
1h
16h
(%) of untreated control
*
DMSO
RO8191
E
0h
1h
16h
(%) of untreated control
****
DMSO
RO8191

Figure 4

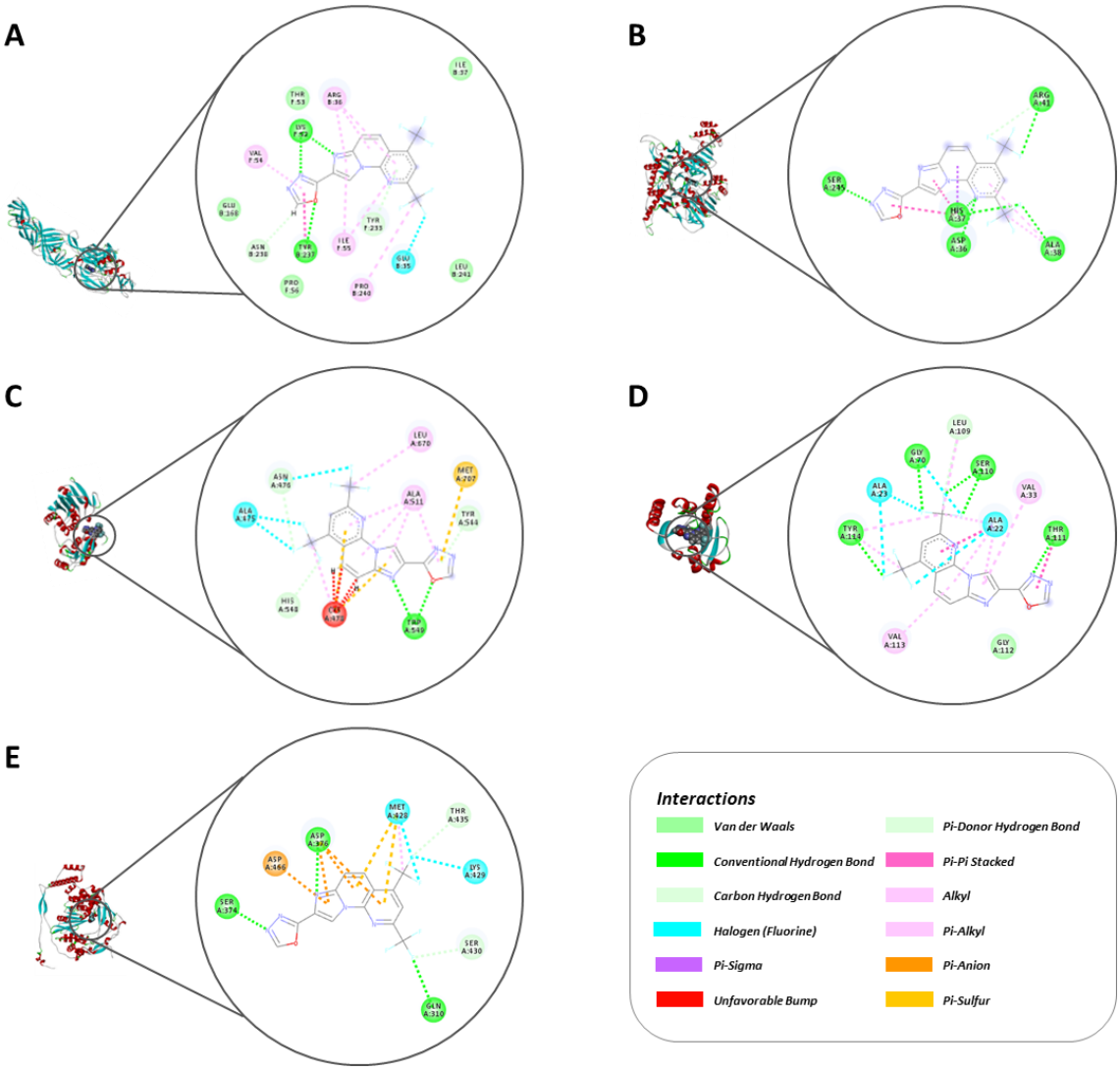
A
B
C
D
E
Interactions
Van der Waals
Conventional Hydrogen Bond
Carbon Hydrogen Bond
Halogen (Fluorine)
Pi-Sigma
Unfavorable Bump
Pi-Donor Hydrogen Bond
Pi-Pi Stacked
Alkyl
Pi-Alkyl
Pi-Anion
Pi-Sulfur

Figure 5

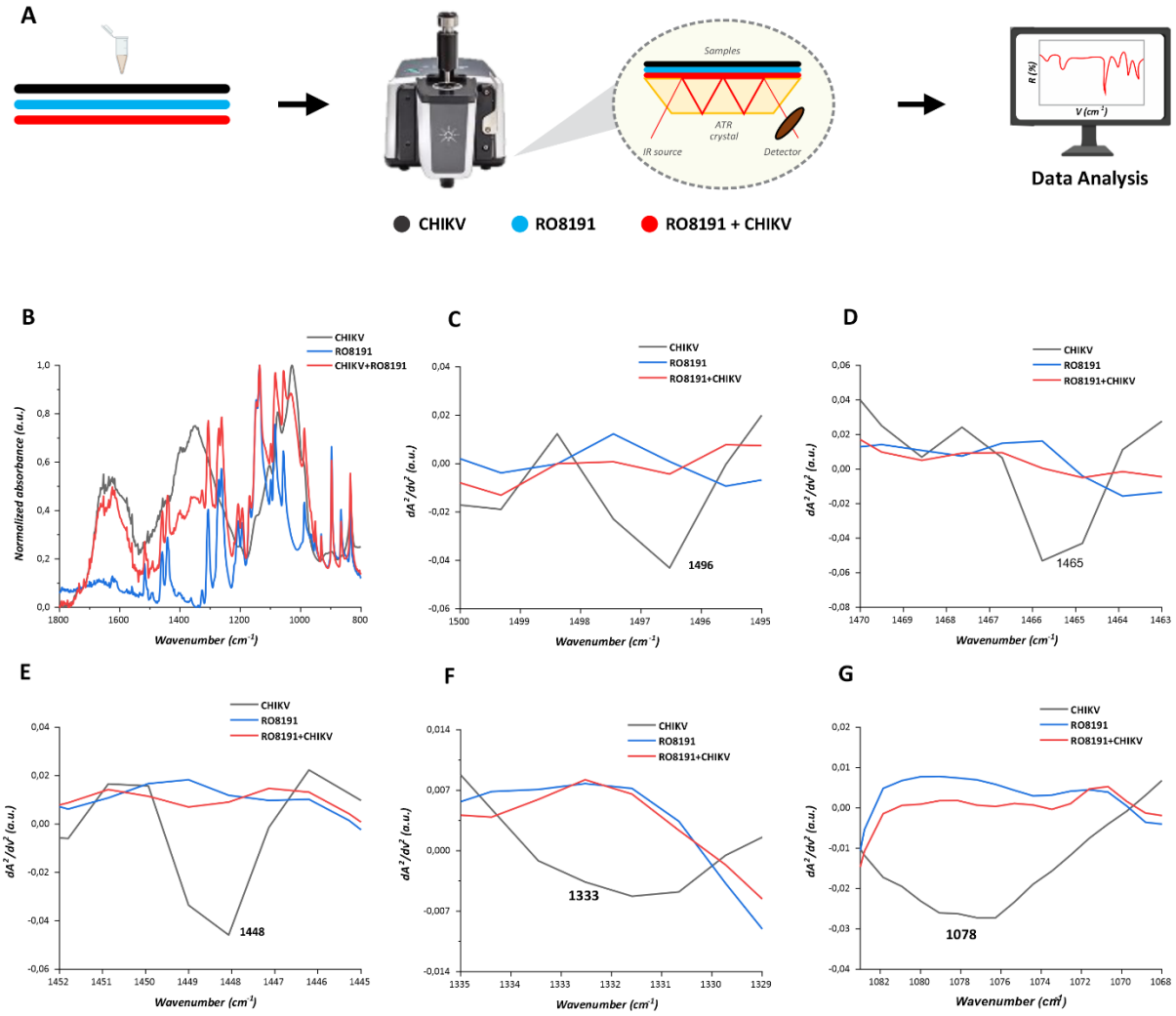
A
Samples
ATR crystal
IR source
Detector
R (%)
V (cm⁻¹)
Data Analysis
CHIKV
RO8191
RO8191 + CHIKV
B
CHIKV
RO8191
CHIKV+RO8191
Normalized absorbance (a.u.)
Wavenumber (cm⁻¹)
C
RO8191+CHIKV
1496
D
1465
E
1448
F
1333
G
1078

SUPPLEMENTARY MATERIAL

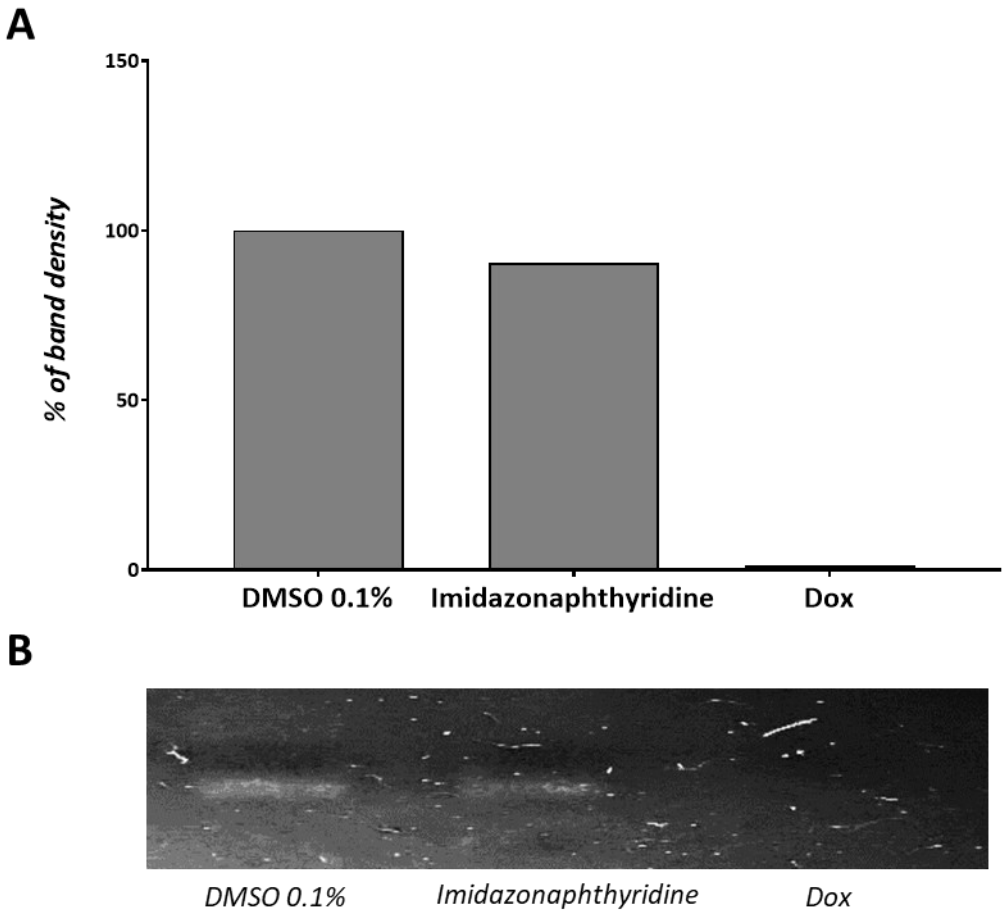

Supplementary Figure 1. RO8191 activity on dsRNA interaction. A-B) RO8191 does not interact with dsRNA (90.4% of bar density) compared with Doxorubicin (1.3% of bar density), a positive control used for this assay. Images were generated using GraphPad Prism 8 and GIMP 2.1v.

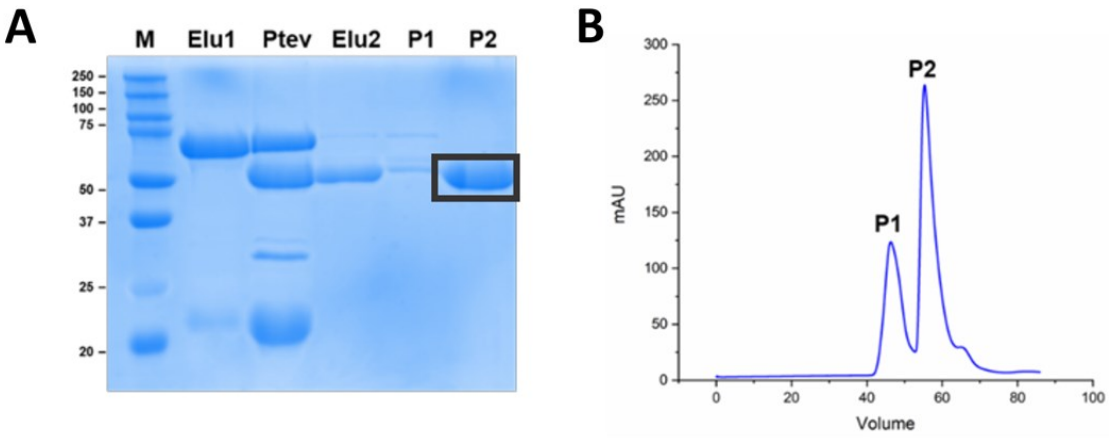

Supplementary Figure 2. nsp4-CHIKV purification. A) Acrylamide gel electrophoresis of nsP4-CHIKV purification steps. M: molecular weight marker; Elu1: fraction eluted after the first affinity chromatography step; Ptev: fraction obtained after TEV protease cleavage; Elu2: fraction eluted after the second affinity chromatography step; P1 and P2: fractions eluted in gel filtration step. The P2 corresponds to the purified nsP4-CHIKV (54.54 kDa). B) Chromatogram of gel filtration step. in which the second peak (P2) corresponds to the purified nsP4-CHIKV (54.54 kDa).

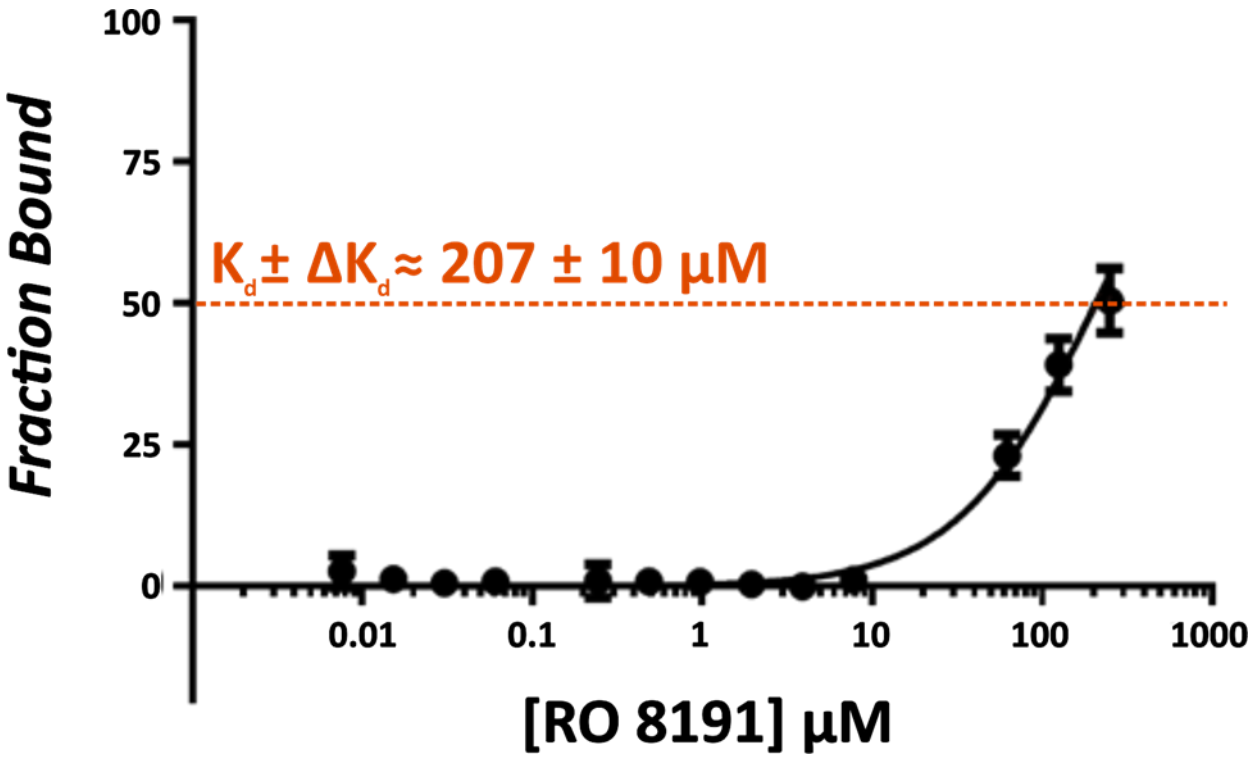

Supplementary Figure 3. Binding affinity of nsP4 and RO8191. The nsP4 binding affinity was performed by MST, using a serial dilution of the compound (250 µM to 0.0076 µM) to obtain the dissociation constant estimated $k_d \pm \Delta k_d = >207 \pm 10$ µM fitting the binding curve with the Hill function.

CAPÍTULO III

CONSIDERAÇÕES FINAIS

Considerações finais

Os resultados deste trabalho demostraram o potencial antiviral do composto RO8191 contra a infecção *in vitro* pelo CHIKV, o qual representa grande importância clínica e preocupação para saúde pública no Brasil. Esperamos que este trabalho possa contribuir na caracterização do modo de ação desta molécula contra o CHIKV. Estudo *in vivo,* registrados na literatura, candidatam o RO8191 como uma alternativa viável para o tratamento desta e de muitas outras doenças virais negligenciadas no mundo.

ANEXOS

ARTIGOS PUBLICADOS

www.nature.com/scientificreports

scientific reports

Check for updates

OPEN

Characterization of the RNA-dependent RNA polymerase from Chikungunya virus and discovery of a novel ligand as a potential drug candidate

Marjorie C. L. C. Freire[1], Luis G. M. Basso [2], Luis F. S. Mendes [3], Nathalya C. M. R. Mesquita [1], Melina Mottin[4], Rafaela S. Fernandes [1], Lucca R. Policastro[1], Andre S. Godoy [1], Igor A. Santos [5], Uriel E. A. Ruiz[5], Icaro P. Caruso [6,7], Bruna K. P. Sousa [4], Ana C. G. Jardim [5,6], Fabio C. L. Almeida [7,8], Laura H. V. G. Gil[9], Carolina H. Andrade [4] & Glaucius Oliva[1]✉

Chikungunya virus (CHIKV) is the causative agent of Chikungunya fever, an acute febrile and arthritogenic illness with no effective treatments available. The development of effective therapeutic strategies could be significantly accelerated with detailed knowledge of the molecular components behind CHIKV replication. However, drug discovery is hindered by our incomplete understanding of their main components. The RNA-dependent RNA-polymerase (nsP4-CHIKV) is considered the key enzyme of the CHIKV replication complex and a suitable target for antiviral therapy. Herein, the nsP4 CHIKV was extensively characterized through experimental and computational biophysical methods.

In the search for new molecules against CHIKV, a compound designated LabMol-309 was identified as a strong ligand of the nsp4-CHIKV and mapped to bind to its active site. The antiviral activity of LabMol-309 was evaluated in cellular-based assays using a CHIKV replicon system and a reporter virus. In conclusion, this study highlights the biophysical features of nsP4-CHIKV and identifies a new compound as a promising antiviral agent against CHIKV infection.

The Chikungunya virus (CHIKV) belongs to the *Togaviridae* family and is the causative agent of Chikungunya fever. The main transmission route occurs through the bite of infected female mosquitoes of the *Aedes* sp. Genus. After CHIKV infection, the proportion of individuals who develop clinical and debilitating symptoms is considered the highest compared to other arboviruses, with an average of 80% of symptomatic cases[1,2]. The control of the mosquito vector remains the best prophylaxis since there are no licensed vaccines or efficient antivirals available[3]. In this scenario, the infection caused by CHIKV has a high social impact and constitutes a serious public health issue[3].

[1]Institute of Physics of Sao Carlos, University of Sao Paulo, Sao Carlos, SP, Brazil. [2]Physical Sciences Laboratory, State University of Northern Rio de Janeiro Darcy Ribeiro (UENF), Campos dos Goytacazes, RJ, Brazil. [3]Departament of Physics, Ribeirao Preto School of Philosophy, Science and Literature, University of Sao Paulo, Ribeirao Preto, SP, Brazil. [4]Laboratory for Molecular Modeling and Drug Design, Labmol, Faculty of Pharmacy, Universidade Federal de Goiás, Goiânia, GO, Brazil. [5]Institute of Biomedical Sciences, Federal University of Uberlandia, Uberlandia, MG, Brazil. [6]Institute of Biosciences, Humanities and Exact Sciences (Ibilce), Sao Paulo State University (Unesp), Campus Sao Jose do Rio Preto, Sao Jose do Rio Preto, SP, Brazil. [7]Institute of Medical Biochemistry (IBqM) Leopoldo de Meis, National Center of Nuclear Magnetic Resonance Jiri Jonas, Federal University of Rio de Janeiro, Rio de Janeiro, RJ, Brazil. [8]National Center of Nuclear Magnetic Resonance (CNRMN), Center of Structural Biology and Bioimaging (CENABIO), Federal University of Rio de Janeiro, Rio de Janeiro, RJ, Brazil. [9]Instituto Aggeu Magalhaes (IAM-FIOCRUZ), Recife, PE, Brazil. ✉email: oliva@ifsc.usp.br

Chikungunya fever presents an acute phase characterized by high fever, arthralgia, myalgia, headaches, edema, periorbital pain and cutaneous rash[4,5]. Later, some patients progress to the so-called chronic phase, mainly characterized by persistent arthralgia and musculoskeletal pain for months and even years[4,6–8]. Since there are no specific antiviral drug treatments, the clinical management targets primarily the relief of symptoms using analgesics and antipyretics in the acute phase; and non-steroidal anti-inflammatory drugs (NSAIDs) and cor- ticosteroids in the chronic phase[5].

CHIKV is a spherical, enveloped, and positive single-stranded RNA virus. As a member of the Alphavirus genus, its genome has approximately 12 kb and codes for two distinct polyproteins: non-structural and structural [9]. The first one is cleaved and gives rise to four non-structural proteins (nsP1, nsP2, nsP3 and nsP4) that form the viral replication complex and have functions in the infection process, such as interaction with host factors[9–11]. The nsP1 has methyltransferase and guanylyltransferase activities, promoting the capping of viral RNA. In addition, this protein also anchors the replication complex in the cell membrane [12]. The nsP2 is a multifunctional protein with NTPase and helicase activities in the N-terminal region. Its C-terminal has a cysteine-protease activity, responsible for processing the non-structural polyprotein [12]. The nsP3 is an accessory protein that recruits host cell factors that participate in and optimize the replicative process [13]. Finally, nsP4 is the RNA-dependent RNA polymerase (RdRp), which is considered the key enzyme of the CHIKV replication complex and acts principally by promoting the synthesis and elongation of viral RNA[14].

On the other hand, the structural polyprotein is cleaved, giving rise to five structural proteins—E1, E2, E3, C and 6 k—which are part of the viral assembly and structure [9]. The envelope proteins, specially E2 and E1, are responsible for virus anchoring, receptor interaction and membrane fusion, promoting virus entry in the host cell[15,16]. Due to its location on the viral surface, envelope proteins are targets of the humoral immune response and thus become targets for vaccine development against CHIKV[17].

Therefore, due to their vital role in the viral life cycle, non-structural proteins emerge as potential targets for developing antiviral drugs, aiming to interrupt the replication process and, consequently, the viral elimination[18]. Among these proteins, nsP4 is an attractive target due to its central role in viral genome replication, transcription and genome repair[14,19]. Recently, the three-dimensional structures of the RdRp domain of Sindbis (SINV) and Ross River (RRV) viruses has been experimentally solved[20]. However, the structure of this domain of CHIKV (nsP4-CHIKV) has not been reported. This fact generates limitations and challenges when the final goal is apply- ing structure- based drug design strategies against this target.

Due to the lack of high-resolution structural information on the nsP4-CHIKV and the need to search for new drugs to treat the infection caused by the virus, we present here a detailed biophysical characterization of this protein. Size exclusion chromatography coupled with multi-angle light scattering was used to infer the oligomeric state of the nsp4-CHIKV protein in solution. A high prevalence of ordered helical secondary struc- tures was observed by circular dichroism, which also showed that the nsP4-CHIKV unfolds under a cooperative transition during thermal denaturation. The thermal denaturation was further studied using differential scanning calorimetry, indicating a kinetically controlled process.

Moreover, in the search for ligands for the development of new inhibitors, we selected 12 compounds for an initial screen using differential scanning fluorimetry experiments. These compounds came from a global collabo- rative project named OpenZika [21,22], through the World Community Grid computational network that enabled massive docking-based virtual screening campaigns for ZIKV proteins as well as other flaviviruses (DENV, YFV, WNV). One compound, LabMol-309, showed a significant effect on nsP4-CHIKV stability and its interaction with the protein was confirmed using a sophisticated combination of experimental and computational strategies.

Furthermore, the inhibitory activity of LabMol-309 was studied in cellular-based antiviral assays using a CHIKV replicon system and a reporter virus, and the results showed that this molecule caused inhibition in these cellular assays and has the potential to be further evaluated as a CHIKV inhibitor. In this way, this work provides novel structural features of nsP4-CHIKV and identifies a new compound that interacts with this protein, generating perspectives in the drug development field to treat the infection caused by CHIKV and potentially other alphaviruses.

Results

nsP4-CHIKV purification and SEC-MALS analysis. The nsP4-CHIKV was bacterially expressed and purified using chromatography systems, and the purity was confirmed by acrylamide gel electrophoresis (Supplementary Fig. 1). The nsP4-CHIKV is formed by 492 amino acids and has a theoretical molecular mass (MM) of 54.54 kDa. This construction covers the entire region of the RNA-dependent RNA polymerase (RdRp) domain, responsible for the nsP4-CHIKV function and where the catalytic aspartic acid residues (Asp371 and Asp466) are located [23]. The Asp466 is in the GDD motif, a highly conserved sequence of viral polymerases [23].

In order to determine the oligomeric state of nsP4-CHIKV in the working buffer solution, Size Exclusion Chromatography coupled with Multi-angle Light Scattering (SEC-MALS) was employed [24]. The SEC-MALS data showed a low polydispersity index and yielded a MM of $(60 \pm 1) kDa$ for nsP4-CHIKV (Fig. 1A). The proximity of the experimental value with the theoretical molecular mass of the protein suggests that the monomeric state is the most populated oligomer under the evaluated conditions.

Evaluation of nsP4-CHIKV secondary structure profile. Circular dichroism (CD) spectroscopy was used to estimate the secondary structure content of nsP4-CHIKV in solution[25]. The CD spectrum of nsP4-CHIKV is characteristic of an α-helical rich protein, with two negative minima at 208 and 222 nm and one positive maximum around 195 nm (Fig. 1B). This profile corroborates with structural features described for viral polymerases and other polymerase structures solved experimentally [23].

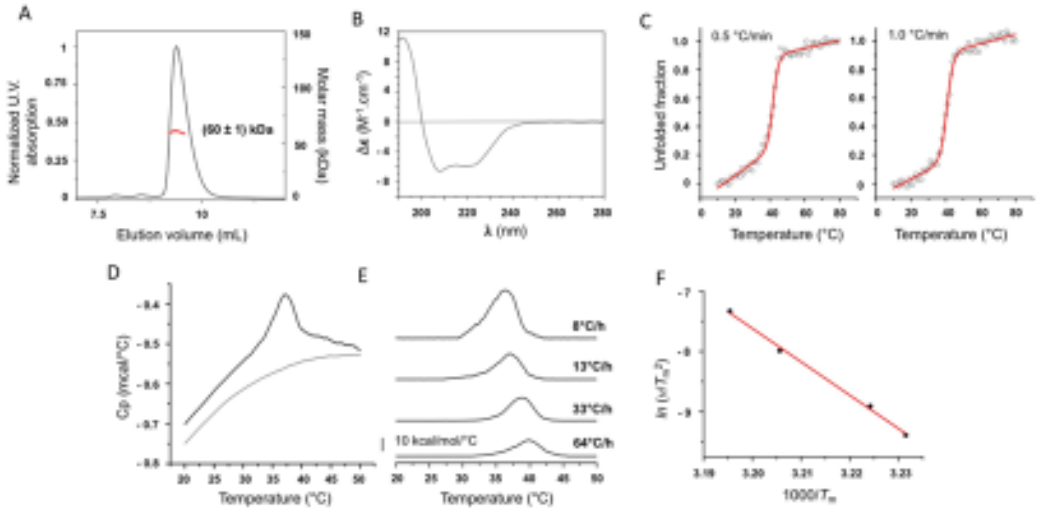

Figure 1. Biophysical characterization of nsP4-CHIKV. (**A**) SEC-MALS analysis of nsP4-CHIKV in solution. The proximity of the estimated molecular weight of (60 ± 1) kDa with the molecular weight of the protein suggests that nsP4-CHIKV is mostly at a monomeric state under the evaluated conditions. (**B**) Secondary structure profile of nsP4-CHIKV by CD spectroscopy. The nsP4-CHIKV spectrum suggests the predominance of helical secondary structures. (**C**) Thermal stability of nsP4-CHIKV probed by CD spectroscopy. The ellipticity at 222 nm as a function of temperature for nsP4-CHIKV was recorded at 0.5 °C/min (left) and 1.0 °C/min (right) and transformed to the protein unfolded fraction. Solid lines are best fits to the CD data using a two-state equilibrium model. The thermodynamic parameters of the protein unfolding transition are summarized in Table 1. (**D**) Scan-rate normalized (13 °C/h) DSC data of the irreversible thermal denaturation of 11.9 µM of nsP4-CHIKV and the corresponding instrumental buffer (50 mM Tris–HCl pH 8.0, 200 mM NaCl e 5% glycerol) baseline. (**E**) Excess heat capacity of nsP4-CHIKV at the indicated scan rates obtained after normalization by protein concentration and subtraction of the buffer baseline. (**F**) Arrhenius-type plot showing the scan rate dependence of the nsP4-CHIKV unfolding temperature, T_m. The slope yields the activation energy for the irreversible denaturation of nsP4-CHIKV.

Rate (°C/min)	T_m (°C)	ΔH_{vH} (kcal/mol)	ΔS_{vH} (cal/mol K)
0.5	41.8 ± 0.2	122 ± 12	387 ± 38
1.0	45.7 ± 0.2	104 ± 8	331 ± 26

Table 1. Thermodynamic parameters of nsP4-CHIKV unfolding by CD spectroscopy. The T_m and the ΔH_{vH} were determined by fitting the CD data to a two-state equilibrium model[33]. The ΔS_{vH} of the unfolding transition at T_m was calculated as $\Delta S_{vH} = \Delta H_{vH}/T_m$, since $\Delta G = 0$ at T_m.

Dichroweb was used in the quantitative analysis of the CD spectrum[36]. The best-fit spectra were obtained with the CDSSRT method[37], which displayed an NRMSD of 0.009 for the SP175 database and 0.012 for Sets 4 and 7, considered the most representative of the secondary structure content of nsP4-CHIKV (Supplementary Table 1). Secondary structure content estimation from the CD spectrum confirmed the higher percentage of α-helix in the nsP4-CHIKV (60%). The remaining fractions were: 6.3% of sheets, 9.6% of turns and 24% of disordered structure.

nsP4-CHIKV thermal stability profile through CD spectroscopy and DSC. The CD technique was also applied to study the thermal behavior of this protein when subjected to temperature variations[38]. The unfolding transition of nsP4-CHIKV was studied by monitoring the ellipticity at 222 nm as a function of temperature[38]. The results showed that the thermal denaturation process occurred cooperatively, exhibiting the transition from folded to unfolded states in a defined way (Fig. 1C).

The thermodynamic parameters of the nsP4-CHIKV unfolding were obtained by adjusting a two-state equilibrium model to the experimental data. Changes in the heat capacity were not considered, and the fitting was performed taking into account the linear changes in pre- and post-transition ellipticity as a function of the temperature[38]. Thus, the melting temperature (T_m), the apparent enthalpy change (ΔH_{vH}), and the apparent entropy change (ΔS_{vH}) for the same protein concentration were obtained at two different heating rates (Table 1).

Concentration (μM)	Rate (°C/h)	T_m (°C)	ΔH_{cal} (kcal/mol)	$\Delta T_{1/2}$ (°C)	ΔS (cal/mol)	ΔH_{VH} (kcal/mol)
9.3	8	36.3	205	4.8	662	142
11.9	13	37.0	102	4.4	330	151
7.4	33	38.8	86	4.3	275	165
7.4	64	39.8	66	4.5	210	150

Table 2. Thermodynamic parameters associated with the nsP4-CHIKV thermal denaturation by DSC. T_m represents the temperature where C_P reaches its maximum value. ΔH_{cal} was calculated as the area under the DSC trace. $\Delta T_{1/2}$ corresponds to the linewidth at half the height of the transition peak. The entropy change at T_m, ΔS, was calculated as $\Delta S = \Delta H_{cal}/T_m$. ΔH_{VH} was calculated as $4RT\frac{2}{m}C_{p,max}/\Delta H_{cal}$. Analyses of the thermograms were performed with MicroCal Origin software. Uncertainties: T_m (± 0.2 °C), ΔH_{cal} (± 1–3 kcal/mol), $\Delta T_{1/2}$ (± 0.2 °C).

The thermodynamic parameters of the nsP4-CHIKV unfolding transition exhibited a dependence on the heating rate. This result suggests that the irreversible nsP4-CHIKV unfolding transition is kinetically dependent[29,30]. The values of the enthalpy and entropy changes obtained from the CD data agree well with those observed for globular proteins[31]. The thermal behavior of nsP4-CHIKV was also evaluated using Differential Scanning Calorimetry (DSC)[32]. Figure 1D shows the temperature-dependence of the heat capacity profile (C_P – sample minus reference) of nsP4-CHIKV and the instrumental buffer baseline, acquired with a scan rate of 13 °C/h. The protein C_P was subtracted from the buffer baseline C_P and normalized to the protein concentration.

DSC experiments were performed at different scan rates to investigate its effect on the DSC profile and the reversibility of the transitions. The temperature- and scan rate dependence of the excess heat capacity profile of nsP4-CHIKV are illustrated in Fig. 1E. The nsP4-CHIKV undergoes an irreversible thermal denaturation, and the values of the calorimetric enthalpy change (ΔH_{cal}) obtained from the analysis of the thermograms are within the range of values observed for other globular proteins[33–36]. Moreover, the transition peak shows a clear scan rate dependence, confirming that all thermodynamic parameters associated with nsP4-CHIKV thermal denaturation depend upon the heating rate (Table 2), as observed in our previous CD analysis. Except for the van't Hoff enthalpy change (ΔH_{VH}), the dependences of the thermodynamic parameters on the heating rate are markedly non-linear (Table 2 and Supplementary Fig. 2). This feature illustrates the non-equilibrium character of the protein denaturation process.

The dependence of T_m on the scan rate was used to calculate the kinetic activation energy, E_a, for the irreversible nsP4-CHIKV thermal denaturation. According to Sanchez-Ruiz et al.[30], the T_m shifts induced by different heating scan rates, v, for an irreversible two-state process can be modeled by the following equation:

$$\frac{\nu}{T_m^2} = \frac{AR}{E_a} e^{-\frac{E_a}{RT_m}}$$

where A is the pre-exponential factor in the Arrhenius equation, and R is the gas constant. Thus, by plotting $ln\ \nu/T_m^2$ against $1/T_m$, the apparent activation energy can be determined from the slope of the curve. The Arrhenius plot showing the scan rate-dependent changes in the T_m is illustrated in Fig. 1F, from which E_a was determined as (110 ± 4) kcal/mol.

Evaluation of nsp4-CHIKV interaction with compounds. In the search for new compounds able to interact and inhibit the nsP4-CHIKV in solution, an initial experimental screening with a series of 12 compounds (Supplementary Table 2) was selected from the OpenZika project[22,37] and performed using differential scanning fluorimetry (DSF or ThermoFluor assay). For nsP4-CHIKV, the T_m in the absence of compounds (only with DMSO) was 37.7 ± 0.4 °C. Among the compounds, LabMol-309 (Fig. 2A) caused the highest thermal shift (~ 4 °C), suggesting the occurrence of interaction with nsP4-CHIKV. Therefore, this compound was chosen to proceed with the other assays.

The interaction between LabMol-309 and nsP4-CHIKV was later analyzed by MicroScale thermophoresis (MST) and solution nuclear magnetic resonance (NMR). The MST data showed an affinity curve with the occurrence of well-defined bound and unbound states (Fig. 2B). From that, the dissociation constant (K_D) for the interaction of nsP4-CHIKV with LabMol-309 was estimated as (6 ± 1) μM.

The interaction of LabMol-309 with nsP4-CHIKV was further evaluated by solution NMR, monitoring the chemical shift perturbation (CSP). Figure 2C shows the spectra obtained for the compound LabMol-309 in the presence (red line) and absence of the protein (blue line). These spectra were superimposed, and the chemical shift differences were identified and mapped according to the respective positions of the proton resonances (Fig. 2C) previously identified in the LabMol-309 assignment (Supplementary Fig. 3).

Therefore, detecting these chemical shifts perturbations is additional evidence for the interaction between nsP4-CHIKV and compound LabMol-309, reinforcing the results obtained using DSF and MST.

The nsP4-CHIKV three-dimensional model and structural analysis. A combined analysis of several biophysical techniques suggests that the nsP4-CHIKV is a monomeric α-helical rich protein capable of forming a complex with the compound LabMol-309 within a moderate dissociation constant (10^{-6} M). The nsP4-CHIKV 3D structural model was obtained using AlphaFold[38]. The model obtained showed a very high

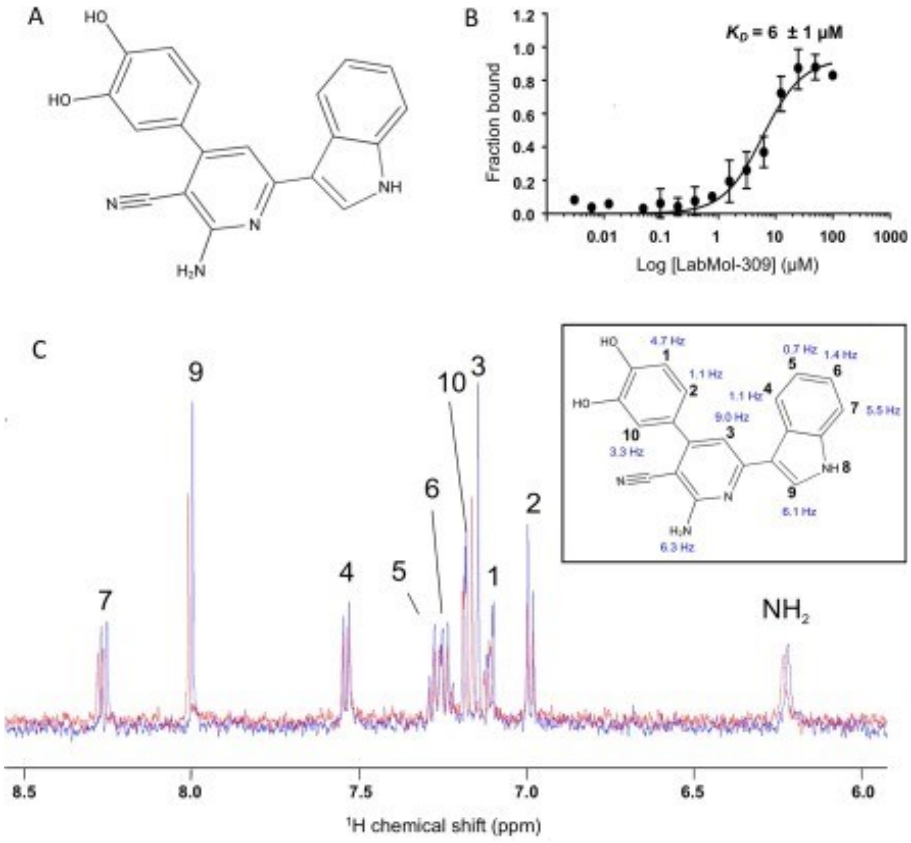

Figure 2. Evaluation of nsp4-CHIKV interaction with the compound LabMol-309. (**A**) LabMol-309 chemical structure. (**B**) Binding affinity curve of nsP4-CHIKV interacting with LabMol-309 by MST. The compound LabMol-309 was titrated in a concentration range of 200 µM to 0.012 µM. The curve was fitted to the Hill function, and the estimated K_D was (6 ± 1 µM). (**C**) Chemical shift perturbation analysis based on the superimposition of LabMol-309 one-dimensional 1H spectra obtained in the presence (red line) and the absence of nsP4-CHIKV (blue line). On the right, chemical shift differences were measured (in Hz) for each proton of the LabMol-309 structure.

per-residue confidence score (pLDDT) for more than 90% of the covered sequence, and only for the N- and C-terminal regions pLDDT were low (Fig. 3A). The full-length nsP4-CHIKV structural model is illustrated in Fig. 3.

In the nsP4-CHIKV structure, we identified the regions corresponding to the *fingers* (residues 93–315), *palm* (residues 316–502) and *thumb* (residues 503–611) domains, which are characteristics of viral polymerases (Fig. 3B). In the palm domain's catalytic site, we also identified the catalytic aspartic acid dyad (Asp371 and Asp466) separated by 7.5 Å. Besides, the nsP4-CHIKV model contains an extra N-terminal domain (*residues 1–92),* forming a coiled-coil.

In the model of nsP4-CHIKV, the electrostatic surface potential of the active site cavity where are located the aspartic acid dyad (Asp371 and Asp466) is remarkably positive, a signature of nucleic acids-interacting motifs (Fig. 3C)[39]. Additionally, the analysis using ConSurf reveals that the catalytic site region and its surroundings are highly conserved (Fig. 3D). These results serve as corroboration for the robustness of the AlphaFold model of nsP4-CHIKV.

Molecular docking and molecular dynamics of LabMol-309 against nsP4-CHIKV. Docking calculations were used to investigate the binding mode of LabMol-309 at the nsP4-CHIKV. The docking results suggest that LabMol-309 binds to the nsP4-CHIKV active site, interacting with the GDD catalytic triad (Asp466 and Asp467), with a docking score of -7.15 kcal/mol^{-1}. LabMol-309 makes H-bonds with Glu369, Asp466, Asp467,

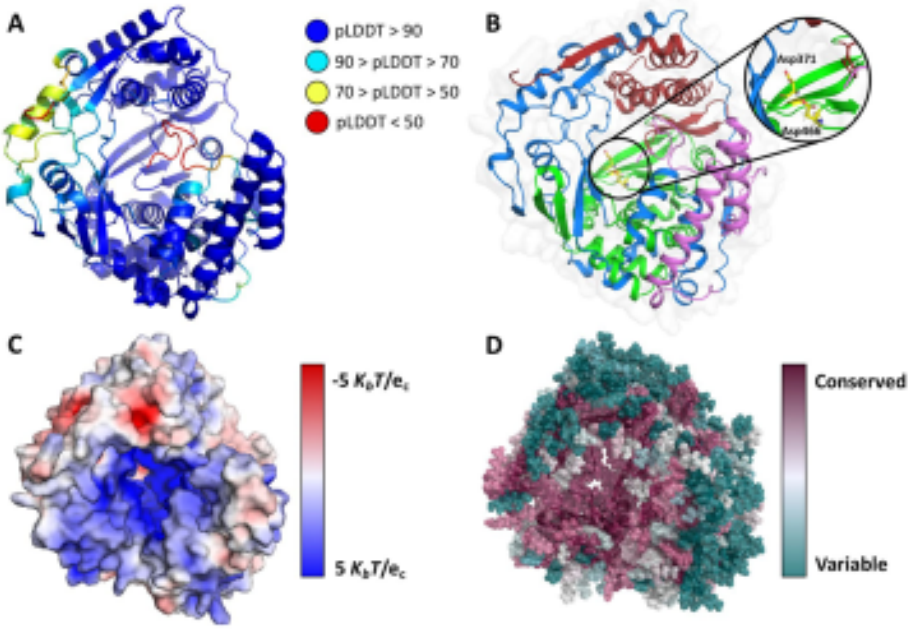

Figure 3. nsP4-CHIKV three-dimensional model by AlphaFold. (**A**) nsP4-CHIKV AlphaFold model colored according to pLDDT. At the top right are shown the pLDDT color scales. (**B**) Model of nsP4-CHIKV colored according to domain assignment. The N-terminal helixes, *finger*, *palm* and *thumb* domains are colored in purple, dark blue, green and red, respectively. A detailed view of predicted catalytic aspartic residues is presented in the inset. (**C**) Electrostatic potential projected on the surface charge of nsP4-CHIKV, calculated with APBS. Positive regions are colored in blue and negative regions are in red. (**D**) ConSurf analysis of nsP4-CHIKV model. The amino acids are colored by their conservation grades using the color-coding bar, with green-through-purple indicating variable-through-conserved.

Gly507, Arg573 and cation–π interactions with Lys295 residue (Fig. 4). The nitrogen atom of the indole group and amine of the pyridine group of LabMol-309 make relevant interactions with Asp466 and Asp467, respec- tively. Additionally, the indole group makes cation–π interaction with Lys295.

The structural stability of the structural model of the nsP4-CHIKV/LabMol-309 complex calculated by docking was evaluated using 100 *ns* molecular dynamics (MD) simulation. Figure 5A presents the values of root mean square deviation (RMSD) for the backbone atoms of the protein and non-hydrogen atoms of the ligand from the initial structure. It is possible to observe that RMSD values are stable after 5 *ns* of simulation and reach plateaus around 0.3 and 0.5 *nm* for the protein and ligand, respectively. Figure 5B shows that the number of contacts < 0.6 nm between nsP4-CHIKV and LabMol-309 does not drop down to zero throughout the MD simu- lation, indicating that the ligand interacts with the protein is persistent. The number of hydrogen bonds is stable throughout the MD simulations and presents an average value of three (Fig. 5C). An evaluation of the hydrogen bonds with significant percentage occupancy (< 5%, Supplementary Table 3) during the MD trajectory reveals that Glu369, Asp371, Asp466, Asp467, Asn468, Lys501, and Arg573 are important for the stabilization of the protein–ligand complex, and further mutagenesis studies may be relevant for confirmation of these interactions. It is worth noting that Glu369 and Asp371 presented percentage occupancies higher than 70%. Considering all MD analyses, it can be concluded that the structural model of the nsP4-CHIKV/LabMol-309 complex is stable throughout the simulation.

Inhibition of CHIKV replication by LabMol-309 through replication-based and viral infection assays. The inhibitory activity of the compound LabMol-309 was evaluated through the replicon-based screenings in a dose-dependent manner to determine its effective and cytotoxic concentrations (EC_{50} and CC_{50}, respectively). Replicon cells were incubated with twofold serial dilutions of compound (from 20 to 0.03 µM for EC_{50} and from 100 to 0.30 µM for CC_{50}), and luciferase signals or cell viability was evaluated after 48 h. Lab- Mol-309 displayed an EC_{50} value of 10.0 ± 0.07 µM and showed a CC_{50} of 17.1 ± 0.6 µM (Fig. 6; Supplementary Table 4 and 5). As a result, the obtained selectivity index (CC_{50}/EC_{50}) of LabMol-309 was 1.7 in the replicon system.

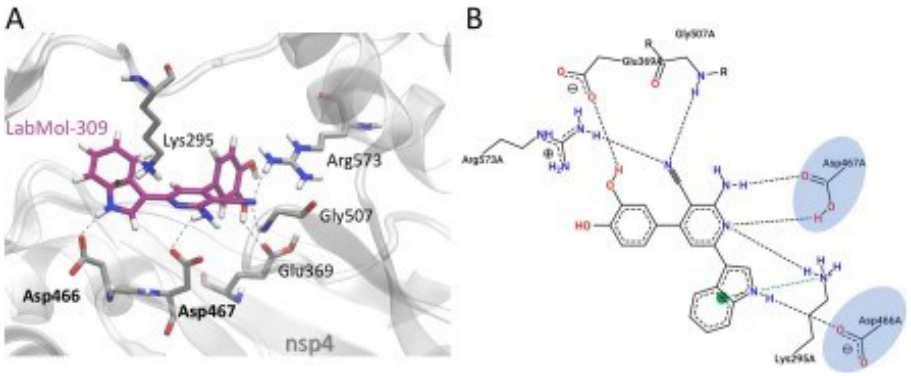

Figure 4. Molecular interactions of LabMol-309 and nsP4-CHIKV, predicted by docking calculations. (**A**) 3D interactions of LabMol-309 and nsP4-CHIKV residues. Hydrogen bonds are shown as gray dashed lines, and cation–π interactions are shown in green dashed lines. Oxygen, nitrogen and hydrogen atoms are shown in red, blue and white, respectively. Carbon atoms of LabMol-309 and protein residues are shown in purple and gray, respectively. Catalytic residues of the GDD triad are highlighted in bold. (**B**) 2D interaction diagram of LabMol-309 and nsP4-CHIKV residues. Hydrogen bonds are shown as gray dashed lines, and cation–π interactions are shown in green dashed lines. Catalytic residues of the GDD triad are highlighted in blue.

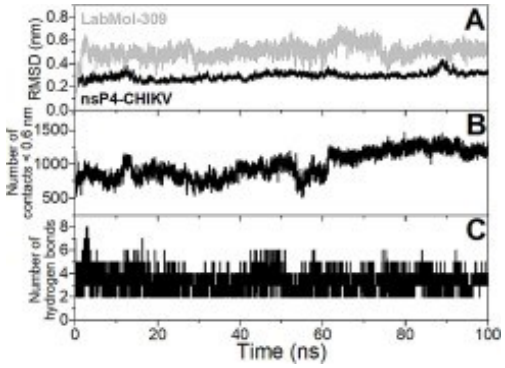

Figure 5. Evaluation of the stability of the structural model of the nsP4-CHIKV/LabMol-309 complex from 100 ns MD simulation. (**A**) RMSDs of backbone atoms of the protein (black line) and non-hydrogen atoms of the ligand (gray line). (**B**) Number of contacts between atoms of the protein and ligand for distances less than
0.6 nm. (**C**) Number of hydrogen bonds formed between the protein and ligand.

To confirm the antiviral activity of the LabMol-309, we carry out the effective concentration of 50% (EC_{50}) and cytotoxic concentration of 50% (CC_{50}) using BHK-21 cells infected with CHIKV-*nanoluciferase*, a recombinant CHIKV that express the Nanoluciferase reporter, at a multiplicity of infection (MOI) of 0.1, with a two-fold serial dilution of LabMol-309 at concentrations ranging from 0.78 to 100 µM. N*anoluciferase* activity levels, proportional to viral replication, were assessed 16 h post-infection (adapted from[40,41]). The cytotoxic concentration of 50% (CC_{50}) was determined in parallel experiments (Fig. 6C). As a result, these assays demonstrated that the LabMol-309 has a EC_{50} of 5.2 µM on BHK-21 cells infected with CHIKV-*nanoluc* and CC_{50} of 52 µM on naive BHK-21 cells, over a period of incubation of 48 h, resulting in a Selectivity Index (SI) of 10 (Table 3; Fig. 6C; Supplementary Table 6).

Discussion

The nsP4-CHIKV polymerase plays a crucial role in viral replication and has been considered a promising target for the search and development of new drugs. Thus, understanding its dynamic and structural features is an important step for studies with this target.

Our biophysical data agree with the structure prediction using Alphafold and point out that nsp4-CHIKV is a monomeric protein enriched with alpha-helix content. These observations also agree with experimental data

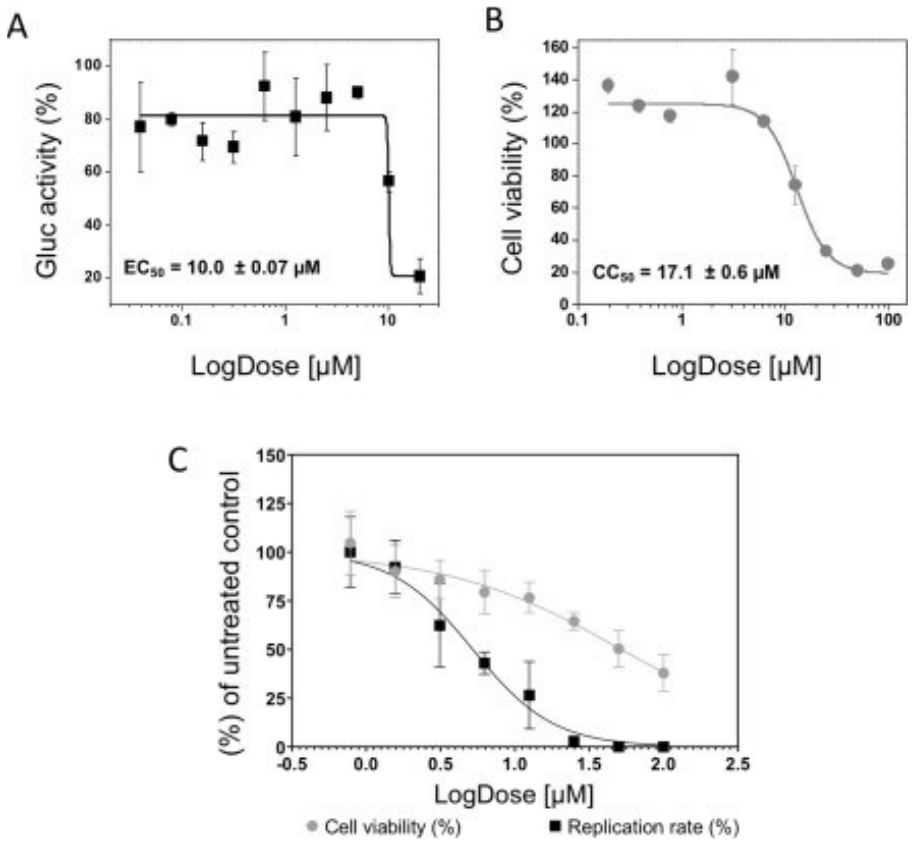

Figure 6. Antiviral activity of LabMol-309. The EC_{50} (**A**) and CC_{50} (**B**) curves from replicon-based assays are shown. CHIKV replicon cells were incubated with the compound at twofold serial dilutions (from 20 µM to 0.03 µM for EC_{50} and from 100 to 0.3 µM for CC_{50}) for 48 h, and Gluc activity/cell viability were measured from cells' supernatant. For the CHIKV-*nanoluc* replication assay evaluation of EC_{50} and CC_{50} (**C**), BHK-21 cells were treated with concentrations of LabMol-309 ranging from 0.78 to 100 µM, in the presence or absence of CHIKV-*nanoluc* for 16 h, and viral replication was quantified by measuring the nanoluciferase activity (indicated by ●) and cellular viability was measured using an MTT assay (indicated by ■). Representative results from two independent experiments performed in duplicates. Error bars represent the standard deviations. Figures and statistical analysis were performed using GraphPad Prism 8.

Compound	Type of the Assay	CC_{50}	EC_{50}	Selectivity index (SI)
LabMol-309	CHIKV-*nanoluc* and BHK-21 cells	52	5.2	10
	BHK-CHIKV replicon	17.1	10.0	1.7

Table 3. Effect of the compound on the viability of BHK-21 cells (CC_{50}) and the viral replication of CHIKV (EC_{50}) in 16 h treatment.

collected for other viral polymerases [2023]. The thermodynamic data showed that when in the in vivo host, this protein can be stable in the vicinity of its thermal denaturation (T_m ~ 40 °C and $\Delta T_{1/2}$ ~ 4–5 °C), and its unfolding is both scan-rate dependent and irreversible under all conditions tested. It was shown before that the T_m might be scan-rate dependent if the scan rate exceeds the unfolding rate [42]. The calorimetric thermograms for the irreversible denaturation of proteins are highly scan-rate dependent, and their shapes are normally asymmetric [43], exactly what is observed for nsp4-CHIKV. Therefore, the kinetics of the thermal denaturation could be treated as a single first-order irreversible step N → D, whose rate of temperature dependence obeys the Arrhenius equation.

The effective activation energy derived from this equation was (110 ± 4) kcal/mol, which fits well within the wide range of the values reported for the thermal denaturation of mammalian tissues and strengthened the thermo- dynamic data collected for this protein [44].

In the search for new nsp4-CHIKV ligands as potential inhibitors, the compound LabMol-309 was identified as a promising candidate through DSF screening. The validation of this interaction through biophysical methods demonstrated that the compound interacts in the low micromolar range. This compound had already been evaluated in virtual screenings for other viral proteins such as ZIKV and other Flaviviruses [21,22], but it was the first time it was reported targeting the nsP4-CHIKV protein.

A three-dimensional model was generated using AlphaFold to analyze the LabMol-309-nsP4-CHIKV complex and their mode of interaction. In this sense, the nsP4-CHIKV model presented the regions corresponding to the *fingers*, *palm* and *thumb* domains, which are characteristics of viral polymerases, and the active site region was remarkably positive and conserved. These structural features were equivalent to the regions presented in the RdRp domain of nsP4 from both RRV and SINV, which were experimentally solved recently (PDB ID: 7F0S, 7VB4, 7VW5)[20]. Therefore, the suggested binding mode for LabMol-309 is through the interaction with residues of the nsP4-CHIKV active site.

Although the data involving the complex formation between nsP4-CHIKV and LabMol-309 are solid, it is still not possible to conclude that this compound has inhibitory activity against this enzyme. The development of an enzymatic assay for the nsP4 polymerase from Alphaviruses in general, has been challenging because this protein cannot effectively perform its function on its own, as previously shown by others [45,46]. Different regions of nsP4 recognize the promoters for *minus* and *plus* strands. However, the binding requires the presence of the other non-structural proteins to form the replication complex and enable the de novo RNA synthesis[11,45–47]. Moreover, the interactions between these proteins with host components during replication have been studied but remain limited and not completely understood[11,46].

Tomar et al.[48] reported that template recognition and the nsP4 activation through protein–protein interac- tions requires the presence of viral polyprotein P123[48]. In another work, the SINV nsP4 was expressed in *E. coli*, and the polymerase activity was observed only when supplied with the viral polyprotein P123[47]. Recently, Lello et al.[46] demonstrated that nsP4 of SINV, CHIKV, ONNV, BFV, RRV, SFV, MAYV, VEEV, and EILV on their own have minimal RNA polymerase activity [46]. Using a trans replicase system consisting of two relatively independent functional modules (nsP4 and P123), they have shown that the nsP4 of all these Alphaviruses was active only when combined with the corresponding P123 polyproteins[46]. Furthermore, Tan et al.[20] evaluated the polymerase activity of SINV and RRV nsP4 and as a result, the isolated proteins showed less efficient polymerase activity than the dengue virus RdRp used as the positive control[20]. Altogether these findings corroborate that bacterially produced nsP4 could not efficiently synthesise RNA unless combined with the viral polyprotein P123 obtained from animal cell extracts [47,49,50].

Given these limitations in establishing an efficient method for evaluating the enzymatic activity of purified recombinant nsP4-CHIKV, in this work the inhibitory effect of the compound LabMol-309 was evaluated using both replicon-based assays and cells infected with the CHIKV expressing the nanoluciferase reporter (CHIKV- nanoluc). Replicon-based systems have been widely used as tools for drug discovery of antiviral agents, and promising replication inhibitors were identified by this method[51]. Specifically to CHIKV, BHK-21 cells har- boring other CHIKV replicon constructs were reported for the high-throughput screening of viral replication inhibitors[52,53]. The same system was also used to evaluate the anti-CHIKV activity of other compounds and different flavonoids[54–56].

The evaluation of LabMol-309 using a replicon-based system was performed in a dose-dependent manner, and its inhibition clearly occurred. Comparing with studies that also used CHIKV replicon, the EC_{50} obtained for LabMol-309 was lower than the values already reported for other compounds[52,55], reinforcing the antiviral potential of this compound. LabMol-309 showed toxicity to the cells, and the resulting low selectivity index of 1.7 may be correlated to a possible negative impact in the cellular factors associated with the viral genome replication. These data suggest that, even with inhibitory activity, chemical modifications would be required to optimize this compound's efficiency and reduce its toxicity. Furthermore, antiviral assays performed with cells infected with a recombinant CHIKV demonstrated that the LabMol-309 decreased CHIKV replication with an EC_{50} of 5.2 µM and an CC_{50} of 52 µM, with a SI of 10 in BHK-21 cells.

The differences in the obtained values using naive BHK-21 or BHK-CHIKV cells (Table 3) are understandable since different factors are involved in these assays. For example, in the infection system the virus is effectively infecting the cells and performing all the stages of the virus replicative cycle. It means that the treatment with Lab- Mol-309 may be acting even before the formation of the replication complexes. Alternatively, in the BHK-CHIKV replicon system, the replication complexes are already formed when the treatment starts, which can impact on the effectiveness of the antiviral activity in a short period of treatment. Additionally, the presence of the replicon might change the cell response to the compound, and explain the higher cytotoxicity shown in the results. This isolated effect predominantly observed in the replicon cells can be explained by the differences in incubation peri- ods used in the antiviral activity experiments (48 h for replicon-based screenings compared to 16 h for the viral infection assays). The prolonged exposure of cells to the compound can result in higher cytotoxicity [57], reinforcing the importance of further studies of the ADME-Tox profile in animal models. Additionally, to the best of our knowledge, this is the first description of LabMol-309 as inhibitor of CHIKV replication, and its low EC_{50} value is in similar level with other inhibitors reported to block CHIKV replication, emphasizing the antiviral potential of this compound[58,59]. In this context, the results obtained from the antiviral assays suggest that LabMol-309 is a potential molecule to be further optimized to reduce its cytotoxicity and increase the selectivity index in cell- based antiviral assays. In summary, this study highlights biophysical features of nsP4-CHIKV, contributing to basic research on alphaviruses polymerase, and identified a new compound as a promising antiviral agent against

CHIKV infection. These findings could contribute to developing novel candidates targeting nsP4-CHIKV and support the progress in therapeutic strategies for CHIKV and other alphavirus infections.

Methods

CHIKV nsP4 cloning and overexpression. The coding region of nsP4-CHIKV (GenBank KP164572.1; PROT-ID AJY53709.1—residues 118 to 611) was subcloned in the pET-SUMO vector using the LIC methodology [60]. This construct encodes an nsP4-CHIKV with an N-terminal 6xHis-tag followed by a TEV protease cleavage site (ENLYFQ ; GAM) and the fusion protein tag SUMO. For protein expression, this plasmid construction was transformed into *E. coli* Rosetta and cultured in Terrific Broth (TB) medium at 37 °C and 200 RPM until an OD_{600} of 1.0. The protein expression was induced with 1 mM of isopropyl-β-thiogalactoside and incubation at 18 °C, 200 RPM for 16 h. The cells were harvested by centrifugation at 5000 × *g* for 30 min at 4 °C and resuspended in buffer A (50 mM Tris pH 8.0, 500 mM NaCl, 10% glycerol). Cells were disrupted by sonication and clarified by centrifugation at 12,000 × *g* for 30 min at 4 °C.

nsP4-CHIKV purification. nsP4-CHIKV was purified using an AKTA Purifier System (GE Healthcare). The first step was affinity chromatography, using a HisTrap HP 5.0 mL column (GE Healthcare) pre-equilibrated with buffer A (50 mM Tris pH 8.0, 500 mM NaCl, 10% glycerol). The elution was performed using 50 mM Tris pH 8.0, 500 mM NaCl, 250 mM imidazole, 10% glycerol. The buffer was exchanged through dialysis to eliminate the imidazole excess. The 6xHis-tag-SUMO was cleaved by TEV protease during overnight incubation at 4 °C. A second affinity chromatography step was performed using the same system to collect the HisTag-less protein obtained after TEV treatment. A final purification step was done using size-exclusion chromatography on an XK 26/1000 Superdex 75 column (GE Healthcare) pre-equilibrated in gel filtration buffer (50 mM Tris pH 8.0, 200 mM NaCl and 5% glycerol). The eluted fractions were collected and analyzed by SDS-PAGE to confirm their purity and mass spectrometry was performed to confirm the presence of nsP4-CHIKV. The final protein sample was concentrated using 30 kDa MWCO centrifugal concentrators (Vivaspin, Sartorius). Protein concentrations were determined spectrophotometrically in a Nanodrop 1000 spectrophotometer, using the measured absorbances at 280 nm and the theoretical extinction coefficient of 36,495 M^{-1} cm^{-1}.

Size exclusion chromatography coupled with multi-angle light scattering (SEC-MALS). The oligomeric state of the purified nsP4-CHIKV was evaluated by size exclusion chromatography coupled with multi-angle light scattering (SEC-MALS) in running buffer composed of 50 mM Tris–HCl pH 8.0 and 200 mM NaCl. For that, 50 µL of purified nsP4-CHIKV at a concentration of 1.5 mg/mL was injected in a Waters 600 HPLC system (Waters) coupled in-line with a UV detector, a mini DAWN TREOS multi-angle light scattering apparatus (Wyatt Technology), a column Superdex 75 Increase 10/300 GL (GE Healthcare), and a refractive index detector Optilab T-rEX (Wyatt Technology). The light scattering detectors were normalized with bovine serum albumin (Sigma-Aldrich) and the flow rate used was 0.5 mL/min. The data were processed using ASTRA7 software (Wyatt Technology) with the following parameters: refractive index of 1.331, 0.890 cP for the viscosity of the solvent, and a refractive index increment of 0.1850 mL/g. Protein solutions were centrifuged for 10 min at 10,000 × *g* at a controlled temperature of 4 °C immediately before use.

Circular dichroism (CD). Far UV-CD spectra (195–280 nm) were measured in a Jasco J-810 spectrometer (Jasco Corporation, Japan) equipped with a Peltier control system and using a quartz cell with a 1 mm pathlength. The spectra were recorded from 280 to 195 nm, with a scanning speed of 100 nm/min, a spectral bandwidth of 1 nm and a response time of 0.5 s. All the protein samples were in a final concentration of 2.5 µM diluted in water. Spectral deconvolution was applied to estimate the secondary structure content using the DICHROWEB web server [26]. Three different methods were combined with three different databases to improve the reliability of the results. The detailed analysis of the results generated by these combinations is provided in Supplementary material (Supplementary Table 1). The estimated values of secondary structure fractions were averaged from each database used. The best fit was determined from the analysis of the NRMSD parameter, which was considered satisfactory when closer to 0 [61]. Thermal denaturation experiments were performed by monitoring the ellipticity at 222 nm in the range from 20 to 80 °C using heating rates of 0.5 °C/min and 1.0 °C/min.

Differential scanning calorimetry (DSC). DSC measurements were carried out with the purified protein solution at 7.4 µM, 9.3 µM and 12 µM, diluted in buffer 50 mM Tris–HCl (pH 8.0), 200 mM NaCl and 5% glycerol. Protein and reference samples (buffer) were degassed for 5 min prior to measurements. The experiments were performed on a VP-DSC MicroCal MicroCalorimeter (Microcal, Northampton, MA, USA) using heating rates of 8 °C/h, 13 °C/h, 33 °C/h and 64 °C/h. The thermograms were recorded from 10 to 70 °C, at a controlled pressure of 1.6 atm. Instrumental buffer baselines were recorded before the protein unfolding experiments to register the thermal history of the calorimeter. The raw DSC traces were subtracted with the buffer baseline and then normalized by protein concentration. The thermogram analysis and the subtraction of the buffer calorimetric response, baseline correction, and integration of the calorimetric peaks referring to the phase transitions were performed using the MicroCal Origin software.

Differential scanning fluorimetry (DSF). In the search for new binders to nsp4-CHIKV, 12 compounds from the OpenZika project were tested [27,27]. The compounds were purchased from Chembridge Library (https://www.chembridge.com/) with a minimum purity of 90%. DSF assays were conducted in a qPCR system Mx3000P (Agilent) for an initial assessment. Protein melting temperatures (T_m), assuming a two-state transition model,

were determined by monitoring the fluorescence intensity variation as a function of temperature for the extrinsic probe SYPRO Orange (Invitrogen). The protein solutions were at a final concentration of 8 µM, diluted in gel fil- tration buffer. Compounds were added at the final concentration of 80 µM and standard samples were prepared only with DMSO. The thermal variations were in the range of 25–75 °C in a stepwise increment of 1 °C/min. The T_m values obtained for each compound were subtracted from the values of the standard samples to identify com- pounds that caused significant T_m changes. For the next steps, the compound that presented the highest thermal shifts (ΔT_m) was selected, considering the deviations of the triplicates [62]. Data were analysed using the software Origin Pro 9.5.1. All experiments were conducted in triplicate.

MicroScale thermophoresis (MST). Experiments were performed on a Monolith® NT.115 instrument (Nanotemper technologies). The nsP4-CHIKV was labelled on cysteine residues with NT-647-Maleimide dye (Nanotemper Technologies) using the Monolith NTTM Protein Labeling Kit RED-MALEIMIDE as per manufacturer's instructions. Samples of 25 nM of cys-labelled nsP4-CHIKV with 5% DMSO were used. An initial binding test was carried out with the compound at the concentration of 100 µM, to check the interaction between the protein and the compound. Then, a serial dilution of the compound from 200 to 0.012 µM (12 nM) was performed to obtain the binding curve. The dissociation constant (K_D) was obtained by fitting the binding curve with the Hill function using GraphPad Prism 8 (Graph Pad Software).

Chemical shift perturbation. The LabMol-309 resonance assignment was performed using a Bruker Avance III 600 MHz. 1H-13C-HSQC, COSY and TOCSY were acquired at 298 K using 1 mM of LabMol-309 in D_2O. The interaction between LabMol-309 and nsP4-CHIKV was studied using a Bruker Avance IIIHD 500 MHz in a solution of 20 mM $(^2H)_{11}$-Tris/HCL pH 7.5, 200 mM NaCl and 250 µM of LabMol-309. One-dimensional ^1H spectra in the presence and absence of 3 µM NSP4-CHIKV were acquired, and the chemical shift difference was analyzed. The data processing and analysis were performed using TopSpin 4.09.

The nsP4-CHIKV tridimensional model and structural analysis. The nsP4-CHIKV sequence (residues 1 to 611) was used to generate the 3D model by AlphaFold2, developed by DeepMind (https://alphafold.ebi.ac.uk/)[38]. The nsP4-CHIKV model was structurally refined for docking calculations at GalaxyRefine server [63]. Surface charge was calculated using APBS[64] and residues conservation was analyzed with ConSurf, following the default parameters [65]. Pymol[66] was used to render the 3D images.

Molecular docking of nsP4-CHIKV and LabMol-309. The docking calculations were performed using the DockThor VS web [67,68], focusing on the active binding site (Asp371 and Asp466 residues). The nsP4-CHIKV and LabMol-309 structures were prepared using the Protein Preparation Wizard [69] and LigPrep tool [70]. The docking grid was centered at the active binding site; grid size 20 Å; and grid coordinates x, y and z of − 27.84 Å, 12.89 Å and 28.25 Å, respectively. The search algorithm precision mode was set up in the standard configuration of genetic algorithm parameters, with the soft docking mode activated. The PLIP server [71] was used to analyze the protein–ligand patterns (hydrogen bonds, hydrophobic interaction, cation-π, π-stacking, water and salt bridge interactions). Poseview server [72,73] was used to generate 2D interaction diagram and VMD program was used to render the 3D images [74].

Molecular dynamics simulations. The initial positions of the nsP4-CHIKV-bound LabMol-309 for the molecular dynamics (MD) simulations were obtained by the molecular docking results, and its topology parameterizations (Molid 814093) were obtained from the ATB server [75]. The MD simulations were performed using GROMACS package version 5.0.7 [76]. The molecular system of the protein–ligand complex was modeled with the GROMOS54A7 force field [77] and SPC water model [78], using a cubic box solvated with 200 mM NaCl. The simulation was realized in ensemble NPT at 25 °C and 1.0 bar using a modified Berendsen thermostat with τ_T = 0.1 ps and Parrinello-Rahman barostat with τ_P = 2.0 ps and compressibility = 4.5×10^{-5}·bar^{-1}. A cutoff value of 12 Å was used for both Lennard–Jones, and Coulomb potentials and long-range electrostatic interactions were calculated using the Particle Mesh Ewald algorithm (PME) [79]. Energy minimization was performed with the steepest descent integrator and conjugate gradient algorithm, using 1000 kJ·mol^{-1}·nm^{-1} as the maximum force criterion. One hundred thousand molecular dynamics steps were performed for each NVT and NPT equilibration, applying force constants of 1000 kJ·mol^{-1}·nm^{-2} to all heavy atoms of the protein–ligand complex. At the end of preparation, a 100 ns MD simulation of the structural model of the protein–ligand complex was carried out for data acquisition. Next, the trajectory was aligned and analyzed according: RMSD of backbone atoms for protein and nonhydrogen atoms for the ligand, number of hydrogen bounds (cutoff distance of 3.5 Å and maximum angle of 30°) between protein and ligand, and number of contacts < 0.6 nm between all atoms of the protein and of the ligand.

Cells and virus. BHK-21 cells were purchased from The Global Bioresource Center (ATCC) and maintained in Dulbecco's modified Eagle's medium (DMEM, Sigma-Aldrich) supplemented with 100U/mL of penicillin (Hyclone Laboratories), 100 mg/mL of streptomycin (Hyclone Laboratories), 1% dilution of stock of non-essential amino acids (Hyclone Laboratories) and 10% of fetal bovine serum (FBS, Hyclone Laboratories) in a humidified 5% CO2 incubator at 37 °C. BHK-21-Gluc-nSP-CHIKV-99659 cell line, harboring a replicative CHIKV replicon expressing *Gaussia* luciferase (Gluc) as a reporter gene, was maintained in DMEM 10% FBS with 500 µg/ml G418 (Sigma-Aldrich). The CHIKV replicon construct includes a T7 bacteriophage promotor followed by the viral 5′ UTR region, the nsp1-4 coding sequence, the CHIKV subgenomic promoter (Sg) followed by the

GLuc sequence and the expression cassette containing a ubiquitination sequence (Ubi) and the neomycin phos- photransferase gene (Neo-resistance gene), and the viral 3′ UTR region. This construction and the development of this replicon cell line will be described elsewhere. The CHIKV expressing *nanoluciferase* reporter (CHIKV- *nanoluc*) used for the antiviral assays is based on the CHIKV isolate LR2006OPY1 (East/Central/South African genotype) and was produced, rescued, and titrated as previously described[40,41].

CHIKV replicon-based screenings. LabMol-309 at 200 mM in 100% DMSO was diluted with assay media to a final concentration of 1% (v/v) DMSO and was evaluated in a dose-dependent manner to determine its effectiveness (EC_{50}) and cytotoxic (CC_{50}) concentrations, as described in[80]. Approximately 2×10^4 replicon cells/well in DMEM 10% FBS were seeded in a 96-well plate. After 16 h of incubation at 37 °C with 5% CO_2, the medium was replaced with fresh DMEM supplemented with 2% FBS and compound was added to the cells at twofold serial dilutions. After a 48 h-incubation, 40 µL of the cells' supernatant containing secreted Gluc were mixed with 50 µl of *Renilla* luciferase Assay Reagent (Promega). The Gluc activity was measured using Spec- traMax i3 Multi-mode Detection Platform (Molecular Devices). Replicon cells in 1% DMSO were used as nega- tive control (0% inhibition). The compound concentration required to inhibit 50% of the Gluc activity (EC_{50}) was estimated using the OriginPro 9.0 software. The cytotoxicity was evaluated through a cell proliferation- based MTT (3-(4,5-dimethylthiazol-2-yl)-2,5-diphenyltetraz olium bromide) assay, as described in[81]. The com- pound concentration required to cause 50% cytotoxicity (CC_{50}) was estimated using the OriginPro 9.0 software. The dose–response curves were performed twice in duplicates. The EC_{50} and CC_{50} values were used to determine the compound's selectivity index ($SI = CC_{50}/EC_{50}$).

Infection assays using CHIKV-nanoluc. To assess the antiviral activity of LabMol-309, BHK-21 cells were seeded at a density of 5×10^4 cells per well into 48 well plates for 24 h. Then, cells were treated with Lab- Mol-309 in a two-fold dilutions ranging from 10.78 to 100 µM in the presence or absence of CHIKV-*nanoluc* at a multiplicity of infection (MOI) of 0.1 PFU/cell. Samples were harvested using *Renilla*-luciferase lysis buffer (Promega®) 16 h post-infection (h.p.i.) and virus replication levels were quantified by measuring *nanoluciferase* activity using the *Renilla* luciferase Assay System (Promega®).

Cell viability assays in BHK-21 cells. As previously described [40,41], cell viability was measured by MTT [3-(4,5-dimethylthiazol-2-yl)-2,5-diphenyl tetraz olium bromide] assay (Sigma-Aldrich®). After this, the medium was replaced with the MTT solution at 1 mg/mL, cells were incubated for 30 min, after which the MTT solution was removed and replaced with 300 µL of DMSO (dimethyl sulfoxide) to solubilize the formazan crystals. The absorbance was measured at 490 nm on the Glomax microplate reader (Promega®). Cell viability was calculated according to the equation (T/C) × 100%, where T and C represent the mean optical density of the treated and untreated control groups, respectively. The values of CC_{50} and EC_{50} were used to calculate the selectivity index ($SI = CC_{50}/EC_{50}$). The cytotoxic concentration of 50% (CC_{50}) and the effective concentration of 50% inhibition (EC_{50}) were calculated using GraphPad Prism 8.0.0 for Windows (GraphPad Software, San Diego, California USA, www.graphpad.com).

Data availability

The datasets generated and/or analysed during the current study are included in the are included in this published article [and its supplementary information files]. The raw data of all cellular assays presented in the manuscript were available in the Supplementary information. Additionally, the three-dimensional model of the protein generated using Alphafold is available upon request to the corresponding author.

Received: 22 February 2022; Accepted: 13 June 2022
Published online: 22 June 2022

References

1. Chastel, C. Infections inapparentes chez l'Homme: Un cheval de Troie pour l'introduction et la diffusion des arbovirus transmis par des moustiques dans les régions non endémiques?. *Bull. la Soc. Pathol. Exot.* **104**(3), 213–219 (2011).
2. Weaver, S. C. & Lecuit, M. Chikungunya virus and the global spread of a mosquito-borne disease. *N. Engl. J. Med.* **372**(13), 1231–1239 (2015).
3. Silva, J. V. J. *et al.* A scoping review of Chikungunya virus infection: Epidemiology, clinical characteristics, viral co-circulation complications, and control. *Acta Trop.* **188**, 213–214 (2018).
4. Thiberville, S.-D. *et al.* Chikungunya fever: Epidemiology, clinical syndrome, pathogenesis and therapy. *Antiviral Res.* **99**(3), 345–370 (2013).
5. Vairo, F. *et al.* Chikungunya: Epidemiology, pathogenesis, clinical features, management, and prevention. *Infect. Dis. Clin. North Am.* **33**, 1003–1025 (2019).
6. Thiberville, S.-D. *et al.* Chikungunya fever: A clinical and virological investigation of outpatients on Reunion island, South-West Indian Ocean. *PLoS Negl. Trop. Dis.* **7**(1), e2004. https://doi.org/10.1371/journal.pntd.0002004 (2013).
7. Simon, F. *et al.* French guidelines for the management of Chikungunya (acute and persistent presentations). *Med. Mal. Infect.* **45**(7), 243–263 (2015).
8. Marimoutou, C., Vivier, E., Oliver, M., Boutin, J. P. & Simon, F. Morbidity and impaired quality of life 30 months after chikungunya infection: Comparative cohort of infected and uninfected french military policemen in Reunion island. *Medicine (United States)* **91**(4), 212–219 (2012).
9. Rausalu, K. *et al.* Chikungunya virus infectivity, RNA replication and non-structural polyprotein processing depend on the nsP2 protease's active site cysteine residue. *Sci. Rep.* **15**, 6 (2016).
10. Lum, F. M. & Ng, L. F. P. Cellular and molecular mechanisms of Chikungunya pathogenesis. *Antiviral Res.* **120**, 165–174 (2015).
11. Rupp, J. C., Sokoloski, K. J., Gebhart, N. N. & Hardy, R. W. Alphavirus RNA synthesis and non-structural protein functions. *J. Gen. Virol.* **96**(9), 2483–2500 (2015).

12. Silva, L. A. & Dermody, T. S. Chikungunya virus: Epidemiology, replication, disease mechanisms, and prospective intervention strategies. *J. Clin. Investig.* **127**, 737–749 (2017).
13. Cunha, M. S. *et al.* Chikungunya virus: An emergent arbovirus to the south American continent and a continuous threat to the world. *Front. Microbiol.* **11**, 1297 (2020).
14. Rashad, A. A., Mahalingam, S. & Keller, P. A. Chikungunya virus: Emerging targets and new opportunities for medicinal chemistry. *J. Med. Chem.* **57**(4), 1147–1166 (2014).
15. Voss, J. E. *et al.* Glycoprotein organization of Chikungunya virus particles revealed by X- ray crystallography. *Nature* **468**(7324), 709–712 (2010).
16. Melton, J. V. *et al.* Alphavirus 6K proteins form ion channels. *J. Biol. Chem.* **277**(49), 46923–46931 (2002).
17. Powers, A. M. *Vaccine and Therapeutic Options to Control Chikungunya Virus* Vol. 31 (American Society for Microbiology, 2018).
18. Bakar, F. A. & Ng, L. F. P. Nonstructural proteins of alphavirus —Potential targets for drug development. Vol. 10, Viruses. MDPI AG (2018).
19. Thiboutot, M. M. *et al.* Chikungunya: A potentially emerging epidemic?. *PLoS Negl. Trop. Dis.* **4**(4), e623. https://doi.org/10.1371/ journal.pntd.0000623 (2010).
20. Tan, Y. B. *et al.* Crystal structures of alphavirus nonstructural protein 4 (nsP4) reveal an intrinsically dynamic RNA-dependent RNA polymerase fold. *Nucleic Acids Res.* **50**(2), 1000–1016. https://doi.org/10.1093/nar/gkab1302 (2022).
21. Ekins, S., Mietchen, D., Coffee, M., Stratton, T. P., Freundlich, J. S., & Freitas-Junior, L., *et al*. Open drug discovery for the Zika virus. *F1000Research*. **5** (2016).
22. Ekins, S., Perryman, A. L. & Horta, A. C. OpenZika: An IBM world community grid project to accelerate Zika virus drug discovery. *PLoS Negl. Trop. Dis.* **10**(10), e0005023 (2016).
23. Choi. K. H. Viral polymerases. *Viral. Mol. Mach.* 2012; 267–304.
24. Some, D., Amartely, H., Tsadok, A. & Lebendiker, M. Characterization of proteins by size -exclusion chromatography coupled to multi-angle light scattering (SEC-MALS). *J. Vis. Exp.* **148**, e59615 (2019).
25. Greenfield, N. J. Using circular dichroism spectra to estimate protein secondary structure. *Nat. Protoc.* **1**(6), 2876–2890 (2007).
26. Whitmore, L. & Wallace, B. A. DICHROWEB, an online server for protein secondary structure analyses from circular dichroism spectroscopic data. *Nucleic Acids Res.* **32**, 668–673 (2004).
27. Johnson, W. C. Analyzing protein circular dichroism spectra for accurate secondary structures. *Proteins Struct. Funct. Bioinform.* **35**(3), 307–312 (1999).
28. Greenfield, N. J. Using circular dichroism collected as a function of temperature to determine the thermodynamics of protein unfolding and binding interactions. *Nat. Protoc.* **1**(6), 2527–2535 (2007).
29. Karantzeni, I., Ruiz, C., Liu, C.-C. & LiCATA, V. J. Comparative thermal denaturation of *Thermus aquaticus* and *Escherichia coli* type 1 DNA polymerases. *Biochem. J.* **374**(3), 785–792 (2003).
30. Sanchez-Ruiz, J. M., Lopez-Lacomba, J. L., Cortijo, M. & Mateo, P. L. Differential scanning calorimetry of the irreversible thermal denaturation of thermolysin. *Biochemistry* **27**(5), 1648–1652 (1988).
31. Khechinashvili, N. N., Janin, J. & Rodier, F. Thermodynamics of the temperature-induced unfolding of globular proteins. *Protein Sci.* **4**(7), 1315–1324 (1995).
32. Durowoju, I. B., Bhandal, K. S., Hu, J., Carpick, B. & Kirkitadze, M. Differential scanning calorimetry—A method for assessing the thermal stability and conformation of protein antigen. *J. Vis. Exp.* **2017**(121), 55262 (2017).
33. Serrão, V. H. B. *et al.* The specific elongation factor to selenocysteine incorporation in *Escherichia coli*: Unique tRNASec recognition and its interactions. *J. Mol. Biol.* **433**(23), 167279 (2021).
34. Scortecci, J. F. *et al.* Initial steps in selenocysteine biosynthesis: The interaction between selenocysteine lyase and selenophosphate synthetase. *Int. J. Biol. Macromol.* **156**, 18–26 (2020).
35. Mota, D. C. A. M. *et al.* Structural and thermodynamic analyses of human TMED1 (p24γ1) Golgi dynamics. *Biochimie* **192**, 72–82 (2022).
36. Micheletto, M. C., Mendes, L. F. S., Basso, L. G. M., Fonseca-Maldonado, R. G. & Costa-Filho, A. J. Lipid membranes and acyl-CoA esters promote opposing effects on acyl-CoA binding protein structure and stability. *Int. J. Biol. Macromol.* **102**, 284–296 (2017).
37. Mottin, M. *et al.* The A–Z of Zika drug discovery. *Drug Discov. Today* **23**(11), 1833–1847 (2018).
38. Jumper, J. *et al.* Highly accurate protein structure prediction with AlphaFold. *Nature* **596**(7873), 583–589 (2021).
39. Sathyapriya, R. & Vishveshwara, S. Interaction of DNA with clusters of amino acids in proteins. *Nucleic Acids Res.* **32**(14), 4109–4118 (2004).
40. de Oliveira, D. M. *et al.* Organometallic complex strongly impairs chikungunya virus entry to the host cells. *Front. Microbiol.* **11**, 3204 (2020).
41. Santos, I. A. *et al.* Chikungunya virus entry is strongly inhibited by phospholipase A2 isolated from the venom of Crotalus durissus terrificus. *Sci. Rep.* **11**(1), 1–12 (2021).
42. Lepock, J. R. *et al.* Influence of transition rates and scan rate on kinetic simulations of differential scanning calorimetry profiles of reversible and irreversible protein denaturation. *Biochemistry* **31**(50), 12706–12712 (1992).
43. Davoodi, J., Wakarchuk, W. W., Surewicz, W. K. & Carey, P. R. Scan-rate dependence in protein calorimetry: The reversible transitions of *Bacillus circulans* xylanase and a disulfide-bridge mutant. *Protein Sci.* **7**(7), 1538–1544 (1998).
44. Wright, N. T. On a relationship between the Arrhenius parameters from thermal damage studies. *J. Biomech. Eng.* **125**(2), 300–304 (2003).
45. Pietilä, M. K., Hellström, K. & Ahola, T. Alphavirus polymerase and RNA replication. *Virus Res.* **234**, 44–57 (2017).
46. Lello, L. S. *et al.* nsP4 is a major determinant of alphavirus replicase activity and template selectivity. *J. Virol.* **95**(20), e00355-e421 (2021).
47. Rubach, J. K. *et al.* Characterization of purified Sindbis virus nsP4 RNA-dependent RNA polymerase activity in vitro. *Virology* **384**(1), 201–208 (2009).
48. Tomar, S., Hardy, R. W., Smith, J. L. & Kuhn, R. J. Catalytic core of alphavirus nonstructural protein nsP4 possesses terminal adenylyltransferase activity. *J. Virol.* **80**(20), 9962–9969 (2006).
49. Thal, M. A., Wasik, B. R., Posto, J. & Hardy, R. W. Template requirements for recognition and copying by Sindbis virus RNA-dependent RNA polymerase. *Virology* **358**(1), 221–232 (2007).
50. Chen, M. W. *et al.* Chikungunya virus nsP4 RNA-dependent RNA polymerase core domain displays detergent-sensitive primer extension and terminal adenylyltransferase activities. *Antiviral Res.* **143**, 38–47 (2017).
51. Fernandes, R. S. *et al.* Reporter replicons for antiviral drug discovery against positive single- stranded RNA viruses. *Viruses* **12**(6), 598 (2020).
52. Pohjala, L. *et al.* Inhibitors of alphavirus entry and replication identified with a stable Chikungunya replicon cell line and virus-based assays. *PLoS ONE* **6**(12), e28923. https://doi.org/10.1371/journal.pone.0028923 (2011).
53. Varghese, F. S. *et al.* Discovery of berberine, abamectin and ivermectin as antivirals against Chikungunya and other alphaviruses. *Antiviral Res.* **126**, 117–124 (2016).
54. Lani, R. *et al.* Antiviral activity of silymarin against Chikungunya virus. *Sci. Rep.* **5**(1), 11421 (2015).
55. Lani, R. *et al.* Antiviral activity of selected flavonoids against Chikungunya virus. *Antiviral Res.* **133**, 50–61 (2016).
56. Albulescu, I. C. *et al.* Suramin inhibits Chikungunya virus replication through multiple mechanisms. *Antiviral Res.* **121**, 39–46 (2015).

57. Eastman, A. Improving anticancer drug development begins with cell culture: misinformation perpetrated by the misuse of cyto- toxicity assays. *Oncotarget* **8**(5), 8854 (2017).
58. Santos, I. A. *et al.* Repurposing potential of rimantadine hydrochloride and development of a promising platinum (II)-rimantadine metallodrug for the treatment of Chikungunya virus infection. *Acta Trop.* **227**, 106300 (2022).
59. Pereira, A. K. S. *et al.* Memantine hydrochloride: A drug to be repurposed against Chikungunya virus?. *Pharmacol. Rep.* **73**(3), 954–961 (2021).
60. Aslanidis, C. & de Jong, P. J. Ligation-independent cloning of PCR products (LIC-PCR). *Nucleic Acids Res.* **18**(20), 6069–6074 (1990).
61. Mao, D., Wachter, E. & Wallace, B. A. Folding of the mitochondrial proton adenosine triphosphatase proteolipid channel in phos- pholipid vesicles. *Biochemistry* **21**(20), 4960–4968 (1982).
62. Wang, B., Shi, W. & Miao, Z. Confidence analysis of standard deviational ellipse and its extension into higher dimensional Euclidean space. *PLoS ONE* **10**(3), e0118537 (2015).
63. Ko, J., Park, H., Heo, L. & Seok, C. GalaxyWEB server for protein structure prediction and refinement. *Nucleic Acids Res.* **40**(W1), W294–W297 (2012).
64. Jurrus, E. *et al.* Improvements to the APBS biomolecular solvation software suite. *Protein Sci.* **27**(1), 112–128 (2018).
65. Ashkenazy, H. *et al.* ConSurf 2016: An improved methodology to estimate and visualize evolutionary conservation in macromol- ecules. *Nucleic Acids Res.* **44**(W1), W344–W350 (2016).
66. The PyMOL Molecular Graphics System, Version 1.8, Schrödinger L. The PyMOL Molecular Graphics System, Version 1.8. (2015).
67. Santos, K. B., Guedes, I. A., Karl, A. L. M. & Dardenne, L. E. Highly flexible ligand docking: Benchmarking of the DockThor program on the LEADS-PEP protein– peptide data set. *J. Chem. Inf. Model.* **60**(2), 667–683 (2020).
68. Guedes, I. A. *et al.* New machine learning and physics-based scoring functions for drug discovery. *Sci. Rep.* **11**(1), 3198 (2021).
69. Schrödinger Release 2015 -2: Protein Preparation Wizard, Schrödinger, LLC (2015).
70. Schrödinger Release 2015-2: LigPrep, Schrödinger, LLC (2015).
71. Salentin, S., Schreiber, S., Haupt, V. J., Adasme, M. F. & Schroeder, M. PLIP: Fully automated protein –ligand interaction profiler. *Nucleic Acids Res.* **43**(W1), W443–W447 (2015).
72. Stierand, K., Maaß, P. C. & Rarey, M. Molecular complexes at a glance: Automated generation of two-dimensional complex dia- grams. *Bioinformatics* **22**(14), 1710–1716 (2006).
73. Fricker, P. C., Gastreich, M. & Rarey, M. Automated drawing of structural molecular formulas under constraints. *J. Chem. Inf. Comput. Sci.* **44**(3), 1065–1078 (2004).
74. Humphrey, W., Dalke, A. & Schulten, K. VMD: Visual molecular dynamics. *J. Mol. Graph.* **14**(1), 33–38 (1996).
75. Malde, A. K. *et al.* An automated force field topology builder (ATB) and repository: Version 1.0. *J. Chem. Theory Comput.* **7**(12), 4026–4037. https://doi.org/10.1021/ct200196m (2011).
76. Abraham, M. J. *et al.* Gromacs: High performance molecular simulations through multi-level parallelism from laptops to super- computers. *SoftwareX.* **1–2**, 19–25 (2015).
77. Schmid, N. *et al.* Definition and testing of the GROMOS force-field versions 54A7 and 54B7. *Eur. Biophys. J.* **40**(7), 843–856 (2011).
78. Berendsen, H. J. C., Postma, J. P. M., van Gunsteren, W. F. & Hermans, J. *Interaction Models for Water in Relation to Protein Hydra- tion* 331–342 (Springer, 1981). https://doi.org/10.1007/978-94-015-7658-1_21.
79. Essmann, U. *et al.* A smooth particle mesh Ewald method. *J. Chem. Phys.* **103**(19), 8577–8593 (1995).
80. Fernandes, R. S. *et al.* Discovery of an imidazonaphthyridine and a riminophenazine as potent anti-Zika virus agents through a replicon-based high-throughput screening. *Virus Res.* **299**, 198388 (2021).
81. Li, J. Q. *et al.* Development of a replicon cell line-based high throughput antiviral assay for screening inhibitors of Zika virus. *Antivir. Res.* **150**, 148–154 (2018).

Acknowledgements

This project was supported by the São Paulo Research Foundation—FAPESP (grants to G.O, 2013/07600-3, M.C.L.C.F 2018/17095-8, L.F.S.M. 2017/24669-8 and 2021/10465-7, R.S.F. 2018/05130-3 and L.R.P. 2021/01706-0) and by the Goias Research Foundation—FAPEG (grants to C.H.A. 202010267000272, M.M. 201710267000[5]. M.M. and I.A.S also thank the CNPq for the fellowships received (300508/2017-4 and 142495/2020–4, respec- tively). ACGJ is grateful to Coordenação de Aperfeiçoamento de Pessoal de Nível Superior (CAPES)—Preven- tion and Combat of Outbreaks, Endemics, Epidemics and Pandemics (#88881.506794/2020–01) and FAPEMIG (Minas Gerais Research Foundation APQ-03385–18). We thank DeepMind Technologies Ltd for generating the AlphaFold 2 ab initio prediction of the CHIKV nsP4 structure before the public availability of their platform. We also thank the Molecular Biophysics Group at Sao Carlos Physics Institute of the University of Sao Paulo for allowing access to the DSC calorimeter and SEC-MALS (FAPESP Grant number: 15/16812-0). We thank Andres Merits (Institute of Technology, University of Tartu, Tartu, Estonia) for the provision of the CHIKV expressing-*nanoluciferase* reporter.

Author contributions

M.C.L.C.F, L.G.M.B, L.F.S.M and G.O. contributed to the ideation and conceptualization of the project. M.C.L.C.F, L.G.M.B, L.F.S.M, F.C.L.A. and N.C.M.R.M. performed the biochemical, biophysical and NMR experiments and analysis. C.H.A., M.M. and B.K.P.S provided the compounds and performed the molecular docking. A.S.G performed structural analysis of 3D model. I.P.C. performed molecular dynamics simulations L.H.V.G.G. provided the replicon system. R.S.F. and L.R.P. performed the cell-based replicon assays and analysis. I.A.S, U.E.A.R. and A.C.G.J. performed the viral assays and analysis. M.C.L.C.F., L.F.S.M., L.G.M.B., F.C.L.A, A.S.G., M.M., C.H.A. and G.O. contributed to the editing and revision of the manuscript.

Competing interests

The authors declare no competing interests.

Additional information

Supplementary Information The online version contains supplementary material available at https://doi.org/10.1038/s41598022-14790-x.

Correspondence and requests for materials should be addressed to G.O.

Reprints and permissions information is available at www.nature.com/reprints.

viruses

MDPI

Article

The Antifungal Itraconazole Is a Potent Inhibitor of Chikungunya Virus Replication

Lucca R. Policastro [1], Isabela Dolci [1], Andre S. Godoy [1], José V. J. Silva Júnior [2,3], Uriel E. A. Ruiz [4], Igor A. Santos [4], Ana C. G. Jardim [4,5], Kirandeep Samby [6], Jeremy N. Burrows [6], Timothy N. C. Wells [6], Laura H. V. G. Gil [7], Glaucius Oliva [1,*] and Rafaela S. Fernandes [1,*]

1 São Carlos Institute of Physics, University of São Paulo, São Carlos 13563-120, Brazil; lrpolicastro@gmail.com (L.R.P.); isabela@estudante.ufscar.br (I.D.); andregodoy@ifsc.usp.br (A.S.G.)
2 Virology Sector, Department of Preventive Veterinary Medicine, Federal University of Santa Maria, Santa Maria 97105-900, Brazil; valter_science@hotmail.com
3 Virology Sector, Laboratory of Immunopathology Keizo Asami, Federal University of Pernambuco, Recife 50670-901, Brazil
4 Institute of Biomedical Sciences, Federal University of Uberlândia, Uberlândia 38405-302, Brazil; uriel.aquino79@gmail.com (U.E.A.R.); igoras244@gmail.com (I.A.S.); jardim@ufu.br (A.C.G.J.)
5 Institute of Biosciences, Humanities and Exact Sciences (Ibilce), São Paulo State University (UNESP), Campus São José do Rio Preto, São Josédo Rio Preto 15054-000, Brazil
6 Medicines for Malaria Venture, P.O. Box 1826, 1215 Geneva, Switzerland; sambyk-consultants@mmv.org (K.S.); burrowsj@mmv.org (J.N.B.); wellst@mmv.org (T.N.C.W.)
7 Aggeu Magalhães Institute, IAM-FIOCRUZ, Recife 50670-420, Brazil; lgilfiocruz@gmail.com
* Correspondence: oliva@ifsc.usp.br (G.O.); rafaela.fernandes@usp.br (R.S.F.)

Abstract: Chikungunya virus (CHIKV) is the causative agent of chikungunya fever, a disabling disease that can cause long-term severe arthritis. Since the last large CHIKV outbreak in 2015, the reemergence of the virus represents a serious public health concern. The morbidity associated with viral infection emphasizes the need for the development of specific anti-CHIKV drugs. Herein, we describe the development and characterization of a CHIKV reporter replicon cell line and its use in replicon-based screenings. We tested 960 compounds from MMV/DNDi Open Box libraries and identified four candidates with interesting antiviral activities, which were confirmed in viral infection assays employing CHIKV-*nanoluc* and BHK-21 cells. The most noteworthy compound identified was itraconazole (ITZ), an orally available, safe, and cheap antifungal, that showed high selectivity indexes of >312 and >294 in both replicon-based and viral infection assays, respectively. The antiviral activity of this molecule has been described against positive-sense single stranded RNA viruses (+ssRNA) and was related to cholesterol metabolism that could affect the formation of the replication organelles. Although its precise mechanism of action against CHIKV still needs to be elucidated, our results demonstrate that ITZ is a potent inhibitor of the viral replication that could be repurposed as a broad-spectrum antiviral.

Keywords: Chikungunya virus; replicon-based assays; drug development; antiviral; Itraconazole

Citation: Policastro, L.R.; Dolci, I.; Godoy, A.S.; Silva Júnior, J.V.J.; Ruiz, U.E.A.; Santos, I.A.; Jardim, A.C.G.; Samby, K.; Burrows, J.N.; Wells, T.N.C.; et al. The Antifungal Itraconazole Is a Potent Inhibitor of Chikungunya Virus Replication. *Viruses* **2022**, *14*, 1351. https://doi.org/10.3390/v14071351

Academic Editor: Rubén Agudo

Received: 14 May 2022
Accepted: 17 June 2022
Published: 21 June 2022

1. Introduction

Chikungunya virus (CHIKV) is an alphavirus first appeared in 1952, which causes periodic and explosive outbreaks of chikungunya fever [1]. The symptoms of this disease include fever, headache, myalgia, and severe polyarthritis that could persist for years [2,3]. In February 2005, a major CHIKV outbreak occurred on the Indian Ocean islands, followed by a high number of infection cases reported in Europe and India in 2006 and 2007, respectively [4,5]. In December 2013, CHIKV emerged in Caribbean, and by the end of December 2015 about 1 million cases had been notified in the Americas [6,7]. Although the most recent outbreak was reported in February 2018 in Mombasa, Kenya, the reemergence of the virus in many parts of the world represents a serious public health concern [8]. Up to date,

no CHIKV-specific antiviral therapy has been approved, being the treatment palliative, to alleviate the symptoms [9].

CHIKV is an enveloped virus with a positive-sense single stranded RNA genome of approximately 12 kb in length, containing two open reading frames (ORFs) flanked by 5′ and 3′ untranslated regions (UTRs) and separated by a non-coding intergenic region. The first ORF encodes a non-structural polyprotein produced by direct translation of the genome, which is proteolytically processed into four non-structural proteins (nsP1-nsP4) [10]. The second ORF encodes five structural proteins (C, E3, E2, 6K, and E1), which are expressed from a subgenomic RNA [11]. The nsPs assemble to form the viral replication complex, which is responsible for RNA synthesis, while the structural proteins assemble into new viral particles [2].

Viral replicon systems, which express all the genetic elements required for their own replication without producing infectious particles, have been widely used as an alternative tool in the search for antiviral drugs [12,13]. In the last decade, CHIKV replicon cell lines have been developed and used to screen inhibitors of the viral replication [14–19]. Among the hit compounds identified, abamectin, ivermectin, and berberine, showed significant inhibitory activities [16]. Berberine, an isoquinoline alkaloid, was shown to reduce virus-induced activation of all major MAP kinase pathways in a follow-up study, and also demonstrated to be effective in alleviating CHIKV-induced inflammatory symptoms in a mouse model [20].

In this study, we describe the development of a stable CHIKV replicon cell line, the BHK-21-T7-Gluc-nSP-CHIKV-99650, which harbors a replicative replicon expressing *Gaussia* luciferase (GLuc) as a reporter gene. Using this cell line in replicon-based assays, we evaluated three MMV/DNDi small-molecule libraries, the Pandemic Response (PRB), Pathogen, and COVID boxes, all containing molecules either marketed or in development, with known or predicted antiviral, antifungal, or antibacterial activities [21–23], for the identification of anti-CHIKV agents. From the tested molecules, the antifungal itraconazole was the most effective, exhibiting a selectivity index (SI) of > 312. Additionally, its antiviral activity was confirmed in viral infection assays (SI > 294), showing that this molecule is a potent inhibitor of CHIKV replication in vitro.

2. Methods

2.1. Cells, Virus, and Compounds

BHK-21 cells, from the Global Bioresource Center (ATCC),were maintained in Dulbecco's Modified Eagle's Medium (DMEM, Sigma-Aldrich, St. Louis, MI, USA) supplemented with 100 U/mL of penicillin 100 mg/mL of streptomycin, 1% dilution of stock of non-essential amino acids (HYCLONE Laboratories, Logan, UT, USA) and 10% of fetal bovine serum (FBS, HYCLONE Laboratories, Logan, UT, USA) in a humidified 5% CO_2 incubator at 37 °C. BHK-21-GLuc-nSP-CHIKV-99650 cells, from the Laboratório de Virologia e Terapia Experimental (LaViTE-Aggeu Magalhães Institute, Recife, Brazil), were maintained in DMEM 10% FBS with 500 µg/mL geneticin (G418-Sigma-Aldrich, St. Louis, MI, USA).The CHIKV expressing *nanoluciferase* reporter (CHIKV-*nanoluc*) [24] used for the viral infection assays was based on the CHIKV isolate LR2006OPY1 (East/Central/South African genotype) and was produced, rescued, and titrated as previously described [25,26]. MMV/DNDi compounds (>90% purity) solubilized in 100% DMSO (*v*/*v*) were further diluted with assay media to a final DMSO concentration of up to 1% (*v*/*v*) for the assays. Suramin (Sigma-Aldrich, St. Louis, MI, USA) was solubilized in 100% DMSO at 20 mM and further diluted in assay media to a final concentration of 10 µM 1% DMSO (*v*/*v*). Itraconazole was purchased as a racemic mixture (CAS number: CAS-84625-61-6).

2.2. Construction of Rep-GLuc-nsP-CHIKV-99659

We constructed a CHIKV reporter subgenomic replicon, termed rep-GLuc-nsP-CHIKV-99659, by recombining four partially homologous fragments: **(i)** fragment 1, covering the T7 RNA polymerase promoter inserted by PCR amplification, and the 5′ UTR and nsP1-nsP4

amplified from the chemically synthesized CHIKV 99659 genome (GenScript, Piscataway, NJ, USA) (GenBank KJ451624); **(ii)** fragment 2, containing the CHIKV subgenomic promoter inserted by PCR amplification, and GLuc amplified from pGLuc-NS (WF10) (kindly provided by Dr. Daniel Perez, University of Georgia, Athens, GA, USA); **(iii)** fragment 3, the ubiquitination sequence and neomycin phosphotransferase (Neo) gene amplified from pBSC-YFV17D-LucNeoIres; and **(iv)** fragment 4 (3′UTR), amplified from the CHIKV 99659 genome (GenScript, Piscataway, NJ, USA).

The four fragments were amplified with Phusion® High-Fidelity DNA Polymerase (New England Biolabs), using the oligonucleotides shown in Table 1 and recombined, in a single-cloning-step, into the pBSC-HDR shuttle vector (Gil et al., unpublished data) previously digested (*Bam*HI nuclease, New England Biolabs) and dephosphorylated (Alkaline Phosphatase, Calf Intestinal, CIAP, Promega, Madison, WI, USA).

Table 1. Oligonucleotides used to construct rep-GLuc-nsP-CHIKV-99659.

Oligonucleotide	Sequence (5′-3′)	Amplicon
pBSC-BamHI-T7Phi2.5-5′CHIKV-F [a]	[b,c] **CAAGCATGTAAATATCGTTTGAGTTG-GATCC**CAGTAATACGACTCACTATT ATGGCTGCGTGAGACACACGTAG	Fragment 1 (T7 RNA polymerase promoter; CHIKV 5′UTR and nsP1-nsP4)
CHIKV-7515R	**GCAAAATAGGTAGCTGTAGTGCGTAC**C TATTTAGGACCGCCGTACAAG	
CHIKV1-GLuc-F	[d] ***GTACGCACTACAGCTACCTATTTTGC****AAA AGCCGACAGCAGGTACCTAAATACCAATCAG CCATA*ATGGGAGTCAAAGTTCTGTTTGCCCTG	Fragment 2 (CHIKV subgenomic promoter and *Gaussia* luciferase gene)
GLuc-Ubiq-R	**CACGAAGATCTGCATGTTTAAACC**GT CACCACCGGCCCCCTTGATC	
Ubiq-F	**GGTTTAAACATGCAGATCTTCGTG**AAG	Fragment 3 (Ubiquitination sequence and neomycin phosphotransferase gene)
CHIKV1-Neo-R	**CTTTAGGGACGCGTATGCCTTCATA CCTAGTTGTCAAG**TCAGAAGAAC TCGTCAAGAAGGCGATAG	
CHIKV-3UTR-F	**CTTGACAACTAGGTATGAAGGCATAC**	Fragment 4 (CHIKV 3′UTR)
pBSC-SpeI-3′CHIKV-R	**ATATGCATAGTACCGAGAAACTAGAACTAG** TTTTTTTTTTTTTTTTTTTTTTTTTTTTTTTTTTTT TTGAAATATTAAAAACAAAATAACATCTCC	

[a] Oligonucleotides pBSC-BamHI-T7Phi2.5-5′CHIKV-F and CHIKV-3′UTR-R (5′-TTTTTTTTTTTTTTTTTTTT TTTTTTTTTTTTTTTTTTTGAAATATTAAAAACAAAATAACATCTCCTACGTCCCTATGGGTAC-3′) were used in full-length PCR; [b] Nucleotides used for homologous recombination are in bold; [c] The T7 RNA polymerase promoter is underlined; [d] The CHIKV subgenomic promoter is in italics.

Homologous recombination was performed in *Saccharomyces cerevisiae* (strain RFY 206, *Mata his3Δ200 leu2-3 lys2Δ201 ura3-52 trp1Δ::hisG*) [27] transformed by lithium acetate (LiAc) [28]. Colonies were screened in Yeast Nitrogen Base (YNB) without tryptophan [29] and cloning was confirmed by PCR, using the oligonucleotides CHIKV-3′UTR-F and pBSC-SpeI-3′CHIKV-R (Table 1). Finally, *Escherichia coli* (strain DH10B) (Invitrogen, Waltham, MA, USA) was transformed with the positive clones [29] and plasmid DNA was extracted (QIAGEN Plasmid Midi Kit, QIAGEN, Germantown, MD, USA) and used as described below.

2.3. Full-Length PCR and In Vitro Transcription

The rep-GLuc-nsP-CHIKV-99659 sequence was linearized and amplified from the DNA plasmid by full-length PCR, using AccuTaq™ LA DNA Polymerase (Sigma) and the oligonucleotides pBSC-BamHI-T7Phi2.5-5′CHIKV-F and CHIKV-3′UTR-R (Table 1). Amplicons were purified by UltraPure™ Phenol: Chloroform: Isoamyl Alcohol (Invitrogen), precipitated with ethanol and sodium acetate (3M), and used as template for in vitro

transcription using the T7 RiboMAX™ Express Large Scale RNA Production System-T7 (Promega, Madison, WI, USA).

2.4. Cell Transfection and Development of the BHK-21-GLuc-nsP-CHIKV-99659 Cell Line

BHK-21 cells were transfected with the in vitro transcribed RNA. Briefly, 2×10^6 cells were resuspended in 100 µL of cytomix buffer (120 mM KCl, 0.15 mM $CaCl_2$, 10 mM K_2HPO_4/KH_2PO_4 pH 7.6, 25 mM HEPES pH 7.6, 2 mM EGTA, 5 mM $MgCl_2$) with 2 mM ATP and 5 mM glutathione, and electroporation was performed in 2 mm cuvette with 140 V and 25 msec pulse (Gene Pulser Xcell, Bio-Rad, Hercules, CA, USA). Three days post-transfection cells were selected in medium supplemented with 700 µg/mL Geneticin® (Gibco, Waltham, MA, USA), and after ten days, cell colonies were removed by Scienceware® cloning discs (Sigma-Aldrich, St. Louis, MI, USA) soaked in trypsin (Gibco, Waltham, MA, USA), seeded individually and amplified in medium with Geneticin® (500 µg/mL). The selected cell line was denominated BHK-21-GLuc-nsP-CHIKV-99659.

2.5. Stability Analysis of BHK-21-GLuc-nsP-CHIKV-99659

Parental and BHK-21-GLuc-nsP-CHIKV-99659 cells (at Passage 3 and 13) were seeded in duplicates in a 96-well plate (10^5 cells/well). Eighteen hours after seeding, 10 µL of the supernatant from each culture was collected and GLuc activity measured using the BioLux Gaussia Luciferase Assay Kit (New England Biolabs, Ipswich, MA, USA) in Mithras LB 940 Multimode Microplate Reader (Berthold Technologies, Bad Wildbad, Germany). Relative light unit (RLU) values of BHK-21-GLuc-nsP-CHIKV-99659 (at p3 and p13) were represented in fold-increase compared to the negative control (parental BHK-21 cell).

2.6. Validation of Replicon-Based Assays Using Suramin

The validation of the replicon-based assays was performed with the anti-parasitic drug suramin, a known inhibitor of CHIKV [19], as previously detailed in [30], with the exception that the GLuc signals were measured from the supernatant of cells (40 µL were mixed with 100 µL of *Renilla* luciferase Assay Reagent [Promega, Madison, WI, USA]). To determine the cytotoxicity of suramin, we performed a MTT (3-(4,5-dimethylthiazol- 2-yl)-2,5-diphenyltetrazolium bromide) assay, as described in [30]. The compound concentration required to inhibit 50% of the GLuc activity (EC_{50}) and cause 50% cytotoxicity (CC_{50}) was estimated using the OriginPro 9.0 software. Two independent assays were performed in duplicates.

2.7. Replicon-Based High-Throughput Screening of MMV/DNDi Libraries

The COVID Box, PRB, and Pathogen Box were screened using the BHK-21-GLuc-nSP-CHIKV-99659 cells. Each compound was tested at 10 µM 1% DMSO for primary screenings in a 96-well HTS format. 1% DMSO (0% inhibition) and suramin (100% inhibition) were used as negative and positive controls, respectively. Statistical analysis of the data were made through the determination of Z'-values, as described in [30]. In parallel, the toxicity of the compounds were evaluated at the same concentration to exclude false-positive hits [12,30]. Compounds that showed inhibition of luciferase activity in $\geq$80% and were not toxic to the cells ($\geq$80% cell viability) were evaluated in a concentration-dependent manner to determine their EC_{50} and CC_{50} values, both used to calculate the selectivity index ($SI = CC_{50}/EC_{50}$). The concentration–response curves were performed twice in duplicates for the selected compounds at a 2-fold or 5-fold serial dilutions, and the CC_{50} and EC_{50} values were calculated as described above (Item 2.6).

2.8. Viral Infection Assays with CHIKV-Nanoluc

To further characterize the antiviral activity of each compound, BHK-21 cells were seeded at a density of 5×10^4 cells/well into 48-well plates for 24 h and infected with CHIKV-*nanoluc* (MOI of 0.1 PFU/cell) in the presence of ITZ, GSK-983, rubitecan, and MMV676270, serially diluted (from 10 to 0.078 µM for ITZ or 100 to 0.78 µM for the other

three compounds). At 16 h post-infection (h.p.i.) samples were harvested, virus replication levels were quantified by luminescence using *Renilla* luciferase Assay Reagent [Promega, Madison, WI, USA], and cell viability was measured, as described in [25,26]. The effective and cytotoxic concentrations (EC_{50} and CC_{50}, respectively) were calculated using OriginPro 9.0 software and used to determine the selectivity index [25,26]. Assays were performed twice in triplicates.

3. Results

3.1. Development, Characterization, and Validation of a CHIKV GLuc Replicon Cell Line

The CHIKV replicon expressing GLuc and Neo sequences was successfully developed by homologous recombination of four DNA fragments in yeast cells (Figure 1A). BHK-21-GLuc-nsP-CHIKV-99659 cell line was obtained after transfection with in vitro transcribed replicon RNA and antibiotic selection. To assess the replicon stability, we compared the GLuc activity of BHK-21-GLuc-nsP-CHIKV-99659 cells in different passages: one corresponding to the third post-selection culture (p3) and another to passage 13 (p13). The GLuc activity signals were very similar between passages, confirming the maintenance of the BHK-21-GLuc-nsP-CHIKV-99659 phenotype throughout the cultivation (Figure 1B).

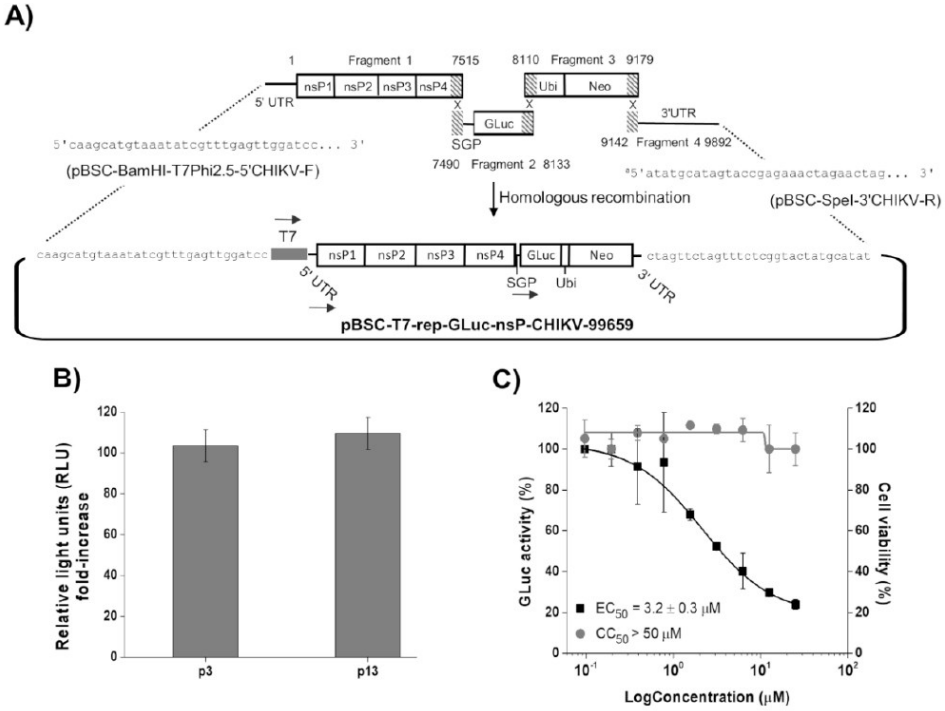

Figure 1. Development and characterization of the BHK-21-GLuc-nsP-CHIKV-99659 cell line. (**A**) Schematic representation of rep-GLuc-nsP-CHIKV-99659 construction. The ligation of fragments 1 and 4 to the pBSC-HDR vector was driven by homologous sequences inserted by the oligonucleotides pBSC-BamHI-T7Phi2.5-5′CHIKV-F and pBSC-SpeI-3′CHIKV-R, respectively (see Table 1). The dashed areas correspond to the overlapping regions between the fragments. The numbers in fragment 1 (1 to

7515 nt), 2 (7490 to 8133 nt), 3 (8110 to 9179 nt), and 4 (9142 to 9892 nt) correspond to the positions in rep-GLuc-nsP-CHIKV-99659. The arrows correspond to transcription driven by the T7 RNA polymerase promoter and the CHIKV genomic (at 5′UTR) and subgenomic promoters (SGP). [a] The sequence in pBSC-SpeI-3′CHIKV-R corresponds to the reverse complement (Table 1). (**B**) Comparison of GLuc activity between passages 3 and 13 of the BHK-21-GLuc-nsP-CHIKV-99659 cell line. The cells' supernatants were subjected to luciferase activity assay to test replicon stability throughout cultivation. (**C**) Antiviral assays of suramin in a 96-well plate format. Replicon cells were incubated with the inhibitor in a serial dilution for 48 h and both the GLuc signal (black squares) and cell viability (gray circles) were measured from the supernatant. Average results of two independent experiments. Error bars represent standard deviations.

Using suramin, we evaluated whether the CHIKV replicon cells would be suitable for the HTS in a 96-well format. As shown in Figure 1C, the compound inhibited GLuc activity in a concentration-dependent manner, with an EC_{50} value of 3.2 ± 0.3 μM, similar to that previously described using an in vitro assay with a replication-transcription complex (RTC) isolated from CHIKV replicon-transfected cells (EC_{50} of 6.7 μM) [31]. Moreover, no cytotoxicity was observed up to 50 μM of the inhibitor.

3.2. Identification of ITZ, GSK-983, Rubitecan, and MMV676270 as Inhibitors of CHIKV Replicon Replication

The replicon-based HTS were performed using 1% DMSO as a negative control and suramin as a positive control. Of the total 960 tested compounds, 55 inhibited the luciferase signals in ≥80%, being 17 from the COVID Box, 33 from the PRB, and 5 from the Pathogen Box (Figure 2). However, only 9 out of those 55 molecules, 3 from each library, exhibited cell viability ≥80% at 10 μM (Figure 2).

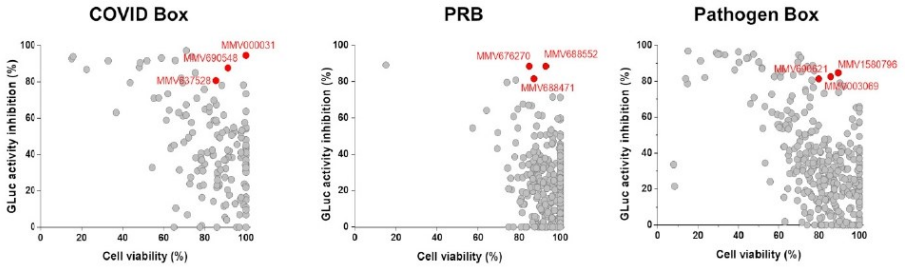

Figure 2. Replicon-based HTS for the COVID Box, Pandemic Response Box (PRB), and Pathogen Box. Scatter plots for the screening results of the 960 compounds in the primary screenings at 10 μM. In y-axis, the relative GLuc activity inhibition, and in x-axis, the relative cell viability. Selected compounds are highlighted in red and identified by their MMV code.

Those 9 selected molecules were evaluated in a concentration-dependent manner and 4 of them, itraconazole (ITZ-MMV637528), GSK-983 (MMV690621), rubitecan (MMV1580796), and MMV676270, showed antiviral activities with EC_{50} values at a nano to low micromolar range (Figure 3). GSK-983 and MMV676270 displayed moderate toxicities to the cells, while ITZ and rubitecan were not toxic up to 100 μM, resulting in SI values ranging from 10 to >714.

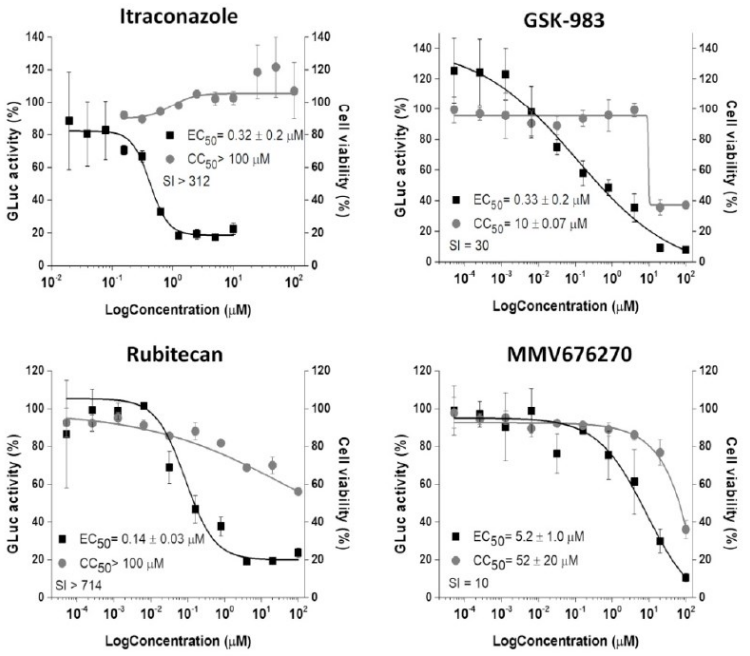

Figure 3. Concentration–response curves (EC_{50} and CC_{50}) of selected compounds. The CHIKV replicon cells were treated with compounds at 2-fold (Itraconazole) or 5-fold (GSK-983, rubitecan, and MMV676270) serial dilutions for 48 h. GLuc signal (black squares) was measured from the supernatant, while cell viability (gray circles) was measured employing MTT assay. Average results of two independent experiments. Error bars represent standard deviations.

Based on the results obtained for ITZ, we additionally tested a panel of ten clinically used azoles in the primary screenings; however, none of them inhibited the GLuc signals in more than 80%, although they did not show significant toxicities (Table 2).

Table 2. Activity of azoles against CHIKV replicon replication.

Compound	GLuc Inhibition	Cell Viability
Voriconazole	13.9%	91.8%
Econazole	43.8%	81.8%
Tioconazole	54.8%	68.4%
Clotrimazole	70.7%	70.2%
Ketoconazole	0%	100%
Fluconazole	0%	94.3%
Posaconazole	11.8%	100%
Ravuconazole	25.4%	100%
Isavuconazole	28.6%	100%
Miconazole	27.8%	100%

The luciferase activity inhibition and cell viability of the ten azoles evaluated in the primary replicon-based screenings at 10 μM are shown.

3.3. ITZ Strongly Inhibits CHIKV Infection In Vitro

Using CHIKV-*nanoluc*, which express *nanoluciferase* as a reporter, we further characterized the antiviral activity of the four inhibitors selected by the replicon-based assay.

BHK-21 cells were infected with CHIKV-*nanoluc* at a MOI of 0.1 and simultaneously treated with two-fold serial dilutions of the compounds. As a result, the treatment with GSK-983, rubitecan, and MMV676270 decreased the viral replication with EC_{50} values at a low micromolar range (Figure 4). MMV676270 displayed a CC_{50} of 59.5 μM, resulting in SI of 3, while GSK-983 and rubitecan were not toxic to BHK-21 cells up to 100 μM, resulting in SI values of >7 and >27, respectively. Notably, ITZ was the most potent antiviral molecule, showing an EC_{50} of 0.34 ± 0.02 μM with no cytotoxic effect on the cell viability up to 100 μM, and SI of >294 (Figure 4).

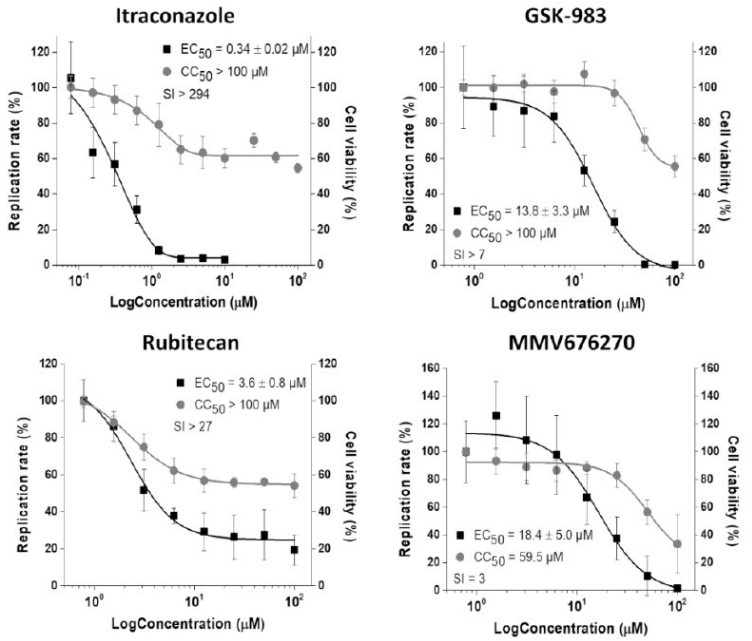

Figure 4. Inhibition of CHIKV-*nanoluc* infection in vitro. Concentration–response curves of selected compounds showing the relative replication rate (y-axis) over the compound concentration in log scale (x-axis). Average results of three independent experiments, each measured in triplicates, are shown, and error bars represent standard deviations.

4. Discussion

CHIKV remains a potential threat to public health with no specific antiviral available [9]. In this study, we successfully constructed a replicative CHIKV reporter replicon using homologous recombination in yeast, a strategy previously used to obtain reverse genetics systems for RNA viruses, such as dengue, yellow fever, bovine viral diarrhea virus and infectious bursal disease virus (IBDV) [29,32–34]. A BHK-21 cell line expressing the GLuc-Neo-CHIKV system, the BHK-21-GLuc-nsP-CHIKV-99659, was developed and demonstrated to persistently express the replicon RNA with no change in GLuc activity over 10 passages. Using replicon-based HTS we evaluated 960 MMV/DNDi compounds and identified rubitecan, GSK-983, MMV676270, and itraconazole with specific anti-CHIKV activities, which were confirmed in viral infection assays using the recombinant CHIKV-*nanoluc*.

The antiviral rubitecan, a camptothecin analog known to inhibit topoisomerase I [35], exhibited a very high SI against CHIKV on replicon-based assays, though this value was considerably lower on the viral infection assays. This compound is orally available, well

tolerated, and was shown to display an anti-HIV effect in infected peripheral blood lymphocytes (PBLs) [36], evidencing its potential to be further studied as an inhibitor of other RNA viruses, such as CHIKV. Another antiviral identified was GSK-983, a tetrahydrocarbazole inhibitor of the dihydroorotate dehydrogenase (DHODH) [37]. DHODH and other enzymes of the pyrimidine biosynthesis pathway are investigated as targets of broad-spectrum antivirals, including the ones with anti-CHIKV activities such as atovaquone, RYL-634, and DD363, but targeting host factors may interfere with cell viability (reviewed in [38]). This could explain the lower CC_{50} observed in replicon-based assays, in which cells are incubated with the compound for a longer period of time than that for the viral infection assays. Compound MMV676270 exhibited the lowest SI among the 4 inhibitors and is not a well-studied molecule with only a reported activity against *Plasmodium falciparum* and *P. berghei* in the chemical database PubChem. The discrepancies between the EC_{50} values for the three compounds resulting from the two different cell-based assays are not surprising because of intrinsic differences among these assays. As an example, the RNA replication levels in replicon-containing cells may differ from that in virus-infected cells, contributing to the system-to-system variation of efficacy (EC_{50}) obtained for a given compound [39,40]. Nevertheless, our results clearly demonstrate that rubitecan, GSK-983, and MMV676270 effectively inhibit CHIKV replication in vitro.

The most noteworthy compound identified was itraconazole (ITZ), a broad-spectrum antifungal agent. With an oral bioavailability of 55%, ITZ is a safe and cheap drug that allows long-period treatments of up to 12 months and regimen doses of up to 200 mg twice daily, making it an ideal candidate for repurposing, thus reducing the costs of developing new drugs against CHIKV [41,42]. Several studies have described in vitro activities of ITZ against +ssRNA viruses, such as enteroviruses, echovirus 30, dengue virus, and SARS-CoV-2 [43–47]. Although its precise mechanism of action has not been elucidated yet, in enteroviruses ITZ was shown to inhibit viral RNA replication by targeting oxysterol-binding protein (OSBP), which is responsible for trafficking of cholesterol and phosphatidylinositol-4-phosphate between membranes, therefore affecting the formation of the replication organelles [43,47]. The antiviral effect of ITZ could be, in part, based on such mechanism, but it is conceivable that it acts on viral replication via multiple mechanisms [45]. Our results also show that the anti-CHIKV effects are exclusive for this member of the azole series.

Recently, Posaconazole (PCZ), a structural analog of ITZ, was identified as a potent inhibitor of alphaviruses replication, showing comparable levels of Semliki Forest virus (SFV) replication inhibition when added at the time of inoculation or at 3 h post-inoculation (h.p.i), suggesting that this molecule acts on entry or early post-entry steps in the viral life cycle. Moreover, PCZ showed no toxic effects up to 100 μM concentration [48]. These findings are in agreement with the anti-CHIKV activity identified herein for ITZ but not for PCZ, as replicon-based screenings allow only the discovery of molecules affecting RNA replication, but not viral entry or assemble/release [12]. In conclusion, our results show that ITZ is a potent inhibitor of CHIKV replication and bring more attention to the potential use of antifungal triazoles as broad-spectrum antivirals. More studies are needed to confirm the *in vivo* efficacy of ITZ treatment on CHIKV infections.

Author Contributions: Conceptualization, R.S.F.; formal analysis, L.R.P., A.S.G., J.V.J.S.J., U.E.A.R., I.A.S., K.S., J.N.B., T.N.C.W. and R.S.F. funding acquisition, G.O.; investigation, L.R.P., I.D., J.V.J.S.J., U.E.A.R. and I.A.S.; project administration, R.S.F.; resources, G.O.; supervision, A.C.G.J., L.H.V.G.G., G.O. and R.S.F.; writing—original draft, L.R.P., J.V.J.S.J., U.E.A.R. and R.S.F.; writing—review and editing, A.S.G., I.A.S. and A.C.G.J. All authors have read and agreed to the published version of the manuscript.

Funding: This work was supported, in whole or in part, by the Bill & Melinda Gates Foundation INV-007155/19-BMGF-006. Under the grant conditions of the Foundation, a Creative Commons Attribution 4.0 Generic License has already been assigned to the Author Accepted Manuscript version that might arise from this submission. GO and RSF received financial support from Fundação de Amparo à Pesquisa do Estado de São Paulo (FAPESP), CEPID grant 2013/07600-3 to GO and grant

2018/05130-3 to RSF. LHVGG received financial support from Conselho Nacional de Desenvolvimento Científico e Tecnológico (CNPq) grant 440773/2019-8. ACGJ received financial support from the FAPEMIG (Minas Gerais Research Foundation APQ-03385-18). ACGJ is grateful to Coordenação de Aperfeiçoamento de Pessoal de Nível Superior (CAPES)—Brasil—Prevention and Combat of Outbreaks, Endemics, Epidemics and Pandemics—Finance Code #88881.506794/2020–01. IAS thanks to CNPq scholarship #142495/2020-4, and UEAR thanks to CAPES scholarship #88887.479203/2020-00.

Institutional Review Board Statement: Not applicable.

Informed Consent Statement: Not applicable.

Data Availability Statement: The data presented in this study are openly available in PubMed Central at [10.3390/v14071351].

Acknowledgments: We thank Andres Merits (Institute of Technology, University of Tartu, Tartu, Estonia) for the provision of the CHIKV expressing-*nanoluciferase* reporter. We would like to gratefully thank the Drugs for Neglected Diseases initiative (DNDi, www.dndi.org) for their support, and the Medicines for Malaria Venture (MMV, www.mmv.org) for the design of the COVID Box, Pandemic Response Box, Pathogen Box, and the azole series and for supplying the compounds. MarvinSketch was used to draw the chemicals, MarvinSketch version 20.17.0, ChemAxon (https://www.chemaxon.com).

Conflicts of Interest: The authors declare no conflict of interest.

References

1. Khongwichit, S.; Chansaenroj, J.; Chirathaworn, C.; Poovorawan, Y. Chikungunya virus infection: Molecular biology, clinical characteristics, and epidemiology in Asian countries. *J. Biomed. Sci.* **2021**, *28*, 1–17. [CrossRef] [PubMed]
2. Silva, L.A.; Dermody, T.S. Chikungunya virus: Epidemiology, replication, disease mechanisms, and prospective intervention strategies. *J. Clin. Investig.* **2017**, *127*, 737–749. [CrossRef]
3. Suhrbier, A. Rheumatic manifestations of chikungunya: Emerging concepts and interventions. *Nat. Rev. Rheumatol.* **2019**, *15*, 597–611. [CrossRef]
4. Schuffenecker, I.; Iteman, I.; Michault, A.; Murri, S.; Frangeul, L.; Vaney, M.-C.; Lavenir, R.; Pardigon, N.; Reynes, J.-M.; Pettinelli, F.; et al. Genome Microevolution of Chikungunya Viruses Causing the Indian Ocean Outbreak. *PLoS Med.* **2006**, *3*, 1058–1070. [CrossRef] [PubMed]
5. Panning, M.; Grywna, K.; van Esbroeck, M.; Emmerich, P.; Drosten, C. Chikungunya Fever in Travelers Returning to Europe from the Indian Ocean Region, 2006. *Emerg. Infect. Dis.* **2008**, *14*, 416. [CrossRef] [PubMed]
6. Wahid, B.; Ali, A.; Rafique, S.; Idrees, M. Global expansion of chikungunya virus: Mapping the 64-year history. *Int. J. Infect. Dis.* **2017**, *58*, 69–76. [CrossRef]
7. Faria, N.R.; Lourenço, J.; de Cerqueira, E.M.; de Lima, M.M.; Pybus, O.; Alcantara, L.C.J. Epidemiology of Chikungunya Virus in Bahia, Brazil, 2014-2015. *PLoS Curr.* **2016**, *8*. [CrossRef]
8. Silva, J.V.J., Jr.; Ludwig-Begall, L.F.; de Oliveira-Filho, E.F.; Oliveira, R.A.S.; Durães-Carvalho, R.; Lopes, T.R.R.; Silva, D.E.A.; Gil, L.H.V.G. A scoping review of Chikungunya virus infection: Epidemiology, clinical characteristics, viral co-circulation complications, and control. *Acta Trop.* **2018**, *188*, 213. [CrossRef]
9. Hucke, F.I.L.; Bugert, J.J. Current and Promising Antivirals Against Chikungunya Virus. *Front. Public Health* **2020**, *8*, 916. [CrossRef]
10. Kendall, C.; Khalid, H.; Müller, M.; Banda, D.H.; Kohl, A.; Merits, A.; Stonehouse, N.J.; Tuplin, A. Structural and phenotypic analysis of Chikungunya virus RNA replication elements. *Nucleic Acids Res.* **2019**, *47*, 9296–9312. [CrossRef]
11. Burt, F.J.; Chen, W.; Miner, J.J.; Lenschow, D.J.; Merits, A.; Schnettler, E.; Kohl, A.; Rudd, P.A.; Taylor, A.; Herrero, L.J.; et al. Chikungunya virus: An update on the biology and pathogenesis of this emerging pathogen. *Lancet Infect. Dis.* **2017**, *17*, e107–e117. [CrossRef]
12. Fernandes, R.S.; Freire, M.C.L.C.; Bueno, R.V.; Godoy, A.S.; Gil, L.H.V.G.; Oliva, G. Reporter replicons for antiviral drug discovery against positive single-stranded RNA viruses. *Viruses* **2020**, *12*, 598. [CrossRef] [PubMed]
13. Hannemann, H. Viral replicons as valuable tools for drug discovery. *Drug Discov. Today* **2020**, *25*, 1026–1033. [CrossRef]
14. Pohjala, L.; Utt, A.; Varjak, M.; Lulla, A.; Merits, A. Inhibitors of Alphavirus Entry and Replication Identified with a Stable Chikungunya Replicon Cell Line and Virus-Based Assays. *PLoS ONE* **2011**, *6*, 28923. [CrossRef] [PubMed]
15. Lani, R.; Hassandarvish, P.; Chiam, C.W.; Moghaddam, E.; Chu, J.J.H.; Rausalu, K.; Merits, A.; Higgs, S.; Vanlandingham, D.; Abu Bakar, S.; et al. Antiviral activity of silymarin against chikungunya virus. *Sci. Rep.* **2015**, *5*, 1–10. [CrossRef]
16. Varghese, F.S.; Kaukinen, P.; Gläsker, S.; Bespalov, M.; Hanski, L.; Wennerberg, K.; Kümmerer, B.M.; Ahola, T. Discovery of berberine, abamectin and ivermectin as antivirals against chikungunya and other alphaviruses. *Antivir. Res.* **2016**, *126*, 117–124. [CrossRef]

17. Wichit, S.; Hamel, R.; Bernard, E.; Talignani, L.; Diop, F.; Ferraris, P.; Liegeois, F.; Ekchariyawat, P.; Luplertlop, N.; Surasombatpattana, P.; et al. Imipramine Inhibits Chikungunya Virus Replication in Human Skin Fibroblasts through Interference with Intracellular Cholesterol Trafficking. *Sci. Rep.* **2017**, *7*, 3145. [CrossRef] [PubMed]
18. Fros, J.J.; Liu, W.J.; Prow, N.A.; Geertsema, C.; Ligtenberg, M.; Vanlandingham, D.L.; Schnettler, E.; Vlak, J.M.; Suhrbier, A.; Khromykh, A.A.; et al. Chikungunya virus nonstructural protein 2 inhibits type I/II interferon-stimulated JAK-STAT signaling. *J. Virol.* **2010**, *84*, 10877–10887. [CrossRef]
19. Albulescu, I.C.; White-Scholten, L.; Tas, A.; Hoornweg, T.E.; Ferla, S.; Kovacikova, K.; Smit, J.M.; Brancale, A.; Snijder, E.J.; van Hemert, M.J. Suramin Inhibits Chikungunya Virus Replication by Interacting with Virions and Blocking the Early Steps of Infection. *Viruses* **2020**, *12*, 314. [CrossRef]
20. Varghese, F.S.; Thaa, B.; Amrun, S.N.; Simarmata, D.; Rausalu, K.; Nyman, T.A.; Merits, A.; McInerney, G.M.; Ng, L.F.P.; Ahola, T. The Antiviral Alkaloid Berberine Reduces Chikungunya Virus-Induced Mitogen-Activated Protein Kinase Signaling. *J. Virol.* **2016**, *90*, 9743. [CrossRef]
21. Samby, K.; Besson, D.; Dutta, A.; Patra, B.; Doy, A.; Glossop, P.; Mills, J.; Whitlock, G.; Hooft van Huijsduijnen, R.; Monaco, A.; et al. The Pandemic Response Box–Accelerating Drug Discovery Efforts after Disease Outbreaks. *ACS Infect. Dis.* **2022**, *8*, 713–720. [CrossRef] [PubMed]
22. Coelho, R.A.; Joffe, L.S.; Alves, G.M.; Figueiredo-Carvalho, M.H.G.; Brito-Santos, F.; Amaral, A.C.F.; Rodrigues, M.L.; Almeida-Paes, R. A screening of the MMV Pathogen Box® reveals new potential antifungal drugs against the etiologic agents of chromoblastomycosis. *PLoS ONE* **2020**, *15*, e0229630. [CrossRef] [PubMed]
23. Choi, R.; Zhou, M.; Shek, R.; Wilson, J.W.; Tillery, L.; Craig, J.K.; Salukhe, I.A.; Hickson, S.E.; Kumar, N.; James, R.M.; et al. High-throughput screening of the ReFRAME, Pandemic Box, and COVID Box drug repurposing libraries against SARS-CoV-2 nsp15 endoribonuclease to identify small-molecule inhibitors of viral activity. *PLoS ONE* **2021**, *16*, e0250019. [CrossRef] [PubMed]
24. Matkovic, R.; Bernard, E.; Fontanel, S.; Eldin, P.; Chazal, N.; Hassan Hersi, D.; Merits, A.; Péloponèse, J.-M.; Briant, L. The Host DHX9 DExH-Box Helicase Is Recruited to Chikungunya Virus Replication Complexes for Optimal Genomic RNA Translation. *J. Virol.* **2019**, *93*, e01764-18. [CrossRef]
25. De Oliveira, D.M.; de Andrade Santos, I.; Martins, D.O.S.; Gonçalves, Y.G.; Cardoso-Sousa, L.; Sabino-Silva, R.; Von Poelhsitz, G.; de Faria Franca, E.; Nicolau-Junior, N.; Pacca, C.C. Organometallic complex strongly impairs chikungunya virus entry to the host cells. *Front. Microbiol.* **2020**, *11*, 608924. [CrossRef]
26. Santos, I.A.; Shimizu, J.F.; de Oliveira, D.M.; Martins, D.O.S.; Cardoso-Sousa, L.; Cintra, A.C.O.; Aquino, V.H.; Sampaio, S.V.; Nicolau-Junior, N.; Sabino-Silva, R.; et al. Chikungunya virus entry is strongly inhibited by phospholipase A2 isolated from the venom of Crotalus durissus terrificus. *Sci. Rep.* **2021**, *11*, 1–12. [CrossRef]
27. Finley, R.L.; Brent, R. Interaction mating reveals binary and ternary connections between Drosophila cell cycle regulators. *Proc. Natl. Acad. Sci. USA.* **1994**, *91*, 12980. [CrossRef] [PubMed]
28. Sambrook, J.; Russel, D.W. *Molecular Cloning: A Laboratory Manual*, 3rd ed.; Cold Spring Harbor Laboratory Press: New York, NY, USA, 2001.
29. Silva, J.V.J.; Arenhart, S.; Santos, H.F.; Almeida-Queiroz, S.R.; Silva, A.N.M.R.; Trevisol, I.M.; Bertani, G.R.; Gil, L.H.V.G. Efficient assembly of full-length infectious clone of Brazilian IBDV isolate by homologous recombination in yeast. *Braz. J. Microbiol.* **2014**, *45*, 1555–1563. [CrossRef]
30. Fernandes, R.S.; de Godoy, A.S.; dos Santos, I.A.; Noske, G.D.; de Oliveira, K.I.Z.; Gawriljuk, V.O.; Gomes Jardim, A.C.; Oliva, G. Discovery of an imidazonaphthyridine and a riminophenazine as potent anti-Zika virus agents through a replicon-based high-throughput screening. *Virus Res.* **2021**, *299*, 198388. [CrossRef]
31. Albulescu, I.C.; van Hoolwerff, M.; Wolters, L.A.; Bottaro, E.; Nastruzzi, C.; Yang, S.C.; Tsay, S.-C.; Hwu, J.R.; Snijder, E.J.; van Hemert, M.J. Suramin inhibits chikungunya virus replication through multiple mechanisms. *Antivir. Res.* **2015**, *121*, 39–46. [CrossRef] [PubMed]
32. Santos, J.J.S.; Magalhães, T.; Silva Junior, J.V.J.; Rangel Da Silva, A.N.M.; Cordeiro, M.T.; Gil, L.H.V.G. Full-length infectious clone of a low passage dengue virus serotype 2 from Brazil. *Mem. Inst. Oswaldo Cruz. Rio Jan.* **2015**, *110*, 677–683. [CrossRef] [PubMed]
33. Kassar, T.C.; Magalhães, T.; Júnior, J.V.J.S.; Carvalho, A.G.O.; Da Silva, A.N.M.R.; Queiroz, S.R.A.; Bertani, G.R.; Gil, L.H.V.G.; Vega, L.H.; Gil, G. Construction and characterization of a recombinant yellow fever virus stably expressing Gaussia luciferase. *An. Acad. Bras. CiencAnnals Braz. Acad. Sci.* **2017**, *89*, 2119–2130. [CrossRef] [PubMed]
34. Arenhart, S.; Silva, J.V.J.; Flores, E.F.; Weiblen, R.; Gil, L.H.V.G. Use of homologous recombination in yeast to create chimeric bovine viral diarrhea virus cDNA clones. *Braz. J. Microbiol.* **2016**, *47*, 993–999. [CrossRef]
35. Clark, J.W. Rubitecan. *Expert Opin. Investig. Drugs* **2006**, *15*, 71–79. [CrossRef]
36. Hung, C.L.; Doniger, J.; Palini, A.; Snyder, S.W.; Radonovich, M.F.; Brady, J.N.; Pantazis, P.; Reza Sadaie, M. 9-Nitrocamptothecin inhibits HIV-1 replication in human peripheral blood lymphocytes: A potential alternative for HIV-infection/AIDS therapy. *J. Med. Virol.* **2001**, *64*, 238–244. [CrossRef] [PubMed]
37. Deans, R.M.; Morgens, D.W.; Ökesli, A.; Pillay, S.; Horlbeck, M.A.; Kampmann, M.; Gilbert, L.A.; Li, A.; Mateo, R.; Smith, M.; et al. Parallel shRNA and CRISPR-Cas9 screens enable antiviral drug target identification. *Nat. Chem. Biol.* **2016**, *12*, 361. [CrossRef]
38. Battisti, V.; Urban, E.; Langer, T. Antivirals against the Chikungunya Virus. *Viruses* **2021**, *13*, 1307. [CrossRef] [PubMed]

39. Puig-Basagoiti, F.; Deas, T.S.; Ren, P.; Tilgner, M.; Ferguson, D.M.; Shi, P.-Y. High-throughput assays using a luciferase-expressing replicon, virus-like particles, and full-length virus for West Nile virus drug discovery. *Antimicrob. Agents Chemother.* **2005**, *49*, 4980–4988. [CrossRef] [PubMed]
40. Lo, M.K.; Tilgner, M.; Shi, P. Potential High-Throughput Assay for Screening Inhibitors of West Nile Virus Replication. *J. Virol.* **2003**, *77*, 12901–12906. [CrossRef] [PubMed]
41. Hardin, T.C.; Graybill, J.R.; Fetchick, R.; Woestenborghs, R.; Rinaldi, M.G.; Kuhn, J.G. Pharmacokinetics of itraconazole following oral administration to normal volunteers. *Antimicrob. Agents Chemother.* **1988**, *32*, 1310. [CrossRef] [PubMed]
42. Pushpakom, S.; Iorio, F.; Eyers, P.A.; Escott, K.J.; Hopper, S.; Wells, A.; Doig, A.; Guilliams, T.; Latimer, J.; McNamee, C.; et al. Drug repurposing: Progress, challenges and recommendations. *Nat. Rev. Drug Discov.* **2018**, *18*, 41–58. [CrossRef] [PubMed]
43. Gao, Q.; Yuan, S.; Zhang, C.; Wang, Y.; Wang, Y.; He, G.; Zhang, S.; Altmeyer, R.; Zou, G. Discovery of itraconazole with broad-spectrum in vitro antienterovirus activity that targets nonstructural protein 3A. *Antimicrob. Agents Chemother.* **2015**, *59*, 2654–2665. [CrossRef]
44. Lee, J.S.; Choi, H.J.; Song, J.H.; Ko, H.J.; Yoon, K.; Seong, J.M. Antiviral Activity of Itraconazole against Echovirus 30 Infection In Vitro. *Osong Public Health Res. Perspect.* **2017**, *8*, 318. [CrossRef] [PubMed]
45. Van Damme, E.; De Meyer, S.; Bojkova, D.; Ciesek, S.; Cinatl, J.; De Jonghe, S.; Jochmans, D.; Leyssen, P.; Buyck, C.; Neyts, J.; et al. In vitro activity of itraconazole against SARS-CoV-2. *J. Med. Virol.* **2021**, *93*, 4454–4460. [CrossRef] [PubMed]
46. Meutiawati, F.; Bezemer, B.; Strating, J.R.P.M.; Overheul, G.J.; Žusinaite, E.; van Kuppeveld, F.J.M.; van Cleef, K.W.R.; van Rij, R.P. Posaconazole inhibits dengue virus replication by targeting oxysterol-binding protein. *Antivir. Res.* **2018**, *157*, 68–79. [CrossRef]
47. Strating, J.R.P.M.; van der Linden, L.; Albulescu, L.; Bigay, J.; Arita, M.; Delang, L.; Leyssen, P.; van der Schaar, H.M.; Lanke, K.H.W.; Thibaut, H.J.; et al. Itraconazole inhibits enterovirus replication by targeting the oxysterol-binding protein. *Cell Rep.* **2015**, *10*, 600–615. [CrossRef]
48. Varghese, F.S.; Meutiawati, F.; Teppor, M.; Jacobs, S.; de Keyzer, C.; Taşköprü, E.; van Woudenbergh, E.; Overheul, G.J.; Bouma, E.; Smit, J.M.; et al. Posaconazole inhibits multiple steps of the alphavirus replication cycle. *Antivir. Res.* **2022**, *197*, 105223. [CrossRef]

Journal of Molecular Structure 1246 (2021) 131261

Contents lists available at ScienceDirect

Journal of Molecular Structure

journal homepage: www.elsevier.com/locate/molstr

Synthesis, spectroscopic characterization and *in vitro* antibacterial and antiviral activities of novel silver(I) complexes with mafenide and ethyl-mafenide

Pedro Gonçalves Esquezaro[a], Carlos Marrote Manzano[a], Douglas Hideki Nakahata[a,b], Igor Andrade Santos[c], Uriel Enrique Aquino Ruiz[c], Mariana Brentini Santiago[d], Nagela Bernadelli Souza Silva[d], Carlos Henrique Gomes Martins[d], Douglas Henrique Pereira[e], Fernando Rodrigues Goulart Bergamini[f], Ana Carolina Gomes Jardim[c], Pedro Paulo Corbi[a,*]

[a] Institute of Chemistry, University of Campinas – UNICAMP, PO Box 6154, 13083-970 Campinas, SP, Brazil
[b] Institute of Chemistry, Federal University of Goiás – UFG, 74690-900 Goiânia, GO, Brazil
[c] Laboratory of Virology, Institute of Biomedical Sciences, Federal University of Uberlândia – UFU, 38405-302 Uberlândia, MG, Brazil
[d] Laboratory of Antimicrobial Testing, Institute of Biomedical Sciences, Federal University of Uberlândia – UFU, 38405-302 Uberlândia, MG, Brazil
[e] Chemistry Collegiate, Federal University of Tocantins – UFT, PO Box 66, 77402-970 Gurupi, TO, Brazil
[f] Laboratory of Synthesis of Bioinspired Molecules, Institute of Chemistry, Federal University of Uberlândia - UFU, 38400-902 Uberlândia, MG, Brazil

ARTICLE INFO

Article history:
Received 19 June 2021
Revised 1 August 2021
Accepted 5 August 2021
Available online 8 August 2021

Keywords:
Silver(I)
Mafenide
Ethyl-mafenide
DFT studies
Antibacterial activity
Antiviral agents

ABSTRACT

Two novel silver(I) complexes with the antibacterial sulfa drugs mafenide (Maf) and ethyl-mafenide (eMaf) are presented in this article. Elemental analysis indicated the 1:1 metal:ligand compositions $AgC_7H_9N_2O_2S$ for Ag-Maf and $AgC_8H_{11}N_2O_2S$ for Ag-eMaf. Infrared (IR), and ^1H and ^{13}C nuclear magnetic resonance (NMR) spectroscopic analyses indicated coordination of the sulfa drugs to silver(I) by the nitrogen and oxygen atoms of the deprotonated sulfonamide (SO_2NH) group in a bidentate chelate mode. The proposition of the coordination mode of the sulfa drugs to silver(I) was also supported by a combination of experimental and theoretical (DFT) data. The Ag-Maf and Ag-eMaf complexes exhibited antibacterial activity over *Staphylococcus aureus, Burkholderia cepacia, Staphylococcus epidermidis*, and *Pseudomonas aeruginosa* aerobic bacteria, with MIC (minimum inhibitory concentration) in the range 21.3–170 μmol L^{-1}, being comparable to the commercial drug silver-sulfadiazine (SSD). Antiviral studies against Chikungunya virus (CHIKV) showed that the complexes exhibit anti-CHIKV activity at non-cytotoxic concentrations to the host cells. Biophysical studies based on gel electrophoresis indicated that the complexes do not interact with albumin and lysozyme, which suggests that proteins are not the main targets of the compounds.

Dedicatory: This work is dedicated to the memory of Professor Oswaldo Luiz Alves (1947-2021) from the Institute of Chemistry of the University of Campinas-UNICAMP, Brazil.

- New silver(I) complexes with mafenide and ethyl mafenide are presented.
- Spectroscopic studies suggest bidentate coordination of the ligands to silver.
- Theoretical data confirms ligand coordination to silver by nitrogen and oxygen atoms.
- The complexes exhibit antiviral activity over Chikungunya virus.
- The complexes were active over aerobic bacteria at concentrations 21.3–170 μmol L^{-1}.

1. Introduction

Infectious diseases (ID) (re)emergence in the last years has become a case of concern to public health systems around the globe [1]. From diseases caused by bacteria to those from viral, fungal and parasite origin, ID account annually for about 4.3 million deaths worldwide [2].

Bacterial infections, for instance, are prone to be the main cause of deaths in the next years, with current antibiotics estimated to lose their effectiveness due to the emergence of resistant strains, indicating the imperativeness of the development of

* Corresponding author.
E-mail address: ppcorbi@unicamp.br (P.P. Corbi).

https://doi.org/10.1016/j.molstruc.2021.131261
0022-2860/

Abbreviation

Ag-Maf	Silver(I) complex with mafenide
Ag-eMaf	Silver(I) complex with ethyl-mafenide
ATCC	American Type Culture Collection
B. cepacia	*Burkholderia cepacia*
BHK-21	Baby Hamster Kidney cells
BSA	Bovine Serum Albumin
CHIKV	Chikungunya virus
C. acnes	*Cutibacterium acnes*
DFT	Density Functional Theory
DNA	Deoxyribonucleic acid
eMaf	Ethyl-mafenide
IR	Infrared absorption spectroscopy
Maf	Mafenide
MIC	Minimum Inhibitory Concentration
MOI	Multiplicity of infection
MTT	[3-(4,5-dimethylthiazol-2-yl)-2,5-diphenyl tetrazolium bromide]
NMR	Nuclear Magnetic Resonance
P. aeruginosa	*Pseudomonas aeruginosa*
QTAIM	Quantum Theory of Atoms in Molecules
SDS-PAGE	Sodium dodecyl sulfate - polyacrylamide gel electrophoresis
SYBR Green	Nucleic acid electrophoresis stain
S. aureus	*Staphylococcus aureus*
S. epidermidis	*Staphylococcus epidermidis*

new effective drugs [3,4]. Viral diseases, in their turn, have also contributed to the overload of health systems, with the SARS-CoV-2 pandemic figuring as one of the current and major causes of concern [1,5]. Other viral diseases, such as the one caused by Chikungunya virus (CHIKV), have become endemic in many tropical countries [1,6]. CHIKV disease encompasses mild to excruciating pain (*e.g.* headache, migraines and polyarthralgia), with no existent treatment or vaccine, also carrying unfortunate prospects of reaching a chronic character that can last up to 2 years [7,8]. As for the case of bacterial infections, many viral strains still lack effective treatments, demanding continuous efforts towards the development of potential therapeutic approaches.

In this context, sulfonamides have been extensively studied due to their anticancer, antimicrobial and antiviral properties [9,10]. From the discovery of the antibacterial activities of Prontosil® to the development of current sulfa drugs, this class of compounds has been employed in the clinics as antimicrobial, anti-inflammatory and antiviral agents [9,11,12]. Some examples are sulfathiazole, sulfamethoxazole, mafenide, amprenavir and sulfasalazine [1,13–15]. Mafenide (Maf, 4-aminomethylbenzenesulfonamide, **Figure 1a**), in special, is the active substance of the drug Sulfamylon®, employed for the treatment of bacterial infections in second and third-degree burn wounds. It has the ability of deep tissue penetration acting effectively against a broad spectrum of bacterial strains such as *Pseudomonas aeruginosa* [16–18]. Structurally similar to Maf, ethyl-mafenide [eMaf, 4-(2-aminoethyl)-benzenesulfonamide, **Fig. 1b**] has shown potent inhibitory activity against carbonic anhydrase [19], an essential enzyme for bacteria.

One of the strategies of enhancing and/or broadening the antimicrobial and antiviral activities of biologically active molecules relies on their coordination to metal ions, which, in their turn, also possess intrinsic antiproliferative and/or antiviral actitivities [20–23]. The synthesis of such coordination compounds potentially offers a synergistic effect, often entailing new modes of action towards other pathogenic microorganisms [24–26].

For instance, silver(I) complexes have been extensively studied due to their intrinsic antibacterial [20,27], antifungal [28], antiproliferative [29] and antiviral [30,31] activities. Silver(I) sulfadiazine (SSD) is a sulfa-bearing polymeric complex encompassing the sulfa drug sulfadiazine and silver(I) [32,33]. It is a drug used as an antibacterial agent [34] and its antiviral activities against clinically isolated *Herpesvirus hominis* has also been explored. This compound showed complete virus inactivation at 10 $\mu g \cdot mL^{-1}$, after 30 min exposure to the drug [1,35].

In the last years, our research group has devoted efforts towards the development of new sulfa-based silver(I) complexes as potential antimicrobial and anticancer agents [10,13,36–38]. Among the new compounds, the silver(I) complexes with sulfathiazole (Ag-SFT) and sulfamethoxazole (Ag-SFM) can be highlighted, since they presented antibacterial activities against *P. aeruginosa* and *Salmonella enterica*, with MIC values of 3.45 and 1.74 mmol L^{-1} for Ag-SFT and Ag-SFM, respectively [13].

Considering the promising antibacterial and antiviral activities of sulfa-bearing silver(I) complexes, we hypothesized that silver(I) compounds encompassing Maf or eMaf could figure as potential antibacterial agents against bacteria related to skin infections. Indeed, as for the case of SSD, the compounds could also be able to inhibit viral infections such as that caused by CHIKV.

Herein we report the synthesis, spectroscopic characterization and Density Functional Theory (DFT) studies of new silver(I) complexes with Maf and eMaf, labeled Ag-Maf and Ag-eMaf, respectively. Antibacterial and antiviral activities of the free sulfa-drugs and complexes were evaluated *in vitro* against *S. aureus, P. aeruginosa, Burkholderia cepacia, Staphylococcus epidermidis* and *Cutibacterium acnes* strains, and over CHIKV. Preliminary biophysical studies encompassing the potential interaction of the complexes with proteins are also presented in this manuscript.

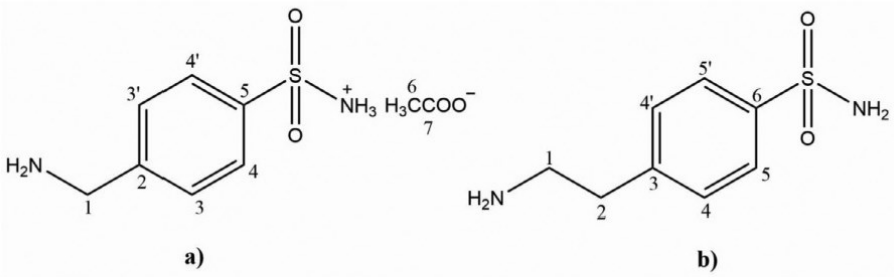

Fig. 1. Molecular structures of (a) mafenide and (b) ethyl-mafenide.

2. Experimental section

2.1. Reagents and equipment

All reagents were of commercial grade and used without further purification. Ethyl-mafenide, or 4-(2-aminoethyl)-benzenesulfonamide (eMaf), was obtained from Merck, and mafenide acetate (Maf) or mafenide hydrochloride (used in the solution-state NMR studies) were obtained from Acros Organics and Merck, respectively. Bovine serum albumin (BSA) and silver nitrate ($AgNO_3$) were purchased from Sigma-Aldrich laboratories. Deoxyribonucleic acid (DNA) Ladder 1Kb Plus was purchased from Invitrogen. Elemental analyses for carbon, hydrogen and nitrogen were performed using a Perkin-Elmer CHNS/O Analyzer Model 2400. Infrared (IR) spectra were obtained in an Agilent Cary 630 FTIR spectrometer, using the Attenuated Total Reflectance (ATR) method, in the range from 4000 to 400 cm^{-1} and with the resolution of 4 cm^{-1}. Solution-state nuclear magnetic resonance (NMR) spectra for the sulfa-drugs were recorded on a Bruker AVANCE III 400 MHz spectrometer. The spectra were acquired in D_2O. Solid-state ^{13}C NMR data for the silver(I) complexes and sulfa-drugs were recorded on a Bruker 400 MHz spectrometer, using the combination of cross-polarization and magic angle spinning (CP/MAS) at 10 kHz.

2.2. Synthesis of Ag-Maf and Ag-eMaf complexes

The silver(I) complexes were prepared as follows: mafenide acetate or ethyl-mafenide (1.0 mmol) were firstly dissolved in water. In the sequence, 1.0 mmol of KOH was added to each of the ligand solutions, which were maintained under magnetic stirring for 15 min without heating. Then, freshly prepared aqueous solutions of silver nitrate (1.0 mmol) were added to the alkaline solutions of the ligands at pH = 10. After 2 h of stirring at room temperature, white solids were obtained and collected by vacuum filtration. The reactions were carried out under the protection of light. The precipitates were then washed with water (~ 50 mL) and dried in a desiccator over P_4O_{10}. Calculated (Calcd.) for Ag-Maf ($AgC_7H_9N_2O_2S$): C, 28.69%; H, 3.10%; N, 9.56%. Found: C, 28.70%; H, 2.91%; N, 9.45%. Yield 78.7%. Calcd. for Ag-eMaf ($AgC_8H_{11}N_2O_2S$): C, 31.29%; H, 3.69%; N, 9.12%. Found (%): C, 31.43%; H, 3.55%; N, 9.07%. Yield 80.3%. No suitable crystals of the complexes were obtained for detailed X-ray diffraction studies even after several attempts. The complexes were insoluble in water and other common organic solvents such as methanol, ethanol, chloroform, dichloromethane, acetone, acetonitrile and dimethylformamide. The complexes have shown to be slightly soluble in dimethylsulfoxide.

2.3. DFT studies

Theoretical calculations for the ligands and complexes were performed using the Density Functional Theory (DFT) with the hybrid functional wB97XD [39]. The 6-31+G(d,p) [40–42] basis set was used for the carbon, hydrogen, oxygen, sulfur and nitrogen atoms. Meanwhile, pseudopotential LANL2DZ [43] basis set was employed for the silver atoms. To assure that the structures were at their minimum energy, frequency calculations were employed and no imaginary frequencies were found. All optimizations and frequency calculations were performed using the Gaussian 09 program [44]. The GaussView program [45] was used to generate the inputs for the calculations. Quantum Theory of Atoms in Molecules (QTAIM) analyses were employed to characterize the bonds between ligands and metal [46–49] and performed by the AIMALL program [50].

2.4. Cell viability assays

Cell viability assays were performed with the complexes, ligands, and $AgNO_3$ at 2, 10, and 50 µmol L^{-1} employing the MTT [3-(4,5-dimethylthiazol-2-yl)-2,5-diphenyl tetrazolium bromide] method [51], as previously described [52]. Briefly, BHK-21 cells (ATCC® CCL-10™), derived from Syrian hamster kidney cells were cultured in 48-well plate at 5 × 10^4 cells/well, and treated with each compound for 16h at 37 °C with 5% of CO_2. After the treatment, the medium containing each compound was removed and 1 mg mL^{-1} solution of MTT was added to each well, which was further incubated for 30 minutes and replaced with 300 μL of DMSO to solubilize the formazan crystals. The absorbance was measured at 490 nm on a Glomax microplate reader (Promega®). Cell viability was calculated according to the equation (T/C) × 100%, in which T and C represented the optical density of the treated and control groups, respectively. Dimethylsulfoxide was employed as non-treated control.

2.5. Antiviral activity assays

The CHIKV expressing *nanoluciferase* reporter (CHIKV-nanoluc) was rescued and titrated as previously described [52]. To assess the antiviral activity of the compounds, BHK-21 cel- ls were seeded at a density of 5 × 10^4 cells per well into 48-well plates 24 h prior to the infection, as previously described [52]. CHIKV-*nanoluc* at a multiplicity of infection (MOI) of 0.1 PFU/cell and the compounds were simultaneously added to the cells [53]. Samples were harvested in Renilla luciferase lysis buffer (Promega®) at 16 h post-infection (h.p.i.) and virus replication was quantified by measuring nanoluciferase activity using the Renilla luciferase Assay System (Promega®).

Data were analyzed for normal distribution to demonstrate the applicability of the parametric or the nonparametric test. Then, Two-way ANOVA test was employed to compare the treatment of each compound with the DMSO or water as control, with a $p < 0.01$.

2.6. Antibacterial activity assays

The minimal inhibitory concentration (MIC) value is defined as the lowest concentration of an antimicrobial agent capable of inhibiting bacterial growth. To determine the MIC of the aerobic and anaerobic bacteria included in this study the microdilution method recommended by the Clinical and Laboratory Standards Institute [54,55] was applied, with some modifications. The isolated compounds were dissolved in dimethylsulfoxide (DMSO, Merck®) or distilled water and diluted with Mueller Hinton broth (Kasvi®) for the aerobic bacteria and Schaedler broth (Difco®) supplemented with hemin (5 mg mL^{-1}, Sigma®) and menadione (1 mg mL^{-1}, Sigma®) for the anaerobic bacterial strain. Then, twelve concentrations of the isolated compounds ranging from 0.195 to 400 μg mL^{-1} were tested in a 96-well microplate.

The bacteria used in this study were obtained from the American Type Culture Collection (ATCC). The following aerobic bacteria were used: *S. aureus* (ATCC BA44), *B. cepacia* (ATCC 25416), *S. epidermidis* (ATCC 12228), *P. aeruginosa* (ATCC 15442) and the anaerobic bacteria *C. acnes* (ATCC 11827). The inocula were adjusted to give a cell concentration of 5 × 10^5 CFU mL^{-1} for the aerobic and 1 × 10^6 CFU mL^{-1} for the anaerobic bacteria. Most of the bacterial strains were chosen due to their close relationship with skin infections [56-59].

The plates containing the aerobic bacteria were incubated at 37 °C for 24 h while the plate containing the anaerobic microorganism was incubated at 37 °C for 72 h (80% N_2, 10% CO_2, 10% H_2) in an anaerobic chamber (Don Whitley Scientific, Bradford, U.K.).

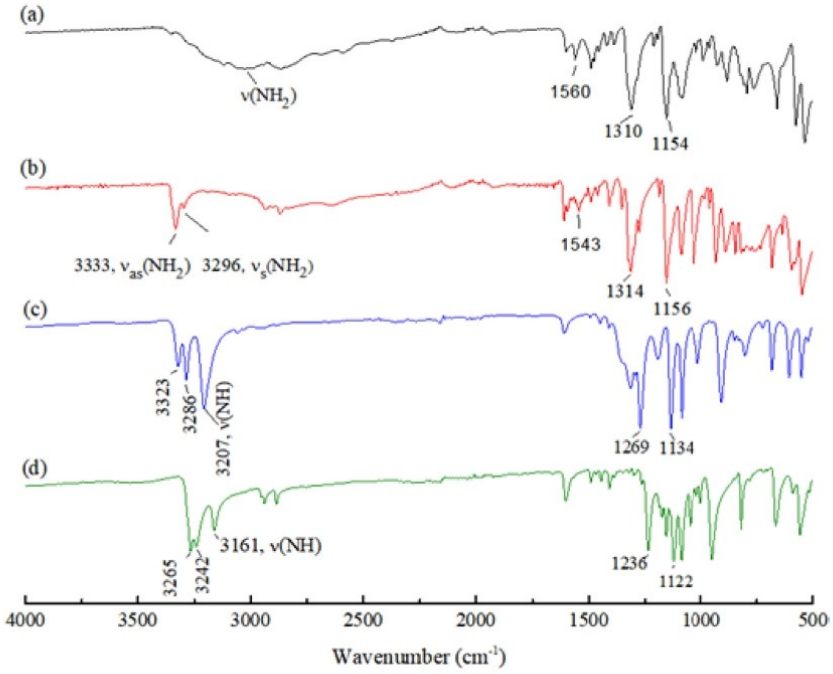

Fig. 2. Infrared spectra of (a) Maf, (b) eMaf, (c) Ag-Maf and (d) Ag-eMaf.

After incubation, 30 μL of 0.02 % aqueous resazurin (Sigma®) solution was added to each well, to reveal bacterial growth [60]. The blue and red colors represent the absence and the presence of microbial growth, respectively. Dimethylsulfoxide 5% (v/v) was used as negative control. As a positive control, gentamicin (0.0115 to 5.9 µg mL^{-1}), vancomycin (0.0115 to 5.9 µg mL^{-1}) and chloramphenicol (7.198 to 5000 µg mL^{-1}) were used for aerobic bacteria and only gentamicin (0.0115 to 5.9 µg mL^{-1}) as a positive control for the anaerobic bacteria. An inoculum was included to monitor ground for bacterial growth. The experiments were carried out in triplicate.

2.7. Gel electrophoresis assay

For polyacrylamide gel electrophoresis assays with bovine serum albumin (BSA) or with lysozyme, solutions of Maf, e-Maf and $AgNO_3$ (1.0 mmol L^{-1}) were prepared in water with 1% (v/v) DMSO. Due to their low solubilities, Ag-Maf and Ag-eMaf complexes were suspended in water with 1% (v/v) DMSO. A volume of 5 µL of the samples were then mixed with 10 µL solution of BSA or lysozyme (250 µmol L^{-1} in phosphate buffer HPO_4^{2-}/ $H_2PO_4^-$, pH = 7.4) followed by 35 µL of phosphate buffer, and incubated at 37 °C for 3 h. After incubation, 50 µL of loading buffer (Tris/HCl 100 mmol L^{-1}, pH 6.8, SDS 4.0%, bromophenol blue 0.2% and glycerol 20.0%) were added to each sample for a final concentration of 50 µmol L^{-1} and 25 µmol L^{-1} of compound and protein, respectively.

The mixture was then heated in a water bath at 96 °C for 5 min. All samples (10 µL) were added to the SDS-polyacrylamide gel electrophoresis (SDS-PAGE, standard 5% polyacrylamide preparation gel for both BSA and lysozyme, 12% polyacrylamide resolution gel for albumin and 18% polyacrylamide resolution gel for lysozyme) and electrophoresed for 2 h (100 V). Each gel was then washed with distilled water and dyed using a Coomassie blue solution. A sample containing only BSA or only lysozyme and the proper buffer was used as control; Precision Plus Protein™ Dual Color Standard was used as protein weight marker.

3. Results and discussion

3.1. Infrared (IR) absorption spectroscopy

The coordination of Maf and eMaf to Ag(I) ions was investigated by IR spectroscopic measurements. The IR spectra of complexes and ligands are presented in **Fig. 2**.

A broad band in the range 3400-2600 cm^{-1} can be observed in the IR spectrum of mafenide acetate, which was assigned to the asymmetric and symmetric stretching modes of NH_2 and CH_2 groups. The broadening of this band can be attributed to the presence of hydrogen bonds between the amino groups of the ligand and/or oxygen atoms from the acetate counterion. In the spectrum of eMaf, the asymmetric and symmetric stretching modes of the NH_2 group were observed at 3333 and 3296 cm^{-1}.

Upon coordination, two well-resolved vibrational bands at 3323 and 3286 cm^{-1} are observed in the IR spectrum of Ag-Maf, while for Ag-eMaf the bands are observed at 3265 and at 3242 cm^{-1}. The presence of such bands correspond, respectively, to the asymmetric and symmetric stretching modes of NH_2 of the uncoordinated aliphatic amine present in the structure of the ligand [13]. There is also a strong and sharp band located in 3207 cm^{-1} in the spectrum of the Ag-Maf complex, which refers to the N-H stretching mode of the SO_2NH group [61]. The same vibrational band is observed at 3161 cm^{-1} in the spectrum of Ag-eMaf. The presence of such absorption band confirms the deprotonation of the former

Table 1
^{13}C NMR assignment and chemical shifts (ppm) for Maf, eMaf, Ag-Maf and Ag-eMaf.

Maf Assignments	δ (ppm)	Ag-Maf Assignments	δ (ppm)	eMaf Assignments	δ (ppm)	Ag-eMaf Assignments	δ (ppm)
C 1	42.7	**C 1**	49.2	**C 1**	42.9	**C 1**	42.1
C 2	142.4	**C 2**	145.8	**C 2**	46.7	**C 2**	47.26
C 3, 3', 4, 4'	127.3	**C 3, 3', 4, 4'**	127.1	**C 3**	145.3	**C 3**	142.0
C 5	138.8	**C 5**	143.0	**C 4, 4', 5, 5'**	129.0	**C 4, 4', 5, 5'**	128.5
C 6	23.8			**C 6**	142.0	**C 6**	140.1
C 7	181.5						

SO_2NH_2 group present in the structure of Maf and eMaf and suggests coordination of the nitrogen atom of this group to silver(I). Vibrational bands were also observed at 1560 and at 1543 cm^{-1} in the IR spectra of mafenide acetate and ethyl-mafenide, respectively. Such bands can be attributed to H-N-H bending mode of the SO_2NH_2 group.

In addition, two absorption bands with their maxima at 1310 and 1154 cm^{-1} in the IR spectrum of Maf, and at 1314 and 1156 cm^{-1} in the spectrum of eMaf are observed. Such bands are assigned to the asymmetric and symmetric stretching modes of the O=S=O group [13]. After coordination, such bands are shifted to low energy values, being observed at 1269 and 1133 cm^{-1} for Ag-Maf and at 1236 and 1122 cm^{-1} for Ag-eMaf. The shift of the asymmetric and symmetric stretching modes of the O=S=O group reinforces the coordination of the ligands to silver(I) by the deprotonated sulfonamide group and also suggests that the oxygen atom from the sulfone group also participates on coordination [13].

3.2. NMR spectroscopic measurements

The NMR assignments of Maf and eMaf were primarily performed by solution state ^1H and ^{13}C NMR spectroscopy (supplementary material, **Figure S1-S4**) in deuterated water (D_2O). For Maf, the salt used in the NMR studies in D_2O was mafenide hydrochloride instead of mafenide acetate. The atoms numbering schemes and NMR assignments are shown in **Fig. 1** and **Table S1** in the supplementary material, respectively.

Due to the low solubility of the complexes in water and other solvents, solid-state NMR spectroscopic measurements were performed to confirm the coordination sites of the ligands to Ag(I). From the solution ^{13}C NMR data it was possible to attribute the ^{13}C NMR signals in the spectra obtained from the solid samples of the compounds. Such spectroscopic technique has proven to be a useful tool to ascribe the sulfonamide coordination sites to metal ions by carbon atoms displacement [62]. The solid-state ^{13}C NMR spectra for the complexes and the respective ligands (mafenide acetate and ethyl-mafenide) are shown in **Fig. 3**, while the ^{13}C NMR assignments and chemical shifts are presented in Table 1.

In the solid-state ^{13}C NMR spectrum of the Ag-Maf complex, carbon atoms of the acetate counterion present in mafenide acetate (Maf) are no longer observed. Such data confirms the loss of the counterion after coordination of Maf to silver(I). The most prominent chemical shifts when the NMR spectra of Maf and Ag-Maf are compared are observed for carbon atoms C1, bonded to the aliphatic NH_2 group, and C5, which is directly bonded to the sulfonamide group. The observed data for carbon atom C5 reinforces coordination of Maf to silver(I) by the sulfonamide moiety as suggested by the IR data. Nevertheless, since carbon atom C1 is also shifted when the ^{13}C NMR spectra of the ligand and complex are compared, coordination by aliphatic NH_2 group cannot be discarded by considering solely this technique.

For Ag-eMaf, the most prominent chemical shifts when compared to eMaf are observed for carbon atoms C3 and C6. Since carbon atom C6 is directly bonded to the sulfonamide group, coordination of eMaf to silver by the deprotonated SO_2NH group can also be proposed as initially suggested when considering the IR data.

Table 2
Energy value and the variation between the structures for the complexes Ag-Maf and Ag-eMaf. Data was determined by the theory wB97XD/6-31+G(d,p)/LANL2DZ.

Complex	Energy (kcal mol^{-1})	ΔE (kcal mol^{-1})
a2	−675095.98	19.05
a3	−675076.93	
b2	−699760.43	17.34
b3	−699743.10	

3.3. Computational Studies

Since no suitable single crystals were obtained to perform a detailed structural characterization of the complexes by X-ray diffraction, DFT studies were employed to support the coordination sites of the ligands to silver as suggested by IR and NMR spectroscopic data. From the IR spectra of ligands and complexes, it was suggested that the coordination occurs by the sulfonamide group. In addition, the observed ^{13}C NMR chemical shifts when ligands and the respective complexes are compared reinforce coordination of Maf and eMaf to silver(I) ions by the sulfonamide group. For the Ag-Maf, coordination by the aliphatic NH_2 group could not be discarded when considering only the ^{13}C NMR. So, based on the experimental data, coordination modes for the Ag-Maf and Ag-eMaf complexes were suggested as presented in **Fig. 4**.

According to the theoretical data, it is possible to infer that the possibilities (**4a1**) and (**4b1**), upon geometrical optimization, converge to complexes (**4a2**) and (**4b2**). In these representations, Maf and eMaf are coordinated in a bidentate mode to silver(I). The coordination occurs by the nitrogen and one of the oxygen atoms present in the deprotonated SO_2NH group. The results agree with those observed in the infrared and NMR spectroscopic analysis where coordination occurs by the sulfonamide group.

Finally, a third coordination mode by the aliphatic NH_2 group represented in **Figs. 4a3** and **4b3** was also investigated. However, such coordination mode is energetically less favored than the bidentate coordination mode by the sulfonamide moiety. Also, the occurrence of the coordination solely by the NH_2 group as represented in **Figs. 4a3** and **4b3** disagrees with the shifts observed in the asymmetric and symmetric IR stretching modes of the O=S=O group upon coordination. The energy values for the complexes and the difference between structures are represented in **Table 2**.

The difference between bidentate coordination by the N,O atoms of the sulfonamide moiety and the coordination only by the aliphatic amine is 19.05 kcal mol^{-1} for Ag-Maf and 17.34 kcal mol^{-1} for Ag-eMaf. The calculated difference in energy led us to infer that the bidentate coordination is indeed the most probable to exist for both complexes in the solid state. Bond lengths obtained by molecular modeling for N•••Ag and O•••Ag in the case of the Ag-Maf complex are, respectively, 2.183 and

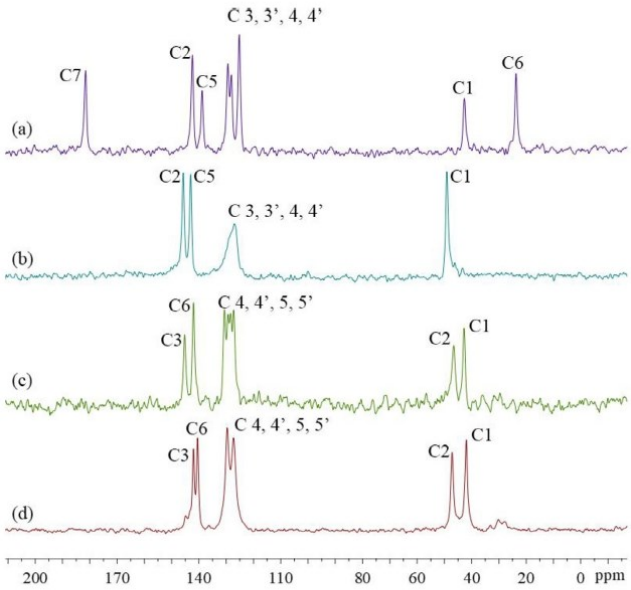

Fig. 3. Solid-state ^{13}C NMR spectra of (a) Maf, (b) Ag-Maf, (c) eMaf and (d) Ag-eMaf.

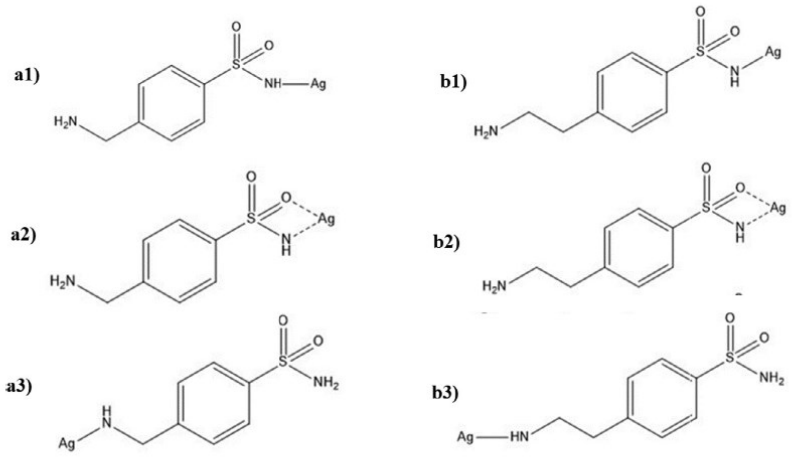

Fig. 4. Simulated coordination modes for a) Ag-Maf and b) Ag-eMaf.

2.527 Å. For the Ag-eMaf complex, bond lengths are 2.181 Å and 2.533 Å for N•••Ag and for O•••Ag, respectively. It is important to notice that bond length values are similar since the coordination site is the same. Also, the values observed in both complexes are in agreement with the values found to similar silver(I) complexes that present the same coordination modes [63].

For a better understanding of electronic effects of the complexes Quantum Theory of Atoms in Molecules (QTAIM) was applied. This methodology can describe the kind of bond or interaction through some parameters as electronic density (ρ(r)), Electronic density Laplacian ($\nabla^2\rho$(r)) and total electronic energy (H (r)) [46–49]. When $\nabla^2\rho$(r) and H(r) values are positive, the interaction or bond is electrostatic, while for $\nabla^2\rho$(r) positive and H(r) negative the bond is considered partially covalent [46–49]. In **Fig. 5** the molecular graphs are represented for the Ag-Maf and Ag-eMaf and their electronic characteristics are presented in **Table S2** (supplementary material).

Values found by QTAIM shows that $\nabla^2\rho$(r) is positive and H(r) is negative for the Ag-O and Ag-N bonds in both complexes, which shows that coordination bonds have a covalent character.

All the theoretical data suggests that the coordination occurs in a bidentate chelate mode. However, these results do not take in consideration the effects of inter and intramolecular interaction in the solid. Therefore, when we compare the observed data obtained for Ag-Maf and Ag-eMaf to other silver(I) complexes presented in literature, including silver sulfadiazine, [1,64], the forma-

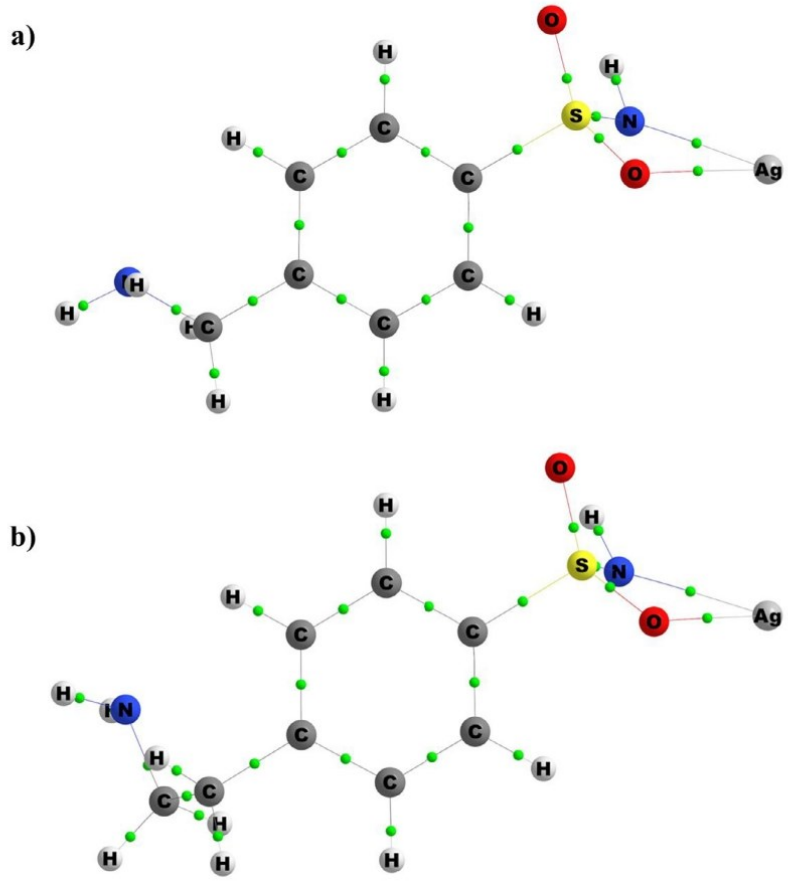

Fig. 5. Molecular plots for the a) Ag-Maf and b) Ag-eMaf complexes. The critical points of attachment are represented by green circles.

tion of polymeric structural arrangements for the complexes Ag-Maf and Ag-eMaf cannot be discarded.

3.4. Antiviral activity assays

First, a cell viability assay was performed in order to evaluate the cytotoxicity of the compounds. For this, BHK-21 cells were treated with Ag-Maf, Ag-eMaf, eMaf, and $AgNO_3$ at 50, 10, and 2 μmol L^{-1} for 16 h, and cell viability was assessed by MTT assay. The results showed that BHK-1 cells were viable in concentrations equal and/or lower than 10 μmol L^{-1} for Ag-Maf, Ag-eMaf, and $AgNO_3$ (**Figure S5** and **Table S3** in supplementary material). For Maf and eMaf, on the other hand, cells were viable for concentrations $\leq$ 50 μmol L^{-1} (**Figure S5** and **Table S3**).

To evaluate the anti-CHIKV activity of the compounds, BHK-21 cells were infected with CHIKV-*nanoluc* and simultaneously treated with compounds at the highest non-cytotoxic concentration, and viral replication was assessed 16 h post-infection (h.p.i.). The results showed that the ligand Maf at concentration of 50 μmol L^{-1} did not inhibit CHIKV replication, whereas eMaf at 50 μmol L^{-1} inhibited 53% of CHIKV replication *in vitro* (**Fig. 6** and the data of **Table S4** in supplementary material). The complexes Ag-Maf at10 μmol L^{-1} and Ag-eMaf at 10 μmol L^{-1} reduced up to 61 and 64 % of virus replication, respectively (**Fig. 6** and the data of **Table S4**). This data suggests that the coordination affected the antiviral activity on virus replication, mainly observed by the stronger activity of the complexes in the treatment at lower concentration than the free ligands. The promising *in vitro* results led us to consider further studies concerning the use of silver-sulfonamide complexes as antiviral agents as just described in the literature for distinct metal ions and ligand classes [1].

3.5. Antibacterial activity studies

The MIC results of the compounds against the five bacterial strains analyzed are shown in **Table 3**. The values ranged from 3.12 to > 400 μg mL^{-1}. The lowest concentration values were found for Ag-Maf and Ag-eMaf over the aerobic bacterial strains *S. aureus, B. cepacia, S. epidermidis* and *P. aeruginosa* with MIC values from 21.3 to 170 μmol L^{-1}. The lowest MIC value was found for the complexes over Gram-negative *P. aeruginosa* strain, which is considered as one of the most common bacteria isolated from chronic wounds [65]. In the case of the anaerobic bacteria *C. acnes*, the lowest MIC value was found for Ag-Maf (682 μmol L^{-1}). For silver sulfadiazine,

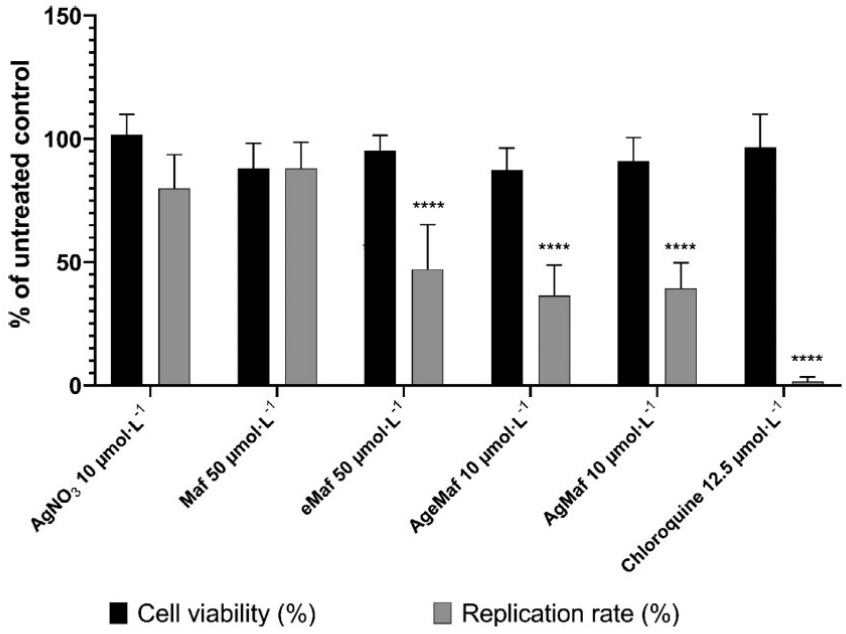

Figure 6. Effect of the highest non-cytotoxic concentration of the compounds upon CHIKV replication. DMSO and water were used as untreated control and Chloroquine at 12.5 µM was used as a positive control. Mean values of one independent experiment each measured in triplicate including the standard deviation are shown. (****) $p < 0.0001$.

Table 3
Minimum inhibitory concentration of isolated compounds against aerobic and anaerobic bacteria. Values are presented in µg mL^{-1} (µmol L^{-1})

Samples	Aerobic *S. aureus* ATCC BA44	*B. cepacia* ATCC 25416	*S. epidermidis* ATCC 12228	*P. aeruginosa* ATCC 15442	Anaerobic *C. acnes* ATCC 11827
Maf	>400 (>1624)	>400 (>1624)	>400 (>1624)	>400 (>1624)	100 (406)
eMaf	>400 (>1997)	>400 (>1997)	>400 (>1997)	>400 (>1997)	>400 (>1997)
Ag-Maf	50 (170)	12.5 (42.6)	12.5 (42.6)	6.25 (21.3)	200 (682)
Ag-eMaf	50 (162.8)	12.5 (40.7)	12.5 (40.7)	12.5 (40.7)	400 (1302)
$AgNO_3$	12.5 (73.6)	3.12 (18.4)	3.12 (18.4)	3.12 (18.4)	100 (587)
SSD[(a)]			(224)	(56)	
Gentamicin	-	-	0.05	1.5	0.4
Vancomycin	0.7	-	-	-	-
Chloramphenicol	-	14.4	-	-	-

(a) from reference 66

which is used in the clinics, the MIC value found in the literature for *P. aeruginosa* (ATCC 15442) was 56 μmol L^{-1}, while for *S. aureus* (ATCC 6538), and *S. epidermidis* (ATCC 12228) the MIC values were higher than 100 μmol L^{-1} [66]. So, the observed MIC values for Ag-Maf and Ag-eMaf are closely related to SSD over *P. aeruginosa* and lower than SSD over *S. aureus* and *S. epidermidis*. Moreover, the observed results indicated that the MIC values for Ag-Maf and Ag-eMaf complexes are 10 to 100 times lower than those for other silver-sulfonamide complexes such as silver sulfathiazole and sulfamethoxazole, where the MIC values were in the range 1.74-6.90 mmol L^{-1} over Gram-positive *S. aureus* and Gram-negative *P. aeruginosa* bacterial strains [13].

Although silver nitrate exhibits MIC values similar to those observed for the Ag-Maf and Ag-eMaf complexes, silver nitrate in concentrations higher than 1% are toxic to tissues [67]. In addition, as described in the literature, the fast and uncontrolled release of silver ions from silver nitrate has limited its application in the clinics [32,37]. The results observed for Ag-Maf and Ag-eMaf, when compared to other similar compounds in the literature and also with SSD *in vitro*, demonstrate that such compounds can be considered as alternatives in the topical treatment of skin lesions. *In vivo* studies are envisaged to validate the potential of application of the complexes in the clinics.

3.6. Biophysical studies (SDS-PAGE)

The biophysical assays were performed to investigate possible molecular targets for the complexes. The interaction between the compounds and the proteins BSA and lysozyme was evaluated by SDS-PAGE. Cisplatin was used as a positive control. The results are present in **Figure S6** (see supplementary material).

The SDS-PAGE experiment with BSA did not show a clear modification on the profile of the protein bands. However, this result is not conclusive because all of bands were broadened. This observation is due to the fact that BSA is a large protein (approximately 66.5 kDa), and it might be difficult to observe and evaluate changes in the electrophoretic pattern when interacted with small molecules.

Lysozyme, when compared to BSA, is a small protein (approximately 14.3 kDa) and so, the effects of the complex in this protein could be more noticeable. However, no significant changes on the electrophoretic profile of lysozyme were observed, which indicates that the complexes and ligands do not have a strong interaction with these proteins.

4. Conclusions

Two new silver(I) complexes with mafenide and ethyl-mafenide of compositions $AgC_7H_9N_2O_2S$ and $AgC_8H_{11}N_2O_2S$, respectively, were obtained. Coordination of the ligands to silver(I) seems to occur by the oxygen and nitrogen atoms of the sulfonamide moiety as indicated by IR and NMR spectroscopic data. Theoretical (DFT) studies reinforce the coordination of Maf and eMaf to silver ions by the nitrogen and oxygen atoms of the sulfonamide group in a bidentate chelate mode. The silver complexes and free sulfonamides were tested as anti-CHIKV agents for the first time. The observed data suggested that the coordination affected the antiviral activity on virus replication, mainly observed by the stronger activity of the complexes in the treatment with low concentration when compared to the free sulfas. The complexes presented antibacterial activity over the aerobic strains *S. aureus, B. cepacia, S. epidermidis* and *P. aeruginosa* with MIC values from 21.3 to 170 μmol L^{-1}, being comparable to those presented by silver sulfadiazine SSD *in vitro*. Further *in vivo* studies are envisaged to evaluate the application of the complexes as alternatives in clinics against bacterial infections. Biophysical studies showed that the complexes do not have a strong interaction with proteins BSA and lysozyme, which indicates that such biomolecules are not the main targets of the compounds.

Disclosure statement

No potential conflict of interest was reported by the authors.

Declaration of Competing Interest

The authors declare that they have no known competing financial interests or personal relationships that could have appeared to influence the work reported in this paper.

CRediT authorship contribution statement

Pedro Gonçalves Esquezaro: Conceptualization, Methodology, Investigation, Validation. **Carlos Marrote Manzano:** Investigation. **Douglas Hideki Nakahata:** Investigation. **Igor Andrade Santos:** Methodology, Investigation, Writing – original draft. **Uriel Enrique Aquino Ruiz:** Investigation. **Mariana Brentini Santiago:** Investigation. **Nagela Bernadelli Souza Silva:** Investigation. **Carlos Henrique Gomes Martins:** Methodology, Investigation, Funding acquisition, Writing – original draft. **Douglas Henrique Pereira:** Methodology, Investigation, Funding acquisition. **Fernando Rodrigues Goulart Bergamini:** Conceptualization, Investigation, Writing – review & editing, Project administration, Supervision, Funding acquisition. **Ana Carolina Gomes Jardim:** Conceptualization, Investigation, Writing – review & editing, Project administration, Supervision, Funding acquisition. **Pedro Paulo Corbi:** Conceptualization, Investigation, Writing – review & editing, Project administration, Supervision, Funding acquisition.

Acknowledgements

We thank Andres Merits (Institute of Technology, University of Tartu, Tartu, Estonia) for the provision of the CHIKV expressing-nanoluciferase reporter. IAS thanks to Conselho Nacional de Desenvolvimento Científico e Tecnológico (CNPq), scholarship # 142495/2020-4. ACGJ is also grateful to Royal Society—Newton Advanced Fellowship (grant reference NA 150195) and to FAPEMIG (Minas Gerais Research Foundation—APQ-00587-14, SICONV 793988/2013 and APQ-03385-18). FRGB and ACGJ are grateful to Coordenação de Aperfeiçoamento de Pessoal de Nível Superior (CAPES)—Brasil—Prevention and Combat of Outbreaks, Endemics, Epidemics and Pandemics—Finance Code #88881.506794/2020-01. FRGB also thanks to he multiusuary laboratory of the Institute of Chemistry at the University Federal Uberlândia for providing the equipment and technical support for the experiments. PPC and CMM thanks to FAPESP 2018/12062-4, 2017/25995-6, CAPES-Print 2464/2018 (Grant # 88881.310539/2018-01 and CAPES-Finance Code 001) and CNPq (grant # 407012/2018-4). DHP also acknowledges the Center for Computational Engineering and Sciences (Financial support from FAPESP, Grants No. 2013/08293-7 and 2017/11485-6) and the National Center for High Performance Processing (CENAPAD) in São Paulo for the computational resources. CHGM thanks to National Council for Scientific and Technological Development (CNPq) Process n° 307974/2019-7.

Supplementary materials

Supplementary material associated with this article can be found, in the online version, at doi:10.1016/j.molstruc.2021.131261.

References

[1] R.E.F. De Paiva, A. Marçal Neto, I.A. Santos, A.C.G. Jardim, P.P. Corbi, F.R.G. Bergamini, What is holding back the development of antiviral metallodrugs? A literature overview and implications for SARS-CoV-2 therapeutics and future viral outbreaks, Dalt. Trans. 49 (2020) 16004–16033, doi:10.1039/d0dt02478c.
[2] World Health Organization, World health statistics 2019 : monitoring health for the SDGs, sustainable development goals, (2019).
[3] M. Babic, A. Hujer, R. Bonomo, What's new in antibiotic resistance? Focus on beta-lactamases, Drug Resist. Updat. 9 (2006) 142–156, doi:10.1016/j.drup.2006.05.005.
[4] A.C. Rios, C.G. Moutinho, F.C. Pinto, F.S. Del Fiol, A. Jozala, M.V. Chaud, M.M.D.C. Vila, J.A. Teixeira, V.M. Balcão, Alternatives to overcoming bacterial resistances: State-of-the-art, Microbiol. Res. 191 (2016) 51–80, doi:10.1016/j.micres.2016.04.008.
[5] I. de A. Santos, V.R. Grosche, F.R.G. Bergamini, R. Sabino-Silva, A.C.G. Jardim, Antivirals against coronaviruses: candidate drugs for SARS-CoV-2 treatment? Front. Microbiol. 11 (2020) 1818, doi:10.3389/fmicb.2020.01818.
[6] S.J.R. da Silva, J.J.F. de Magalhães, L. Pena, Simultaneous circulation of DENV, CHIKV, ZIKV and SARS-CoV-2 in Brazil: an inconvenient truth, One Heal 12 (2021) 100205, doi:10.1016/j.onehlt.2020.100205.
[7] L. Dupuis-Maguiraga, M. Noret, S. Brun, R.Le Grand, G. Gras, P. Roques, Chikungunya disease: Infection-associated markers from the acute to the chronic phase of arbovirus-induced arthralgia, PLoS Negl. Trop. Dis. 6 (2012) e1446, doi:10.1371/journal.pntd.0001446.
[8] D.O.S. Martins, I.D.A. Santos, D.M. De Oliveira, V.R. Grosche, A.C.G. Jardim, Antivirals against chikungunya virus: is the solution in nature? Viruses 12 (2020) 272, doi:10.3390/v12030272.
[9] A. Casini, A. Scozzafava, C.T. Supuran, Sulfonamide derivatives with protease inhibitory action as anticancer, anti-inflammatory and antiviral agents, Expert Opin. Ther. Pat. 12 (2002) 1307–1327, doi:10.1517/13543776.12.9.1307.
[10] R.E.F. de Paiva, C. Abbehausen, A.F. Gomes, F.C. Gozzo, W.R. Lustri, A.L.B. Formiga, P.P. Corbi, Synthesis, spectroscopic characterization, DFT studies and antibacterial assays of a novel silver(I) complex with the anti-inflammatory nimesulide, Polyhedron 36 (2012) 112–119, doi:10.1016/j.poly.2012.02.002.
[11] L.M. Lima, B.N.M. da Silva, G. Barbosa, E.J. Barreiro, β-lactam antibiotics: an overview from a medicinal chemistry perspective, Eur. J. Med. Chem. 208 (2020) 112829, doi:10.1016/j.ejmech.2020.112829.
[12] E. Scholar, Sulfonamides, in: XPharm Compr. Pharmacol. Ref., Elsevier, 2007: pp. 1–4. doi:10.1016/B978-008055232-3.61013-X.
[13] J.H. Bormio Nunes, R.E.F. de Paiva, A. Cuin, W.R. Lustri, P.P. Corbi, Silver complexes with sulfathiazole and sulfamethoxazole: synthesis, spectroscopic characterization, crystal structure and antibacterial assays, Polyhedron 85 (2015) 437–444, doi:10.1016/j.poly.2014.09.010.
[14] A. Afshari, L. Nguyen, S.A. Kahn, B. Summitt, 2.5% Mafenide Acetate, J. Burn Care Res. 38 (2017) e42–e47, doi:10.1097/BCR.0000000000000425.

[15] A.S. Pereira, K.B. Kenney, M.S. Cohen, J.J. Eron, R.R. Tidwell, J.A. Dunn, Determination of amprenavir, a HIV-1 protease inhibitor, in human seminal plasma using high-performance liquid chromatography- tandem mass spectrometry, J. Chromatogr. B Anal. Technol. Biomed. Life Sci. 766 (2002) 307–317, doi:10.1016/S0378-4347(01)00512-6.
[16] M.G. White, M.J. Asch, Acid-base effects of topical mafenide acetate in the burned patient, N. Engl. J. Med. 284 (1971) 1281–1286, doi:10.1056/NEJM197106102842302.
[17] J.S. Glasser, C.H. Guymon, K. Mende, S.E. Wolf, D.R. Hospenthal, C.K. Murray, Activity of topical antimicrobial agents against multidrug-resistant bacteria recovered from burn patients, Burns 36 (2010) 1172–1184, doi:10.1016/j.burns.2010.05.013.
[18] Z. Pang, R. Raudonis, B.R. Glick, T.J. Lin, Z. Cheng, Antibiotic resistance in Pseudomonas aeruginosa: mechanisms and alternative therapeutic strategies, Biotechnol. Adv. 37 (2019) 177–192, doi:10.1016/j.biotechadv.2018.11.013.
[19] M. Durgun, H. Turkmen, M. Ceruso, C.T. Supuran, Synthesis of Schiff base derivatives of 4-(2-aminoethyl)-benzenesulfonamide with inhibitory activity against carbonic anhydrase isoforms I, II, IX and XII, Bioorganic Med. Chem. Lett. 25 (2015) 2377–2381, doi:10.1016/j.bmcl.2015.04.007.
[20] S. Medici, M. Peana, V.M. Nurchi, M.A. Zoroddu, Medical uses of silver: history, myths, and scientific evidence, J. Med. Chem. 62 (2019) 5923–5943, doi:10.1021/acs.jmedchem.8b01439.
[21] S. Medici, M. Peana, G. Crisponi, V.M. Nurchi, J.I. Lachowicz, M. Remelli, M.A. Zoroddu, Silver coordination compounds: a new horizon in medicine, Coord. Chem. Rev. (2016) 349–359 327–328, doi:10.1016/j.ccr.2016.05.015.
[22] A.L. Semeykina, V.P. Skulachev, Submicromolar Ag+ increases passive Na + permeability and inhibits the respiration-supported formation of Na + gradient in Bacillus FTU vesicles, FEBS Lett 269 (1990) 69–72, doi:10.1016/0014-5793(90)81120-D.
[23] F.R.G. Bergamini, M.A. Ferreira, R.E.F. de Paiva, A.F. Gomes, F.C. Gozzo, A.L.B. Formiga, F.C.A. Corbi, I.O. Mazali, D.A. Alves, M. Lancellotti, P.P. Corbi, A binuclear silver complex with l-buthionine sulfoximine: synthesis, spectroscopic characterization, DFT studies and antibacterial assays, RSC Adv 2 (2012) 10372, doi:10.1039/c2ra21433d.
[24] K.D. Mjos, C. Orvig, Metallodrugs in medicinal inorganic chemistry, Chem. Rev. 114 (2014) 4540–4563, doi:10.1021/cr400460s.
[25] S. Medici, M. Peana, V.M. Nurchi, J.I. Lachowicz, G. Crisponi, M.A. Zoroddu, Noble metals in medicine: latest advances, Coord. Chem. Rev. 284 (2015) 329–350, doi:10.1016/j.ccr.2014.08.002.
[26] X. Liang, S. Luan, Z. Yin, M. He, C. He, L Yin, Y. Zou, Z. Yuan, L Li, X. Song, C. Lv, W. Zhang, Recent advances in the medical use of silver complex, Eur. J. Med. Chem. 157 (2018) 62–80, doi:10.1016/j.ejmech.2018.07.057.
[27] I.L. Paiva, G.S.G. De Carvalho, A.D. Da Silva, P.P. Corbi, F.R.G. Bergamini, A.L.B. Formiga, R. Diniz, W.R. Do Carmo, C.Q.F. Leite, F.R. Pavan, A. Cuin, Silver(I) complexes with symmetrical Schiff bases: synthesis, structural characterization, DFT studies and antimycobacterial assays, Polyhedron 62 (2013) 104–109, doi:10.1016/j.poly.2013.06.031.
[28] Y.-H. Ou, R.-K. Du, S.-P. Zhang, Y. Ling, S. Li, C.-J. Zhao, W.-Z. Zhang, L. Zhang, Synthesis, crystal structure and in vitro antifungal activity of two-dimensional silver(I)-voriconazole coordination complexes, J. Mol. Struct. 1215 (2020) 128229, doi:10.1016/j.molstruc.2020.128229.
[29] C.N. Banti, S.K. Hadjikakou, Anti-proliferative and anti-tumor activity of silver(I) compounds, Metallomics 5 (2013) 569, doi:10.1039/c3mt00046j.
[30] S.S. Jeremiah, K. Miyakawa, T. Morita, Y. Yamaoka, A. Ryo, Potent antiviral effect of silver nanoparticles on SARS-CoV-2, Biochem. Biophys. Res. Commun. 533 (2020) 195–200, doi:10.1016/j.bbrc.2020.09.018.
[31] O. Sánchez, S. González, Á.R. Higuera-Padilla, Y. León, D. Coll, M. Fernández, P. Taylor, I. Urdanibia, H.R. Rangel, J.T. Ortega, W. Castro, M.C. Goite, Remarkable in vitro anti-HIV activity of new silver(I)- and gold(I)-N-heterocyclic carbene complexes. Synthesis, DNA binding and biological evaluation, Polyhedron 110 (2016) 14–23, doi:10.1016/j.poly.2016.02.012.
[32] C.L. Fox, S.M. Modak, Mechanism of silver sulfadiazine action on burn wound infections, Antimicrob. Agents Chemother. 5 (1974) 582–588, doi:10.1128/AAC.5.6.582.
[33] C.L. Fox, Silver sulfadiazine—a new topical therapy for pseudomonas in burns: therapy of pseudomonas infection in burns, Arch. Surg. 96 (1968) 184–188, doi:10.1001/archsurg.1968.01330200022004.
[34] S.M. Modak, C.L. Fox, Binding of silver sulfadiazine to the cellular components of Pseudomonas aeruginosa, Biochem. Pharmacol. 22 (1973) 2391–2404, doi:10.1016/0006-2952(73)90341-9.
[35] T.W. Chang, L. Weinstein, In vitro activity of silver sulfadiazine against Herpesvirus hominis, J. Infect. Dis. 132 (1975) 79–81, doi:10.1093/infdis/132.1.79.
[36] L.M. Yamamoto, J.H.B. Nunes, M.A. Ribeiro, A.M. da C. Ferreira, W.R. Lustri, P.P. Corbi, Copper(II) and silver(I) complexes with sulfamethizole: synthesis, spectroscopic characterization, ESI-QTOF mass spectrometric analysis, crystal structure and antibacterial activities, Polyhedron 138 (2017) 168–176, doi:10.1016/j.poly.2017.09.034.
[37] A.T.M. Fiori, D.H. Nakahata, A. Cuin, W.R. Lustri, P.P. Corbi, Synthesis, crystallographic studies, high resolution mass spectrometric analyses and antibacterial assays of silver(I) complexes with sulfisoxazole and sulfadimethoxine, Polyhedron 121 (2017) 172–179, doi:10.1016/j.poly.2016.09.046.
[38] D.H. Nakahata, W.R. Lustri, A. Cuin, P.P. Corbi, Crystal structure, spectroscopic characterization and antibacterial activities of a silver complex with sulfameter, J. Mol. Struct. 1125 (2016) 609–615, doi:10.1016/j.molstruc.2016.07.049.
[39] J.-D. Chai, M. Head-Gordon, Long-range corrected hybrid density functionals with damped atom–atom dispersion corrections, Phys. Chem. Chem. Phys. 10 (2008) 6615, doi:10.1039/b810189b.
[40] R. Ditchfield, W.J. Hehre, J.A. Pople, Self-consistent molecular-orbital methods. ix. an extended gaussian-type basis for molecular-orbital studies of organic molecules, J. Chem. Phys. 54 (1971) 724–728, doi:10.1063/1.1674902.
[41] W.J. Hehre, R. Ditchfield, J.A. Pople, Self—consistent molecular orbital methods. XII. Further extensions of Gaussian—type basis sets for use in molecular orbital studies of organic molecules, J. Chem. Phys. 56 (1972) 2257–2261, doi:10.1063/1.1677527.
[42] P.C. Hariharan, J.A. Pople, The influence of polarization functions on molecular orbital hydrogenation energies, Theor. Chim. Acta. 28 (1973) 213–222, doi:10.1007/BF00533485.
[43] P.J. Hay, W.R. Wadt, Ab initio effective core potentials for molecular calculations. Potentials for the transition metal atoms Sc to Hg, J. Chem. Phys. 82 (1985) 270–283, doi:10.1063/1.448799.
[44] J. Frisch, G.W. Trucks, H.B. Schlegel, G.E. Scuseria, M.A. Robb, J.R. Cheeseman, G. Scalmani, V. Barone, B. Mennucci, G.A. Petersson, H. Nakatsuji, M. Caricato, X. Li, H.P. Hratchian, A.F. Izmaylov, J. Bloino, G. Zheng, J.L. Sonnenberg, M. Hada, M. Ehara, K. Toyota, R. Fukuda, J. Hasegawa, M. Ishida, T. Nakajima, Y. Honda, O. Kitao, H. Nakai, T. Vreven, J.A. Montgomery, J.E. Peralta, F. Ogliaro, M. Bearpark, J.J. Heyd, E. Brothers, K.N. Kudin, V.N. Staroverov, R. Kobayashi, J. Normand, K. Raghavachari, A. Rendell, J.C. Burant, S.S. Iyengar, J. Tomasi, M. Cossi, N. Rega, J.M. Millam, M. Klene, J.E. Knox, J.B. Cross, V. Bakken, C. Adamo, J. Jaramillo, R. Gomperts, R.E. Stratmann, O. Yazyev, A.J. Austin, R. Cammi, C. Pomelli, J.W. Ochterski, R.L. Martin, K. Morokuma, V.G. Zakrzewski, G.A. Voth, P. Salvador, J.J. Dannenberg, S. Dapprich, A.D. Daniels, Ö. Farkas, J.B. Foresman, J.V. Ortiz, J. Cioslowski, D.J. Fox, Gaussian09, Revision D.1, Gaussian, Inc., Wallingford, CT, 2009.
[45] R. Dennington, T. Keith, J. Millam, Gauss View, Version 5, Semichem Inc., Shawnee Mission, 2009.
[46] N.M. O'boyle, A.L. Tenderholt, K.M. Langner, cclib: A library for package-independent computational chemistry algorithms, J. Comput. Chem. 29 (2008) 839–845, doi:10.1002/jcc.20823.
[47] R.F.W. Bader, H. Essén, The characterization of atomic interactions, J. Chem. Phys. 80 (1984) 1943–1960, doi:10.1063/1.446956.
[48] T.A. Keith, R.F.W. Bader, Y. Aray, Structural homeomorphism between the electron density and the virial field, Int. J. Quantum Chem. 57 (1996) 183–198, doi:10.1002/(SICI)1097-461X(1996)57:2⟨183::AID-QUA4⟩3.0.CO;2-U.
[49] D.T. Reis, I.H.S. Ribeiro, D.H. Pereira, DFT study of the application of polymers cellulose and cellulose acetate for adsorption of metal ions (Cd2+, Cu2+ and Cr3+) potentially toxic, Polym. Bull. 77 (2020) 3443–3456, doi:10.1007/s00289-019-02926-5.
[50] AIMAll (Version 17.11.14), Keith TA, (2017) TK Gristmill Software, Overland Park KS, USA (aim.tkgristmill.com)
[51] N.T.H. Nga, T.T.B. Ngoc, N.T.M. Trinh, T.L. Thuoc, D.T.P. Thao, Optimization and application of MTT assay in determining density of suspension cells, Anal. Biochem. 610 (2020) 113937, doi:10.1016/j.ab.2020.113937.
[52] I.A. Santos, J.F. Shimizu, D.M. de Oliveira, D.O.S. Martins, L. Cardoso-Sousa, A.C.O. Cintra, V.H. Aquino, S.V. Sampaio, N. Nicolau-Junior, R. Sabino-Silva, A. Merits, M. Harris, A.C.G. Jardim, Chikungunya virus entry is strongly inhibited by phospholipase A2 isolated from the venom of Crotalus durissus terrificus, Sci. Rep. 11 (2021) 8717, doi:10.1038/s41598-021-88039-4.
[53] R. Matkovic, E. Bernard, S. Fontanel, P. Eldin, N. Chazal, D.Hassan Hersi, A. Merits, J.-M. Péloponèse, L. Briant, The Host DHX9 DExH-Box Helicase is recruited to Chikungunya virus replication complexes for optimal genomic RNA translation, J. Virol. 93 (2019) e01764-18, doi:10.1128/JVI.01764-18.
[54] CLSI, Methods for Antimicrobial Susceptibility Testing of Anaerobic Bacteria; Approved Standard, 2007. www.clsi.org. (Accessed 31 May 2021).
[55] CLSI, Methods for Dilution Antimicrobial Susceptibility Tests for Bacteria That Grow Aerobically, Approved Standard, 2012. www.clsi.org. (Accessed 31 May 2021).
[56] B. Dietl, I. Sánchez, P. Arcenillas, E. Cuchi, L. Gómez, F.J. González de Molina, L. Boix-Palop, J. Nicolás, E. Calbo, Ceftolozane/tazobactam in the treatment of osteomyelitis and skin and soft-tissue infections due to extensively drug-resistant Pseudomonas aeruginosa: clinical and microbiological outcomes, Int. J. Antimicrob. Agents. 51 (2018) 498–502, doi:10.1016/j.ijantimicag.2017.11.003.
[57] J.E. Song, Y.G. Kwak, T.H. Um, C.R. Cho, S. Kim, I.S. Park, J.H. Hwang, N. Kim, G.B. Oh, Outbreak of Burkholderia cepacia pseudobacteraemia caused by intrinsically contaminated commercial 0.5% chlorhexidine solution in neonatal intensive care units, J. Hosp. Infect. 98 (2018) 295–299, doi:10.1016/j.jhin.2017.09.012.
[58] T. Li-Geng, T.C. Geraci, N. Narula, F.N. Zervou, P.J. Prasad, A.G. Decano, S. Sterling, I.M. Zacharioudakis, Recognizing Cutibacterium acnes as a cause of infectious pericarditis: a case report and review of literature, Anaerobe 69 (2021) 102359, doi:10.1016/j.anaerobe.2021.102359.
[59] W. Zhou, M. Spoto, R. Hardy, C. Guan, E. Fleming, P.J. Larson, J.S. Brown, J. Oh, Host-specific evolutionary and transmission dynamics shape the functional diversification of staphylococcus epidermidis in human skin, Cell 180 (2020) 454–470 e18, doi:10.1016/j.cell.2020.01.006.
[60] S.D. Sarker, L. Nahar, Y. Kumarasamy, Microtitre plate-based antibacterial assay incorporating resazurin as an indicator of cell growth, and its application in the in vitro antibacterial screening of phytochemicals, Methods 42 (2007) 321–324, doi:10.1016/j.ymeth.2007.01.006.

[61] R.M. Silverstein, F.X. Webster, D. Kiemle, Spectrometric Identification of Organic Compounds, 7th Edition, Wiley, 2005. https://books.google.com.br/books?id=mQ8cAAAAQBAJ.
[62] N.T. Zanvettor, C. Abbehausen, W.R. Lustri, A. Cuin, N. Masciocchi, P.P. Corbi, Silver sulfadoxinate: synthesis, structural and spectroscopic characterizations, and preliminary antibacterial assays in vitro, J. Mol. Struct. 1082 (2014) 180–187, doi:10.1016/j.molstruc.2014.11.004.
[63] L.L. Marques, G. Manzoni de Oliveira, E. Schulz Lang, M.M. Anraku de Campos, L.R. Soccol Gris, New gold(I) and silver(I) complexes of sulfamethoxazole: Synthesis, X-ray structural characterization and microbiological activities of triphenylphosphine (sulfamethoxazolato-N2)gold(I) and (sulfamethoxazolato)silver(I), Inorg. Chem. Commun. 10 (2007) 1083–1087, doi:10.1016/j.inoche.2007.06.005.
[64] X.-Y. Yu, R. Zhang, S.-L. Li, S.-H. Yu, L. Gao, W.-F. Yan, J. Jin, Y.-N. Luo, A new silver-organic coordination polymer: synthesis, crystal structure, fluorescence and antibacterial activity, Inorg. Chem. Commun. 116 (2020) 107897, doi:10.1016/j.inoche.2020.107897.
[65] R. Serra, R. Grande, L. Butrico, A. Rossi, U.F. Settimio, B. Caroleo, B. Amato, L. Gallelli, S. De Franciscis, Chronic wound infections: the role of Pseudomonas aeruginosa and Staphylococcus aureus, Expert Rev. Anti. Infect. Ther. 13 (2015) 605–613, doi:10.1586/14787210.2015.1023291.
[66] U. Kalinowska-Lis, A. Felczak, L. Checińska, K. Zawadzka, E. Patyna, K. Lisowska, J. Ochocki, Synthesis, characterization and antimicrobial activity of water-soluble silver(I) complexes of metronidazole drug and selected counter-ions, Dalt. Trans. 44 (2015) 8178–8189, doi:10.1039/c5dt00403a.
[67] B.S. Atiyeh, M. Costagliola, S.N. Hayek, S.A. Dibo, Effect of silver on burn wound infection control and healing: Review of the literature, Burns 33 (2007) 139–148, doi:10.1016/j.burns.2006.06.010.